Aalto University

School of Engineering

Department of Energy Technology

Variable Valve Actuation and Dual-Fuel Combustion

Master's Thesis

3.8.2015

Juhani Törmänen

Supervisor: Prof. Martti Larmi

Instructor: Lis. Sc. (Tech.) Teemu Sarjovaara

Aalto University
School of Engineering

Aalto University, P.O. BOX 11000, 00076
AALTO
www.aalto.fi

Abstract of master's thesis

Author Juhani Törmänen		
Title of thesis Variable Valve Actuation and Dual-Fuel Combustion		
Degree programme Energy Technology		
Major/minor Personal minor		**Code** K9002
Thesis supervisor Prof. Martti Larmi		
Thesis advisor(s) Lis. Sc. (tech.) Teemu Sarjovaara		
Date 03.08.2015	**Number of pages** 85	**Language** English

Abstract

The constantly increasing interest in alternative fuels in transportation has given birth to new strategies in the internal combustion engine technology. The tightening emissions regulations further boost this development. The dual-fuel technology is one of the most promising new concepts for natural gas-fuelled engines and it has already been widely adopted by the marine and power generation industry. However, the transition from Diesel to dual-fuel engines in road and off-road traffic has not been as rapid. The relatively high hydrocarbon emissions are one of the drawbacks that hinder the use of dual-fuel engines.

This Master's thesis focuses on combustion and emissions research in a dual-fuel research engine with VVA. VVA is commonly used in passenger car engines but rarely in heavy-duty Diesel engines, even though it offers some indisputable benefits. Five different valve actuation profiles were used with several Diesel substitution rates. The effects of each parameter combination on the cylinder pressure and engine-out emissions were recorded. The analysis of the engine phenomena was mainly based on calculations utilizing the cylinder pressure data.

The research engine was a conventional Diesel engine converted to run in dual-fuel mode. The conversion included a new exhaust system, methane feed line including injectors, several new sensors and other devices related to the methane injection. Moreover, the engine control system was updated for dual-fuel operation.

The results of the engine tests can be concluded as follows: The dual-fuel combustion is very sensitive to IEGR, most likely due to high mixture temperature. High temperatures promote the partial pre-combustion oxidation of methane which causes a substantial increase in the heat release rate even with very lean mixtures. Low temperatures have the opposite effect, although it is not as pronounced. A significant amount of the HC emissions originate from the scavenging if methane is injected prior to the exhaust valve closing. Furthermore, high substitution ratios tend to increase the cycle-to-cycle variation.

Keywords dual-fuel, gas engines, alternative fuels, variable valve actuation

Aalto-yliopisto
Insinööritieteiden
korkeakoulu

Aalto-yliopisto, PL 11000, 00076 AALTO
www.aalto.fi

Diplomityön tiivistelmä

Tekijä Juhani Törmänen	
Työn nimi Muuttuva venttiiliajoitus ja dual-fuel-palaminen	
Koulutusohjelma Energiatekniikka	
Pää-/sivuaine Henkilökohtainen sivuaine	**Koodi** K9002
Työn valvoja Professori Martti Larmi	
Työn ohjaaja(t) Tekniikan lisensiaatti Teemu Sarjovaara	
Päivämäärä 03.08.2015 **Sivumäärä** 85	**Kieli** Englanti

Tiivistelmä

Jatkuvasti kasvava kiinnostus vaihtoehtoisia polttoaineita kohtaan liikennekäytössä on synnyttänyt uusia lähestymistapoja polttomoottoritekniikassa. Kiristyvät päästömääräykset yhä vauhdittavat tätä kehitystä. Dual-fuel-teknologia on yksi lupaavimmista uusista maakaasua hyödyntävistä moottorikonsepteista ja se onkin saavuttanut jo vankan jalansijan merenkulku- ja voimalaitostekniikassa. Tieliikenne- ja työkonekäytössä muutos ei kuitenkaan ole ollut näin nopeaa. Verrattain korkeat hiilivetypäästöt ovat yksi dual-fuel-moottoreiden yleistymistä haittaavista tekijöistä.

Tämä diplomityö paneutuu palamisen ja päästöjen tutkimukseen muuttuvalla venttiiliohjauksella varustetun dual-fuel-tutkimusmoottorin avulla. Muuttuvaa venttiiliohjausta käytetään yleisesti henkilöautojen moottoreissa, mutta varsin harvoin raskaan kaluston puristussytytteisissä moottoreissa. Tässä työssä käytettiin viittä erilaista venttiiliohjausstrategiaa ja useita eri korvaavuusasteita. Jokaisen yhdistelmän vaikutukset palamiseen ja päästöihin tallennettiin. Tutkittujen ilmiöiden analyysi pohjautui pitkälti sylinteripainetietoon ja sitä hyödyntäviin laskelmiin.

Tutkimusmoottori oli dual-fuel-käyttöiseksi muunnettu Diesel-moottori. Muunnos sisälsi muun muassa uuden pakokaasujärjestelmän, metaanisyötön laitteineen, useita uusia antureita sekä muista metaanin ruiskutukseen liittyviä laitteita. Lisäksi moottorin ohjausjärjestelmä päivitettiin dual-fuel-järjestelmää ja mittauksia varten.

Tutkimuksen tuloksista voidaan nostaa esille useita pääkohtia: Dual-fuel-palaminen on hyvin herkkä sisäiselle EGR:lle, mikä todennäköisesti johtuu seoksen lämpötilan noususta. Korkea lämpötila edistää metaanin osittaista hapettumista ennen varsinaista palamista, mikä puolestaan lisää huomattavasti seoksen palamisnopeutta myös hyvin laihoilla seoksilla. Matalilla lämpötiloilla on päinvastainen vaikutus, vaikka vaikutus on huomattavasti vähäisempi. Merkittävä osa hiilivetypäästöistä syntyy kaasunvaihdon aikana, jos metaani ruiskutetaan ennen pakoventtiilin sulkeutumista. Korvaavuusasteella vaikuttaisi olevan syklistä variaatiota lisäävä vaikutus.

Avainsanat dual-fuel, kaasumoottorit, vaihtoehtoiset polttoaineet, muuttuva venttiiliajoitus

Preface

This thesis was conducted in the Aalto University Internal Combustion Engine Laboratory. The project was funded by the Henry Ford Foundation in Finland and by the Aalto University Department of Energy Technology. I want to thank these organizations for the financial aid.

I am particularly grateful to my instructor Lis. Sc. Teemu Sarjovaara and my supervisor Professor Martti Larmi for the opportunity to write this thesis. I also want to express my gratitude to the following people that have helped me during my work in the laboratory: Otto Blomstedt, Olli Ranta, Rasmus Pettinen, Alberto Murillo, Tuomo Hulkkonen, Kari Hujanen and Karri Keskinen.

Finally, I thank my friends and family for all the support in my studies and in my life outside the university.

Hyvinkää, May 2015

Juhani Törmänen

Table of Contents

Nomenclature

Abbreviations:

A/D	Analogue/Digital
AFR	Air-Fuel Ratio
ABDC	After Bottom Dead Centre
ATDC	After Top Dead Centre
BBDC	Before Bottom Dead Centre
BDC	Bottom Dead Centre
CAD	Crank Angle Degrees
CLD	Chemiluminescence Detector
CNG	Compressed Natural Gas
COV	Coefficient of Variance
CP	Charge Pressure
DF	Dual-Fuel
DOC	Diesel Oxidation Catalyst
E%	Percentage of Energy
ECU	Electronic Control Unit
EGR	Exhaust Gas Recirculation
EHVA	Electro-Hydraulic Valve Actuation
ETC	European Transient Cycle
EVC	Exhaust Valve Closing
EVT	Exhaust Valve Timing
FID	Flame Ionisation Detector
GHG	Greenhouse Gas
HCCI	Homogeneous Charge Compression Ignition
HP	High-Pressure
HPDI	High-Pressure Direct Injection
HR	Heat Release
HRR	Heat Release Rate
ICE	Internal Combustion Engine
IEA	International Energy Agency
IEGR	Internal Exhaust Gas Recirculation
IMEP	Indicated Mean Effective Pressure

IVC	Inlet Valve Closing
IVT	Inlet Valve Timing
LHV	Lower Heating Value
LNG	Liquefied Natural Gas
LP	Low-Pressure
LPG	Liquid Petroleum Gas
MN	Methane Number
$\dot{m}_a$	Air Mass Flow
$\dot{m}_{DI}$	Diesel Mass Flow
$\dot{m}_{CH4}$	Methane Mass Flow
NG	Natural Gas
NGV	Natural Gas Vehicle
NVO	Negative Valve Overlap
OFAT	One-Factor-At-Time
PCCI	Premixed Charge Compression Ignition
PID	Proportional-Integral-Derivative (Control)
PPCI	Partially Premixed Compression Ignition
r_c	Compression Ratio
RCCI	Reactivity Controlled Compression Ignition
r_e	Expansion Ratio
ROI	Return on Investment
RTC	Real-Time Computer
SCR	Selective Catalytic Reaction
SECA	Sulphur Emission Control Area
SR	Substitution Rate
TTL	Transistor-Transistor Logic
VSI	Vapour Sequential Injection
VVA	Variable Valve Actuation
VVE	Variable Valve Event
VVL	Variable Valve Lift
VVT	Variable Valve Timing
WHTC	World Harmonized Transient Cycle
WI	Wobbe-Index

Chemical Compounds and Emissions:

CH	Hydrocarbon(S)
CH_4	Methane
C_2H_6	Ethane
C_3H_8	Propane
CO	Carbon Monoxide
CO_2	Carbon Dioxide
$CO(NH_2)_2$	Urea
HO_2	Hydroperoxyl
NO	Nitric Oxide
NO_2	Nitrogen Dioxide
N_2O	Nitrous Oxide
NO_x	Nitrogen Oxides
O_2	Oxygen Gas
O_3	Ozone
PAH	Polyaromatic Hydrocarbon

Greek Letters:

γ	Ratio of Specific Heats
λ	Air-Fuel Ratio (relative to stoichiometric)
ρ	Density
σ	Standard Deviation

1 Introduction

As the race for cleaner climate escalates and conventional energy sources become increasingly expensive, natural gas has been adopted as fuel for internal combustion engines in various applications. The natural gas market is constantly spreading and natural gas becomes more easily available throughout the world. According to International Energy Agency's scenario 'The Golden Age of Gas', the production of natural gas is will likely increase by 50% from the level of 2010 by 2035. [1]

There are several incentives for wider natural gas usage in internal combustion engines. Tightening legislation and regulations concerning engine-out emissions compel operators to either invest in expensive after-treatment devices or change the fuel to something less polluting. Natural gas is seen as one of such fuels while liquefied natural gas technology has made it particularly interesting for marine engines. However, probably the strongest driver for increased natural gas popularity is the fuel price. The new fuel sulphur content limits in the sulphur emission control areas (SECAs) has boosted this development as the use of cheap heavy fuel oil in marine engines has become increasingly difficult [2].

The dual-fuel technology has been widely adopted in marine industry as a means of utilising natural gas as the main fuel while maintaining the possibility to switch to Diesel operation if natural gas in not available. Dual-fuel is now trending in heavy-duty road traffic as well in areas where natural gas infrastructure is developed. There are some problems that hinder the widespread adoption of the technology even though the experiences from dual-fuel engines in road traffic are positive. The most acute problems related to the dual-fuel technology in road traffic are the difficulty of natural gas transportation and the rather high hydrocarbon emissions that may exceed the latest emission standard levels. Moreover, the combustion control of very lean mixtures at part load conditions is often problematic.

Lean combustion control is the key to low engine-out hydrocarbon emissions which may be achieved by advanced engine control strategies. The goal of this thesis was not to develop a low-emission engine but rather to study and understand the behaviour of lean dual-fuel combustion and emissions relative to variable valve actuation.

This thesis focuses on the study of dual-fuel combustion phenomena and emissions in a high-speed research engine. A conventional single-cylinder Diesel engine has been converted to run in dual-fuel mode with methane and Diesel simultaneously. The objectives of this thesis are to study and analyse the effects of substitution rate and variable valve actuation and related parameters on dual-fuel combustion phenomena and emissions. Namely the effects of variable valve actuation strategies on lean-burn dual-fuel combustion and emissions are subjects of interest.

The thesis is divided into three main sections: The Background section is a literature review which explains the dual-fuel concept and covers the most important topics related to the research objective. The Research System and Methods section presents the tools, devices, calculations and theories that were used during the experiments and analysis. Finally, the Experiment Results and Analysis section presents the results obtained from the engine tests and combustion and emissions analysis based on these results.

2 Background

2.1 Natural Gas as Diesel Fuel Substitute in Dual-Fuel Engines

2.1.1 Dual-Fuel Engine Fundamentals

A dual-fuel engine always mixes two different fuels, hence the name, to form the combustion event. There are multiple fuels that have been successfully implemented into the dual-fuel concept: liquid petroleum gas (LPG), natural gas (NG), gasoline, ethanol and Diesel to name a few [3]. In this thesis, the mix of NG and Diesel is considered which is a common combination in marine and road traffic applications [4].

The term 'dual-fuel' (DF) can refer to a variety of combustion strategies in the literature. However, this chapter defines the context and relevance of the term as it is considered in this thesis. The DF process combines the aspects of the Otto and Diesel processes in a unique manner and the classification to either is obscure. A major part of the bulk energy of the combustion originates from a premixed air-fuel mixture which is more or less homogeneous. The DF engine is compression ignited and another fuel is used to provide the ignition energy. Fundamentally, high-reactivity fuel is used to ignite the fuel-air-mixture while low-reactivity fuel comprises the main part of the energy content in the combustion. [5]

The inlet and compression strokes of the DF cycle are depicted in Figure 2.1. The primary fuel used to form the premixed mixture is NG. NG is admitted in the inlet ports or manifold during or prior to the inlet cycle. The methane-air is mixed in the inlet ports and it continues to mix in the cylinder. At the end of the compression phase, a small amount of Diesel fuel is injected to commence the combustion. The Diesel ignites after the ignition delay period and ignites the premixed NG-air mixture. The expansion and exhaust strokes follow as in any four-stroke engine. [5]

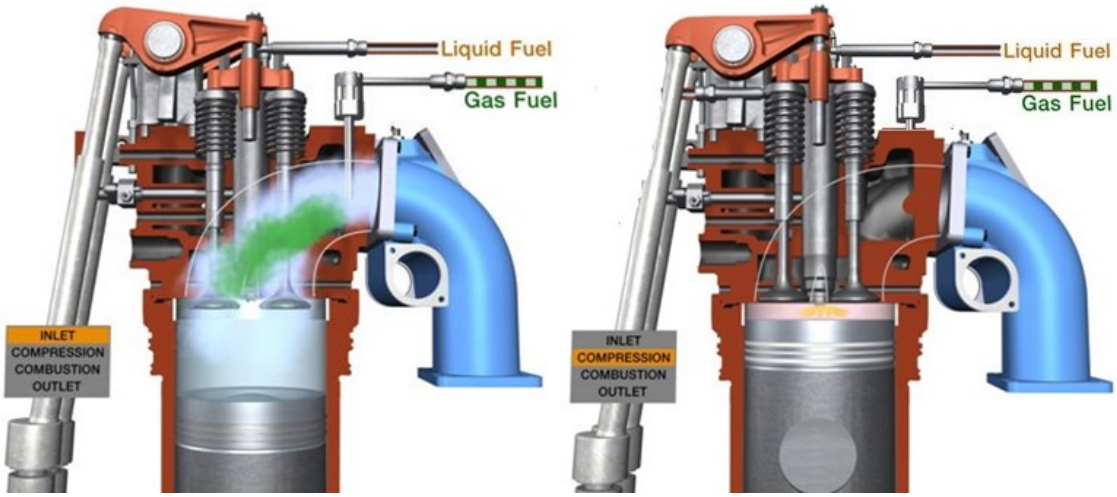

Figure 2.1. Conventional dual-fuel inlet (left) and compression (right) strokes. The methane fuel is indicated with green and Diesel with gold color. [6]

The Diesel injection is often termed pilot injection, particularly with small injection amounts. The pilot injection behaves in the same manner as it would in conventional Diesel mode and undergoes the same pre-ignition processes. The DF engine may operate on relative Diesel amounts of 1 to 100 % of the total fuel energy [5]. The maximum and minimum limits of natural gas are set by the mixture formation, compression ratio and the properties of the Diesel injector. The natural gas fraction of total fuel energy content is referred to as the substitution rate (SR). A high substitution rate is usually desired in order to fully benefit from the more economical and cleaner natural gas [7].

The main advantages of the DF engine over the conventional Diesel engine are:

- Low fuel costs
- fuel flexibility
- reduction in NO_x, PM and CO_2 emissions

NG is generally substantially cheaper than Diesel oil and the price is expected to remain below that of the conventional fuels in the future [1]. In addition, DF engine may generally be operated in full Diesel mode if NG is not available so that the original performance is maintained. Moreover, the concentrations of certain harmful exhaust gas components are significantly lower in DF engines than in Diesel operation. Namely the nitrogen oxides (NO_x), particulate matter (PM, soot) and carbon dioxide (CO_2) are reported to decrease [8].

Some of the main disadvantages of the DF engine are:

- the need of two parallel fuel systems
- more complicated engine control
- difficulties in low-load operation
- increased HC and CO emissions

Two fuel systems increase the cost of the vehicle and require more space which is often very limited in vehicles. Particularly the fuel tanks of compressed natural gas (CNG) may be problematic [9]. Furthermore, the combustion control is more complex and prone to load variations than the Diesel engine [7]. Lastly, the increased HC and CO emissions may require the use of additional after-treatment devices unless very sophisticated engine control is used [10].

As stated before, there are a variety of terms associated to the DF combustion. These terms refer to different combustion strategies that are used with the DF concept. Some of the most commonly used combustion strategies are briefly explained below.

The combustion strategy shown in Figure 2.1 is referred to as partially premixed compression ignition (PPCI). This denotes that the methane-air mixture is premixed outside the cylinder whereas the Diesel is injected very late in the compression cycle. The Diesel combustion is mostly mixing controlled while a small fraction is premixed. The purpose of the Diesel fuel is purely to ignite the bulk mixture and control the ignition timing [5]. The combustion strategy used in the experimental engine for this thesis can be categorized as PPCI and henceforth the term dual-fuel (DF) refers to this combustion method.

Premixed charge compression ignition (PCCI) utilises earlier Diesel injections than a PPCI process. This strategy uses a mixture where both fuels are premixed with air. However, it is important to notice that the mixture is not homogeneous which indicates that the combustion chamber is divided into phases where Diesel and NG concentrations are dissimilar. The ignition of the charge is not completely decoupled from the injection timing so that some control is retained. The onset of the combustion is further controlled with the use of exhaust gas recirculation (EGR). [11]

If the Diesel injection is further advanced, the mixing of the two fuels and air is more complete and the charge is considered homogeneous. This combustion strategy is referred to as homogeneous charge compression ignition (HCCI). HCCI relies on very early Diesel injections after the bottom dead centre (BDC). As the mixture becomes homogeneous, the ignition control via injection timing is lost. The HCCI combustion is divided into two phases. In the first phase, the long carbon chains of the Diesel fuel rupture and release heat which increases the mixture temperature. This is referred to as the low-temperature combustion. In the second phase, the mixture ignites and burns nearly instantaneously. The second phase is called the high-temperature combustion. There are multiple ignition start locations which cause a rapid heat release. The HCCI mixture ignition timing is mainly controlled with EGR. [11]

A combustion strategy that utilises the different reactivity of the fuels is called reactivity controlled compression ignition (RCCI). RCCI combustion is controlled by the mixture reactivity which, in turn, is controlled by the relative proportions of the fuels in the mixture. RCCI requires a high-reactivity fuel, such as Diesel and a low-reactivity fuel, such as natural gas so that the combustion event can be formed as desired. [12]

2.1.2 Heavy Duty Gas Engine Emissions Legislation

Heavy duty engine emissions in Europe are regulated for both on- and off-road vehicles. The Euro 1 standard was first introduced in 1992 which was followed by the Euro 2 regulation in 1996. Since then, the Euro standards have been gradually updated to the present Euro 6 standard, each standard introducing more stringent emissions regulation than the previous [13]. The evolution of the Euro emissions regulations is presented in Figure 2.2.

The regulated emissions include carbon monoxide (CO), hydrocarbons (HC), nitrogen oxides (NO_x) and particulate matter (PM). The HC emissions are further classified into non-methane hydrocarbons (NMHC) and methane (CH_4) in the Euro regulations. All regulated emissions except CH_4 are so called local emissions. This implies that the emissions have an adverse impact on the local air quality and ecosystems. On the contrary, the effects of CH_4 are considered global [14]. Figure 2.2 shows how the total emission limits have decreased by 83% since the introduction of Euro 1. PM emission limits have decreased nearly to zero [13]. However, further reduction of the NO_x, HC and CO emissions becomes increasingly difficult and expensive as the regulations become more stringent.

More detailed regulations for Diesel and natural gas engines in Euro 4, 5 and 6 standards are presented in Table 2.1. The presented regulations apply to the European Transient Cycle (ETC) or World Harmonized Transient Cycle (WHTC) tests. The steady state cycle

emissions regulations are not specified for gas-powered engines in the Euro standards. [13][15][16]

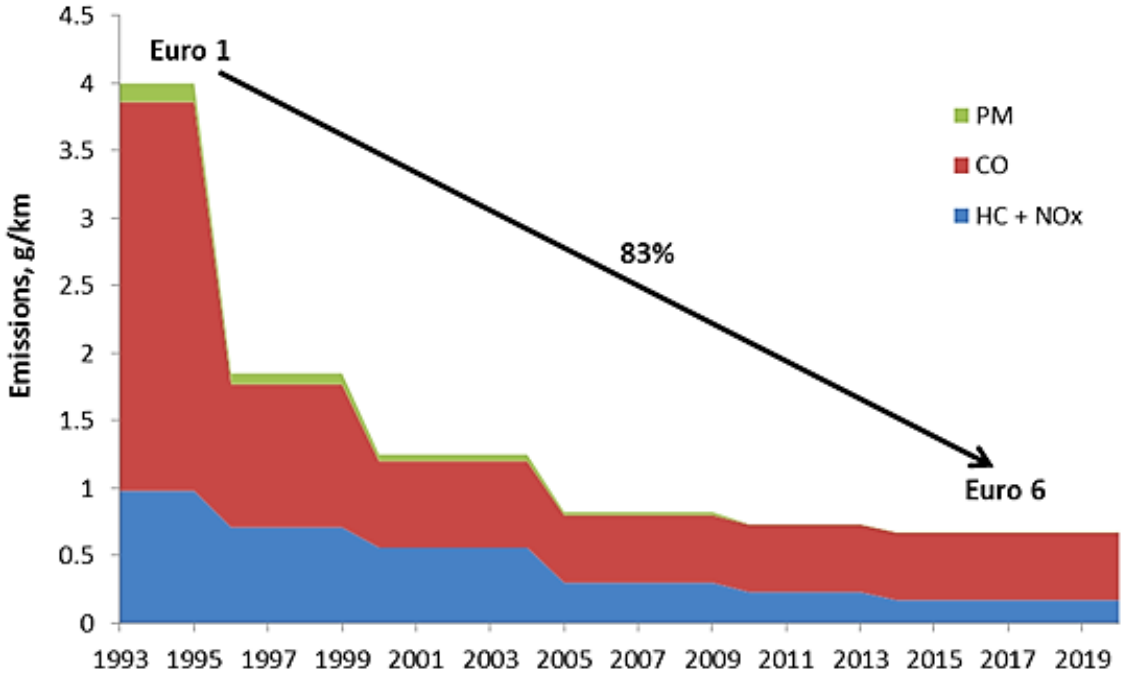

Figure 2.2. The evolution of the Euro emissions regulations. [17]

In addition to fixed emissions limits, the Euro standards specify emission durability periods. A vehicle must fulfil the regulated emission limits up to a certain age or mileage. The durability limit for heavy vehicles is 500 000 km or 7 years in Euro 4 and 5 and consequently 700 000 km or 7 years in Euro 6. For lighter trucks and buses, this limit is 200 000 km or 6 years in Euro 4 and 5 and 300 000 km or 6 years in Euro 6.

Table 2.1 Heavy duty road vehicle emissions regulations from Euro 4 to Euro 6. [13, 15, 16]

Standard	Date applied	Test Cycle	CO	NMHC	CH4	NOx	PM
			g/kWh				
Euro 4	Oct. 2005	ETC	4.0	0.55	1.1	3.5	0.03
Euro 5	Oct. 2008	ETC	4.0	0.55	1.1	2.0	0.03
Euro 6	Jan. 2013	WHTC	4.0	0.16	0.5	0.46	0.01

The emissions from non-road engines are regulated in separate standards where the emission limits are dependent on the nominal engine power. Stage 4 is the latest standard succeeding Stage 3B. The emission limits for the two largest power ranges in Stage 3B and Stage 4 and the proposed limits for the upcoming Stage 5 standard are presented in Table 2.2. The figures presented in table 2.2 concern Diesel engines as there is no current separate legislation for gas-powered non-road engines. The HC emission limit in Stage 5 is multiplied by a factor of 1.10 for gas engines. [18]

Table 2.2 Heavy duty non-road emission regulations from Stage 3B to proposed Stage 5. [18]

Standard	Date applied	Power range (kW)	CO	HC	NOx	PM
			g/kWh			
Stage 3B	Jan. 2012	$75 \leq P < 130$	5.0	0.19	3.3	0.025
	Jan. 2011	$130 \leq P \leq 560$	3.5	0.19	2.0	0.025
Stage 4	Oct. 2014	$75 \leq P < 130$	5.0	0.19	0.4	0.025
	Jan. 2014	$130 \leq P \leq 560$	3.5	0.19	0.4	0.025
Stage 5	2020**	$56 \leq P < 130$	5.0	0.19*	0.4	0.015
	2019**	$130 \leq P \leq 560$	3.5	0.19*	0.4	0.015

** Multiply by 1.10 for gas engines*
*** To be announced*

Dual-fuel engines generally require higher limits for HC emissions due to the unburned methane in the exhaust gases. It can be argued that the 1.10 factor proposed in Stage 5 HC emissions for gas engines is too low. On the other hand, it may be possible to comply with the Euro 6 CH_4 emissions limit of 0.5 g/kWh with modern DF engines [7]. It would be reasonable to separate the CH_4 emissions from the NMHC emissions also in the non-road engine legislation as these species have very different environmental impacts.

2.1.3 Dual-Fuel In-Cylinder Mixture Formation and Combustion

The mixture formation in a dual-fuel engine is dependent on both the spray and ignition attributes of the Diesel injection and the properties and concentration of the gaseous fuel used. There are two combustible fuels and thus the physical and chemical interactions prior to and during the combustion are rather complex. [4]

As the piston approaches the top dead centre (TDC) during the compression stroke, the premixed gaseous fuel-air mixture is subjected to increasing temperature and pressure. The pre-ignition processes commence as the temperature rises to a certain level and the methane, the main component of natural gas, starts to oxidize. Part of the methane oxidizes to formaldehydes and active radicals and subsequently to CO during the late compression stroke. This is sometimes referred to as low-temperature combustion as no flame front exists. The low-temperature combustion can substantially increase the in-cylinder temperature toward the TDC. [19]

The Diesel is injected close to the TDC and this commences the combustion. The combustion of NG-air mixture ignited with a small amount of Diesel is presented in Figure 2.3. The outer regions of the Diesel spray mix with air and a combustible mixture is formed. With small Diesel pilot quantities, a major portion of the Diesel will be mixed with air prior to combustion. When the in-cylinder temperature rises to the autoignition level of the premixed Diesel, the mixture ignites in several locations nearly simultaneously. The number of ignition locations depends on the number of injector holes in the Diesel injector. The premixed part of the Diesel fuel burns quickly and the partially oxidized methane in the immediate vicinity of the Diesel flame contributes to the heat released during the early combustion. As the flame front propagates, the bulk of the gas-air mixture burns until the whole volume is engulfed. [20]

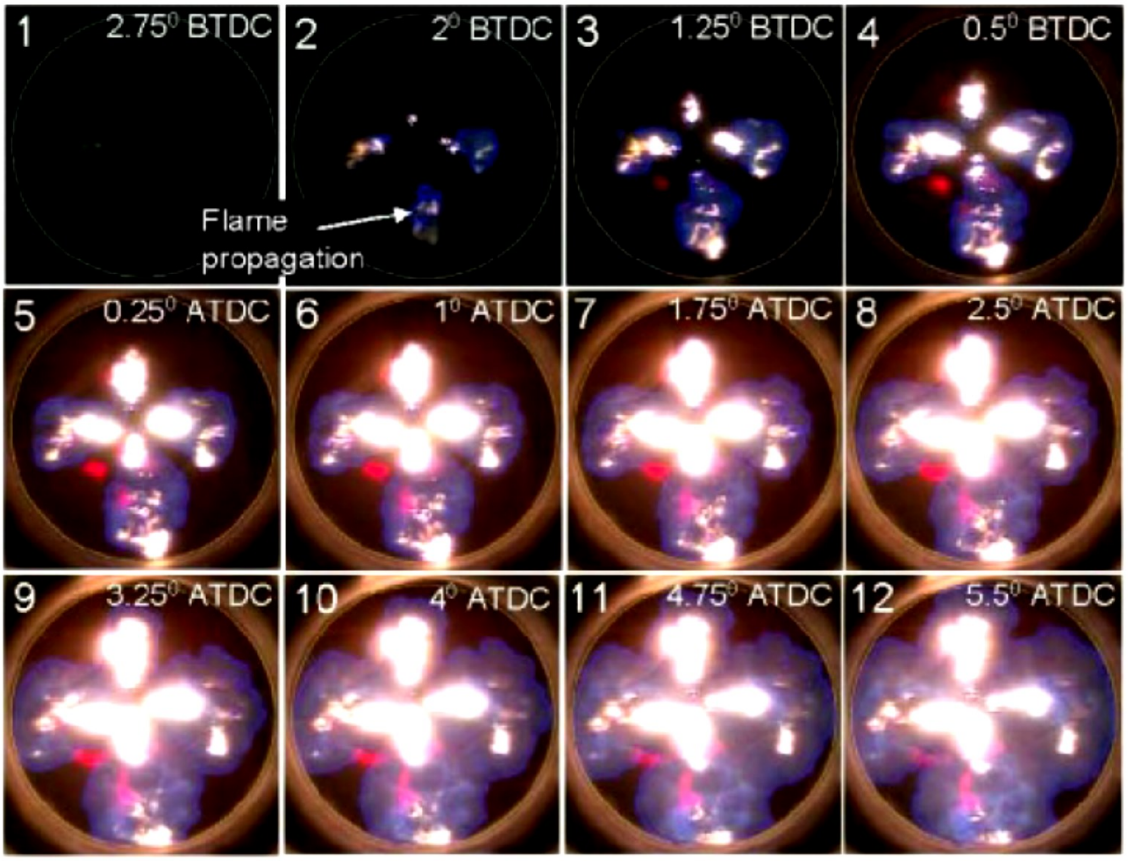

Figure 2.3. Micro-pilot ignited dual-fuel combustion with natural gas (88% CH4, 6% C2H6, 4% C3H8, 2% n-C4H10). Diesel injector has 4 holes and injection pressure of 40 MPa. Diesel injection quantity 2 mg. [20]

The dual-fuel heat release can be divided into three components which overlap each other. The first component is the combustion of the pilot fuel or the premixed part of the Diesel. The second component originates from the combustion of gaseous fuel in the immediate vicinity of the Diesel flame. The first two components cause a steep increase in the heat release rate (HRR). The third component is the combustion of the lean mixture across the rest of the volume. This lean mixture combustion is rather slow and ignites due to propagating turbulent flame or auto-ignition [4]. In some cases, a fourth component can be identified. This is the possible bulk ignition of the end gas causing a rapid pressure rise rate rather late in the cycle and may lead to knocking combustion [7]. The three main components of the DF combustion heat release rate are shown in Figure 2.4.

At heavy load (Figure 2.4 left side), the premixed gas-air mixture is richer in fuel and the total amount of energy in the mixture is high. Thus the relative proportions of the second and third components are large. The Diesel pilot causes a high, rapidly rising peak of the NG combustion and the propagating flame front burn the bulk mixture rather rapidly. On the contrary, at light load as the mixture becomes very lean, the influence of the pilot on the total combustion becomes more pronounced while especially the contribution of the third component to the total heat release diminishes. This is mostly due to the increase in the relative proportion of the pilot fuel of the total energy content in very lean mixtures, which leads to relatively larger amount of gaseous fuel being in the immediate vicinity of the pilot flame. Moreover, the flame propagation in the lean mixture is quite slow. Hence, the third component diminishes while the first and second become more dominant. [4]

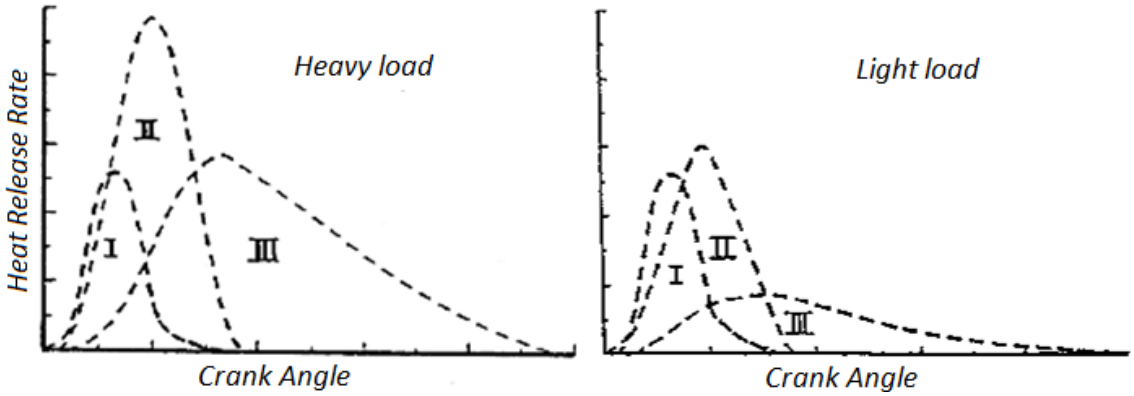

Figure 2.4. The dual-fuel heat release rate components: I) premixed Diesel, II) partially oxidized NG and NG near the Diesel flame, III) combustion of the lean bulk mixture. Left side: heavy load combustion. Right side: light load combustion. [4]

This significantly promotes the progress of the pre-ignition processes especially with certain reactive fuels. However, even with methane operation, some pre-ignition reactions occur during the compression stroke without the implementation of the pilot fuel. The reactions during the compression stroke before the ignition can substantially raise the temperature of the charge near the TDC. The pre-ignition reactions are often referred to as cold combustion. Furthermore, the reactions produce some partial oxidation products including aldehydes, radicals and CO. These products contribute directly to the combustion process in the vicinity of the pilot flame. [4]

The stable, high-energy ignition provided by the Diesel pilot is one of the main advantages of the DF combustion. The ignition energy is substantially higher than in spark-ignited engines which enables the use of very lean NG-air mixtures [21]. However, the DF combustion is rather prone to pre-ignitions and knock due to the high compression ratios used with a partially premixed mixture [11]. The optimum operating window is therefore rather narrow. The operating window of large Wärtsilä DF engines is shown in Figure 2.5. With relatively low air-fuel ratios, the engine load output is limited by pre-ignitions and knock whereas with very lean mixtures misfiring and incomplete combustion occur. The optimum operating window is therefore well on the lean side (lambda > 2) but the lean limit of methane combustion is not exceeded [22].

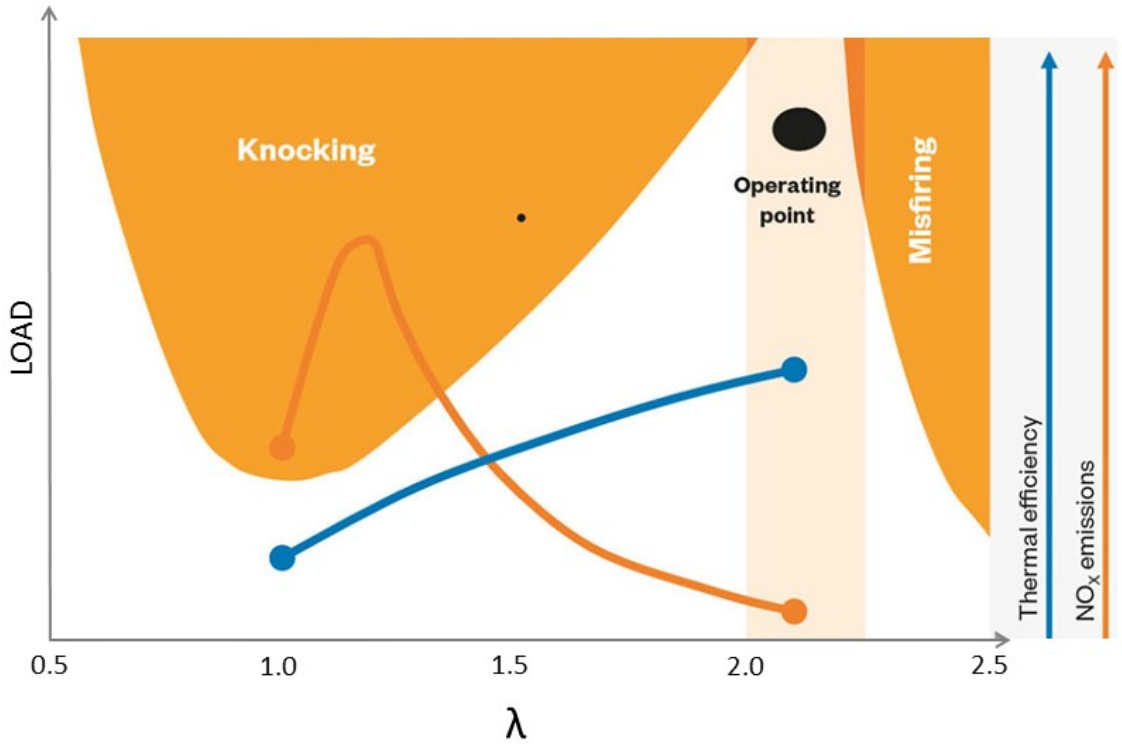

Figure 2.5. The operating window of the Wärtsilä dual-fuel engines. [23]

2.1.4 Natural Gas Fuel Properties

Instead of pure methane, compressed natural gas (CNG) or liquefied natural gas (LNG) is used as transportation fuel. The natural gas used in internal combustion engines (ICEs) varies in composition depending on the region. NG mainly consists of methane (CH_4) but other alkanes such as propane (C_3H_8) and ethane (C_2H_6) may exist in small concentrations. Moreover, inert gases such as CO_2 and nitrogen gas (N_2) are often present. [24]

Natural gas is a fossil fuel and thus contributes to the CO_2 burden of the atmosphere when burned. However, methane-rich biogas can be enriched from gas obtained from landfill sites, waste water sludge, gasification of wood and from other organic sources. Raw biogas consists mainly of CH_4, CO_2 and N_2. The CH_4 content is often too low for ICE use without enrichment. The enriched or upgraded biogas consists of approximately 97…98 m% CH_4 which corresponds to the CH_4 content of the most commonly used (in Europe) Russian NG. Wood gasification produces nearly pure CH_4 and thus the gas can be used without enrichment [25]. Some gas compositions of natural gas and biogas from different sources are presented in Table 2.3.

NG and biogas are classified to L-gas and H-gas according to their heating value. L-gas is regarded as low-calorific value gas whereas H-gas is high-calorific value gas. The heating value is affected by the presence of combustible and inert species. In Table 2.3 for example, NG from Russia and Norway is regarded as H-gases whereas the rest are L-gases due to the high amounts of N_2 and CO_2. [26]

Table 2.3. Typical natural gas and biogas compositions (VOL-%) from different sources. [25]–[27]

Area →	NG Russia	NG Norway	NG the Netherlands	Landfill gas (raw)	Food stock gas (raw)
CO_2	0.1	2.0	1.8	50…60	50…60
N_2	0.8	1.0	9.9	0…15	< 10
CH_4	97.6	87.8	83.2	45…55	40…50
C_2H_6	1.0	7.6	4.1	-	-
C_3H_8	0.3	1.3	0.7	-	-
Higher HC	0.1	0.3	0.3	-	-

The combustion properties of the fuel gas are described with the methane number (MN) and the Wobbe-index (WI). MN is a dimensionless value that represents the fuel's ability to resist autoignition. Thus, MN is similar to octane rating but the reference fuels are pure methane and hydrogen gas (H_2) instead of iso-octane and n-heptane. CH_4 and H_2 are given reference values of 100 and 0, respectively. A gas with a methane number of 90 would behave as a mixture of 90% CH_4 and 10% H_2. Generally any higher alkanes, such as C_2H_6 and $C3H_8$, decrease the MN whereas the non-combustible gases, such as CO_2 and N_2, increase the MN. [25][26]

The Wobbe-index of a gas can be calculated as follows: [28]

$$WI = \frac{LHV}{\sqrt{\frac{\rho_{fuel}}{\rho_{air}}}} \quad (1)$$

Where LHV is the lower heating value of the fuel and $\rho_{fuel}$and ρ_{air} are the densities of the fuel gas and air, respectively.

The Wobbe-index is used to evaluate the interchangeability of different gaseous fuels. A comparison between the heating values of different gaseous fuels can be misleading due to the differences in density whereas the Wobbe-index comparison is more relevant. Fuels with similar WIs are often interchangeable. [28]

The main hindrance to NG becoming a more common engine fuel in road traffic is the difficulty of transportation. NG requires infrastructure, namely gas pipes, in order to be transported in gaseous form. Furthermore, NG can be transported in a liquid state but this requires extremely cold temperatures of approximately -163 °C. In order to maintain such temperatures, cryogenic tanks are needed. Moreover, some of the liquefied NG has to be allowed to boil off to maintain the temperature. The difficulty of transportation also applies to vehicles that carry NG in their fuel tanks. LNG is often inconvenient for road traffic use and unavailable to public but some LNG systems have been successfully used in some long-haul freight trucks. CNG is usually more suitable but requires relatively large pressure tanks in order to maintain satisfactory operating range for the vehicle due to the lower energy density of NG in a gaseous state. [29]

Despite the disadvantages of handling gaseous fuel, methane-rich natural gas has some attributes that make it exceptionally good fuel for ICEs. The high octane number of methane enables the use of methane in compression ignited engines without changing the

compression ratio thus making dual-fuel conversions more easily available [7]. Moreover, the heat capacity of methane is higher than that of air which leads to lower compression temperatures of the fuel-air mixture which helps reducing the NO_x emissions [28]. Some properties of methane and Diesel are listed in Table 2.4.

Table 2.4. A comparison of methane and Diesel properties. [30][31] [32]

Fuel	Diesel	Methane
Stoichiometric AFR	14.5	17.2
Mixture energy density (λ=1) [MJ/m^3]	3.79	3.40
Lower heating value [MJ/kg]	41.7	48.8
Density (NTP) [kg/m^3]	856	0.72
Energy density (liquid) [GJ/m^3]	35.7	23.6
Energy density (CNG. 230 bar) [GJ/m^3]	-	9.5
Carbon content [m%]	87	74
Boiling point [°C]	125	-162
Research octane number (RON)	-	120
Specific CO_2 emissions [g/MJ]	72	56

A significant incentive for using methane-powered engines is the low well-to-wheel CO_2 emissions. Methane has a low carbon-to-hydrogen ratio and thus methane combustion emits less CO_2 and more H_2O than the conventional liquid fuels. The reduction of CO_2 emissions from the vehicle tailpipe is approximately 25 % when Diesel is substituted with methane [33]. Contemplating from a well-to-wheel perspective, natural gas still offers substantial reduction of CO_2 emissions when compared with petroleum Diesel. However, methane itself is a very potent greenhouse gas (GHG) and care must be taken in order to minimize the methane emissions during the whole well-to-wheel cycle. [14][34]

Biogas is a very promising alternative fuel in the battle against the global warming. Instead of allowing the methane from natural decomposition processes to slip into the atmosphere unrestrained, it is processed and used to power combustion engines. This reduces the harmful emission load in the atmosphere and the well-to-wheel GHG emissions can be considered as negative. [14]

2.2 Current Technology, Problems and Solutions

2.2.1 Dual-Fuel Retrofitting

A conventional Diesel engine may be retrofitted with DF equipment rather easily without any modifications the mechanical parts of the engine. An engine optimized for operation on high Diesel substitution rates requires more modifications. The natural gas can be stored in either compressed gaseous form (CNG) or in a liquid state (LNG) in cryogenic tanks. The suitability of LNG is dependent on application. Marine engines use LNG for obvious reasons but heavy duty road and off-road vehicles are often more suitable for CNG. In some cases LNG may be applicable to road traffic (e.g. long-haul freight trucks). In either case, the fuel system is unquestionably the largest single modification in a retrofitted DF engine. [33]

The design parameters for a retrofitted DF system are [33]:

- high fuel substitution rate
- short return on investment (ROI)
- unaffected Diesel operation (fuel flexibility)
- operating range
- system reliability

A high fuel substitution rate is desired to achieve as short a ROI time as possible. Often fuel cost savings vary between 15 and 50 % compared with a Diesel-powered engine. The ROI time is naturally dependent on the taxation and current fuel prices in the region [33]. Moreover, fuel flexibility is often important to fleet operators as natural gas is not always available and Diesel must be used. The fuel flexibility is closely related to the operating range on natural gas. The operating range can be increased by installing larger fuel tanks for natural gas. Even LNG has approximately 35% lower energy density than Diesel whereas CNG requires four times more space for Diesel equivalent energy content (see Table 2.4) [32]. In addition, the DF conversion must not significantly increase the maintenance costs or degrade the reliability of the engine.

The measures for dual-fuel conversion can be divided into necessary and optional. The necessary changes include changes in the fuel system that enable the use of a simple DF system at a basic level whereas the optional measures optimise the performance of the DF engine and may be needed to comply with the newest emissions legislation.

The necessary system components and changes are:

- LNG or CNG tanks with safety equipment
- Fuel gas piping, pressure regulators and sensors
- NG injectors or a gas admission valve
- NG electronic control unit (ECU) and wirings

The optional measures are for example [37]:

- Exhaust piping update without flammable gas traps
- Exhaust gas after-treatment system update
- Lambda control with throttle
- Optimised NG admission
- Compression ratio change
- Minimisation of combustion chamber crevices
- Diesel injector update
- Sophisticated mixture control methods (e.g. HPDI)

A typical natural gas feed system for heavy duty vehicles using CNG is presented in Figure 2.6. The fuel is stored in 200…250 bar pressure in a vessel from where it is lead through a filter to a pressure regulator. The pressure regulator lowers the gas pressure to the desired injection pressure. The gas is then lead to the NG injector rail which distributes the fuel to the gas injectors. The air flow from the compressor is controlled by a throttle valve and the AFR is metered with the air mass flow sensor in the inlet air pipe and with the oxygen sensor located in the exhaust pipe. The Diesel system is similar to that of any Diesel engine. The high-pressure pump pressurises the Diesel fuel to the desired rail

pressure. The pump is usually controlled with pulse width modulation (PWM). The Diesel injectors are connected to a common rail which supplies the injectors for all cylinders. [35]

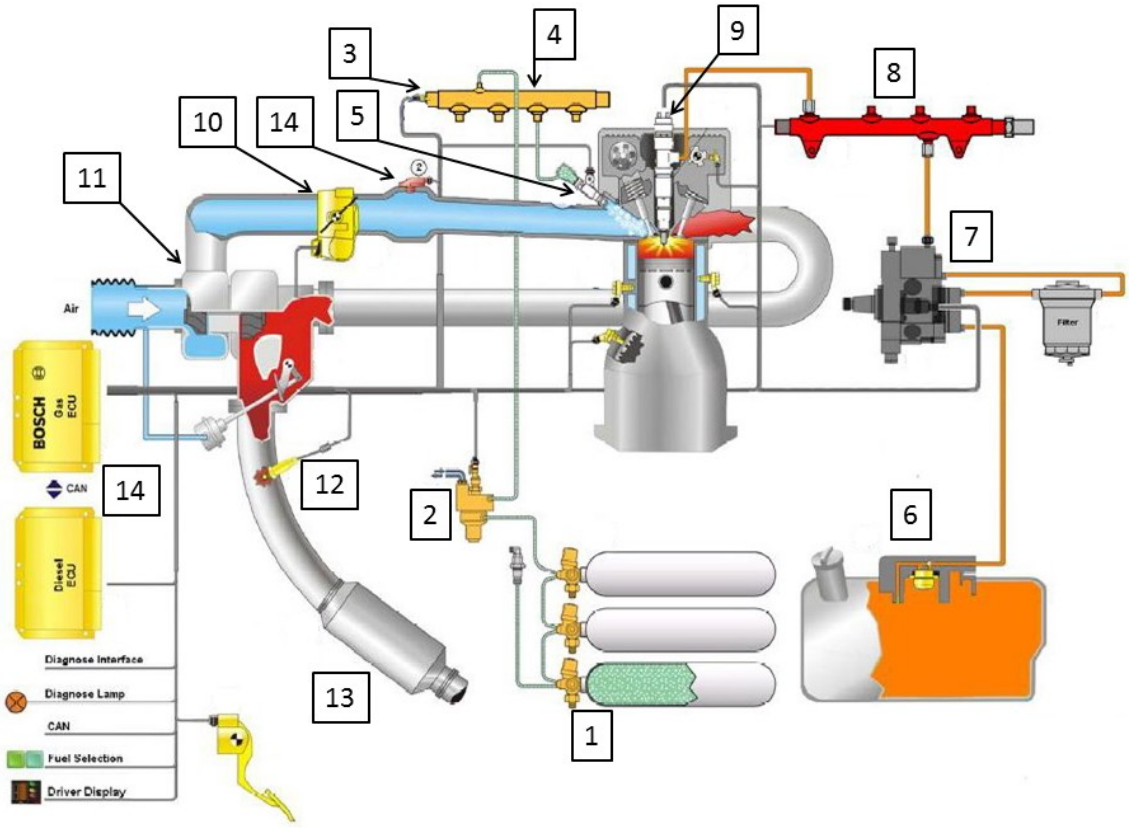

Figure 2.6. A typical dual-fuel system. Components: 1) CNG tanks, 2) pressure regulator, 3) gas pressure and temperature sensor, 4) NG rail, 5) NG injector, 6) Diesel tank, 7) Diesel HP pump, 8) Diesel common rail, 9) Diesel injector, 10) throttle valve, 11) turbocharger, 12) oxygen sensor, 13) oxidation catalyst, 14) electronic control units. [35]

The fuel gas may be introduced to the inlet air stream before the compressor, in the inlet manifold, inlet ports individually for each cylinder or directly injected in the cylinders with high-pressure direct injection (HPDI) of NG. The latter is difficult to implement and rarely used in retrofitted systems. A comparison of gas admission strategies is presented in Table 2.5. Fuel gas feed at the compressor inlet is easiest to install as it requires no changes to the inlet manifold or the cylinder head. On the contrary, the manifold or port-injected type requires injector mounting points in the inlet manifold or in the cylinder head. If the gas is directly injected in the cylinder, a special injector must be used and a mounting point in the cylinder head is required. In addition, an additional compressor is needed for pressurising the fuel gas to adequate injection pressure. [36][37]

If accurate mixture control is desired, natural gas feed at the compressor inlet cannot be considered. If the gas feed is located far away from the cylinders, some fuel may linger in the inlet pipes between cycles which contributes to the cyclic variation. Instead, each cylinder must be equipped with an individual gas admission valve or injector in the cylinder head or in the inlet manifold. In addition, the gas admission duration may be timed to occur only when the exhaust valve is closed during the inlet stroke. This reduces the methane slip directly from the inlet to the exhaust. [7][22]

Table 2.5. Comparison of different methane admission methods. [22][37][38]

	Gas admission method		
	At compressor inlet	**Manifold/port injected**	**HPDI**
Gas feed pressure	Below atmospheric	1…10 bar relative	Up to 300 bar
NG mixture formation	Premixed	Premixed	Non-Premixed/Stratified
Gas admission type	Gas admission valve	LP injectors/Gas valve	HP injector/Dual injector
Fuel amount control per cycle	Challenging	Accurate	Very Accurate

Methane emissions in the exhaust gas are rather difficult to remove with after-treatment methods and it may be necessary to update the emissions system in order to effectively reduce methane emissions. In addition, natural gas use may significantly decrease the Diesel oxidation catalyst (DOC) lifetime due to thermal and chemical interactions with the catalyst material. This is further discussed in the next chapter. Furthermore, unburned methane emissions especially in case of several consecutive misfires may gather in the exhaust pipe and cause an explosion. Therefore the exhaust pipe must be designed so that it prevents the build-up of flammable gas in the pipe. [10]

In order to operate on high Diesel substitution rates (> 80 %), the compression ratio of the standard Diesel engine may have to be reduced. The compression ratio is a compromise between the reliable ignitability of the Diesel fuel and stable combustion of the lean natural gas charge. Furthermore, a robust cold start must be achieved. The optimal compression ratio is suspected to lie slightly below that of a Diesel engine with similar output. However, decreasing the compression ratio has an adverse effect on the Diesel operation efficiency and hence this measure is a step toward a more dedicated DF engine. Another modification needed for high substitution rate operation is the air flow control with a throttle valve in the inlet pipe. This allows the accurate control of the gas-air AFR. [7]

The combustion chamber crevices need to be minimized in order to effectively reduce the engine-out HC emissions. The most critical dead volume contributing to the emissions appears to be the clearance between the piston top and the cylinder liner [22]. The volume can be decreased by moving the upper compression ring upwards. The highest position of the ring is limited by the temperature at which the burning lubrication oil deposits on the piston ring. If the ring is moved upwards, more efficient cooling of the ring groove or reduced heat load may have to be implemented. [7]

The standard Diesel injector may be used in most dual-fuel applications. However, with very low Diesel injection amounts a special injector with a pilot injection may be used in order to ensure stable ignition. Also natural gas HPDI requires special injectors. [37]

When optimizing DF engines beyond conventional limits, advanced control systems must be adopted. In addition to methane injection timing, the pressure may have to be varied. This would allow more degrees of freedom for methane injection timing control [38]. Furthermore, advanced lambda and load control methods have potential to substantially

improve throttled DF efficiency [7]. These methods include skip firing that is used in marine engines or cylinder deactivation currently in use in some modern gasoline engines [22].

2.2.2 Dual-Fuel Emissions After-Treatment

The emissions of internal combustion engines can be divided into local and global emissions. Local emissions are problematic in tightly populated urban areas where they affect human health when inhaled and may increase the probability of respiratory diseases and even shorten life expectancy. Global emissions, in turn, do not have direct effect on human health but are suspected to contribute to the global climate warming or deterioration of the ozone layer. Local emissions are categorized into unburned hydrocarbons (HC), carbon monoxide (CO), nitrogen oxides (NO_x) and particulate matter (PM). Common global tailpipe emissions are carbon dioxide (CO_2) and methane (CH_4). Methane is also measured as HC but the negative effects are global rather than local and it is often separated from other HC emissions. [39][40]

The tailpipe emissions can be reduced either by improving the engine-out emissions or by after-treatment of the exhaust gases. Usually, both methods coexist in order to reach the emission standards. By substituting Diesel with natural gas, substantial reduction in NO_x and PM emissions can be reached. In addition, CO_2 emissions may be reduced up to 25 %. However, this comes with a cost of increased HC and CO emissions. The HC in DF engines is mainly CH_4. [10][39]

The stability of the simple CH_4 molecule is often beneficial in internal combustion engines but also makes it difficult to oxidize in catalytic converters. The light-off temperature at which methane begins to oxidize in an oxidation catalyst is very high at above 300 °C and the conversion efficiency remains poor until about 450 °C. A comparison of HC and CO conversion efficiencies are presented in Figure 2.7. Even at very high temperatures the conversion efficiency of CH_4 may linger under 100%. [10]

The high temperature needed to oxidize methane is problematic due to two reasons: On one hand it is difficult to maintain high enough temperatures in the exhaust gas in turbocharged engines after the turbine. On the other hand, the high temperature results in shorter lifespan due to thermal ageing of the catalyst coating. The thermal ageing is a phenomenon where the catalyst metal coating is either alloyed with the matrix material or the reactive molecules are sintered together into lumps. Both phenomena result in decreased reactive surface area and thus reduced conversion efficiency. Interestingly only the conversion efficiency of methane seems to be vulnerable to thermal ageing. [10]

Moreover, oxidations catalysts are prone to the so called chemical ageing. The effect on methane conversion efficiency is similar to that of thermal ageing but the cause is fouling molecules contained in the fuel and burning lubrication oil. Chemical ageing reduces the active surface area of the catalytic coating via two mechanisms: Catalyst fouling is a consequence of carbon and zinc (Zn) deposits that block the pores in the catalyst washcoat. This mechanism is non-selective as it does not form chemical bonds with the precious metals in the catalyst. Catalyst poisoning is a selective ageing mechanism where certain compounds chemically attach to the precious metal particulates in the washcoat. Contaminants found in chemically aged catalyst include phosphorus (P), calcium (Ca)

and magnesium (Mg). The ageing mechanisms of gas engine catalysts are depicted in Figure 2.8. [10]

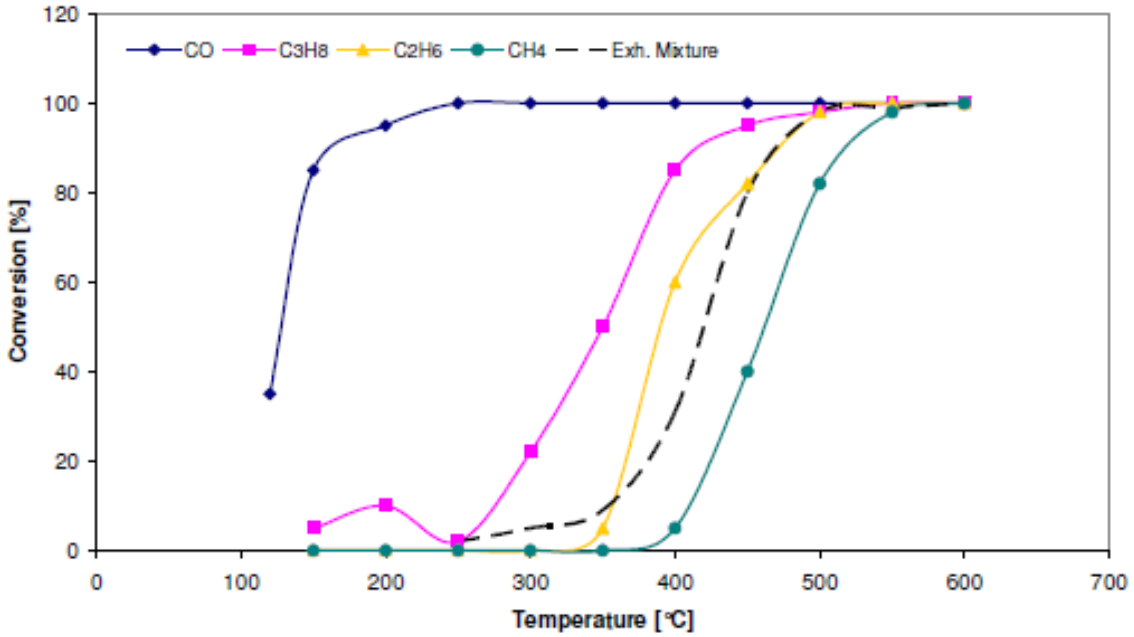

Figure 2.7. Oxidation catalyst conversion efficiencies of different carbon molecules as a function of temperature. [10]

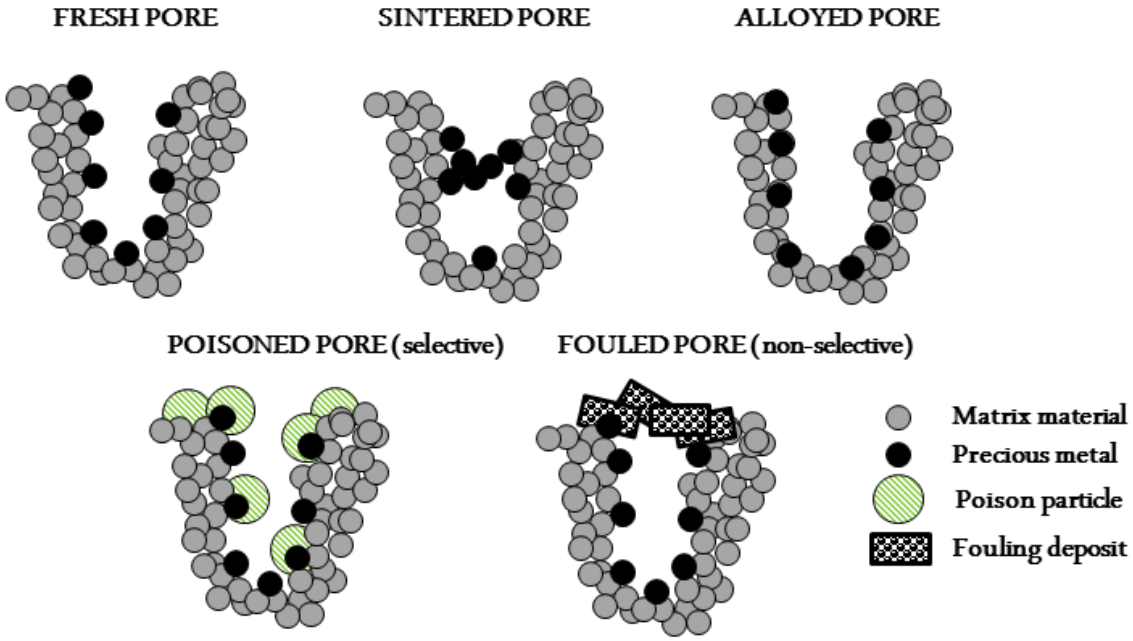

Figure 2.8. Different ageing mechanisms of gas engine catalysts. [10]

The oxidation catalyst can be optimized for methane operation for increased lifespan and conversion efficiency. Natural gas vehicle (NGV) converters have increased washcoat thermal stability which may be achieved e.g. with increased ZrO2 content and modified precious metal composition. [10]

Due to the good mixing of the gaseous methane, PM formation is low and is not considered a problem at present with high substitution rates. Future legislation may, however, require the use of a Diesel particulate filter (DPF) in order to meet the tightening demands. On the other hand, if fuel flexibility is desired, it might be necessary to install a Diesel particulate filter (DPF) in the exhaust line. [7]

NO_x emissions in DF engines are generally significantly lower than in Diesel engines of comparable output. Selective catalyst reaction (SCR) is used in Diesel engines in order to lower the NO_x emissions by injecting urea (CH_4N_2O) into the exhaust stream. The lower NO_x-concentrations of DF engines may enable running the engine without an SCR converter while maintaining low NO_x. [8][41]

2.2.3 Current Problems in Dual-Fuel Engines

As promising as the DF engine may seem in various applications, there are still several obstacles that hinder the widespread adoption of the technology. Excellent combustion control is required in order to meet the future emissions regulations, low specific fuel consumption and high specific power. The main problems in current DF engines are [7], [42]:

- Occurrence of pre-ignition and knock
- CH4 emissions
- Low load combustion control
- Cycle-to-cycle variation

In addition, some lesser and less common problems exist. These are for example [7][43]:

- Thermal issues and injector nozzle coking
- Valve seat wear

Possibly the greatest problem in DF engines regarding the combustion control is the occurrence of knock and preignition and the resulting rapid pressure rise rate. The cylinder pressure curves of a preignited combustion cycle and knocking combustion cycle in a spark-ignited engine are shown in Figure 2.9. Preignition is generally more dominant of these phenomena in DF engines but both knock and preignition often coexist. As the term implies, preignition causes the bulk mixture of premixed gas to ignite before the Diesel spray when the mixture temperature and pressure exceed the autoignition tolerance of the mixture. This results in a high pressure peak on either side of the top dead centre. Pre-ignition may further lead to knocking combustion. [7]

Knock is a phenomenon where the end gas of the bulk mixture is compressed and heated to the auto-ignition temperature due to relatively slow flame front propagation. The end gas ignites spontaneously in a remote location before the flame front arrives. The combusting end gas sends forth a pressure wave across the cylinder volume which reflects back and forth at a high frequency and causes the specific ringing noise of knocking combustion. The superimposing high-pressure waves increase the surface temperatures of the components in the combustion chamber which may result in material creep and failure. [40][44]

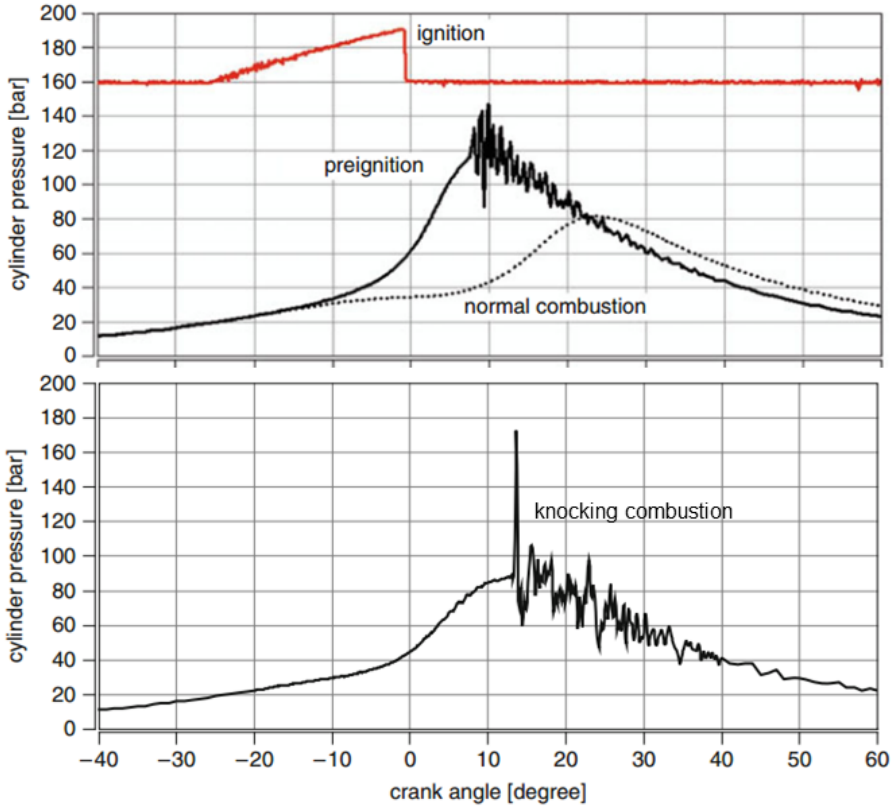

Figure 2.9. Above: preignited combustion and a normal cylinder pressure curve in a spark-ignited engine. Below: a knocking combustion pressure curve. [40]

There are several root causes that may lead to preignitions and knock [7][40]:

- Lubrication oil ignition
- Hot spot ignition
- Ignition from glowing carbon deposits
- Ignition from hot soot
- Ignition from residual exhaust gases
- Low-speed preignition
- Diesel injector leakage or dribble

In spark-ignited engines knock and rapid cylinder pressure rise may be controlled by retarding the ignition timing. The same principle may be used in dual-fuel engines by retarding the Diesel injection timing. However, pre-ignitions can become self-sustaining and accelerating and occur completely independent of the Diesel injection. In such a situation, the only option is to quickly reduce the cylinder load. Knock on the other hand, can be countered by increasing the in-cylinder turbulence as the flame front propagation increases and the end gas has less time to reach the autoignition temperature before the flame front arrives. [7]

Another significant problem in DF engines is the AFR or lambda control at part-load operation. The lambda ratio may be controlled by throttling the engine, which enriches the mixture and promotes efficient combustion while the pumping losses tend to increase. The control of the cyclic variation and HC emissions with combustion lambda conflict with the needs of efficient part-load operation. On one hand it is desired to maintain a

lean mixture in order to minimize the pumping losses but on the other hand, a lean mixture causes combustion instability and flame quenching resulting in high HC emissions. The lean operation window may be further widened by increasing the in-cylinder air motion. [7]

Variations in the cylinder pressure and heat release rate are a common problem in DF engines with high Diesel substitution rates. The pressure variation results in output torque fluctuation. This cycle-to-cycle variation generally originates from the non-uniform mixture formation of the port-injected methane and air. Cycle-to-cycle variation generally increases as the substitution rate is increased. It is essential that the amount of CH_4 in the inlet channels between cycles is minimized. Optimally all fuel injected during and prior to the inlet stroke is inducted into the cylinder [11]. Some cycle-to-cycle variation is believed to originate from the variation of Diesel injection dispersion and the resulting variation in ignition stability. This phenomenon is pronounced with smaller Diesel injection amounts [42].

A possible mechanical problem in gas-powered engines is excessive exhaust valve seat wear. The valve seat wear is mainly caused by mechanical adhesion and abrasion [45]. It is probable that the lack of oxidation of the seat material surface contributes to the wear rate. An iron and chromium oxide film forming on the valve and seat surfaces appears to be the key inhibitor of wear. Absence of this film has been recorded in gas engines, although the problem is mainly occurring in spark-ignited gas engines. As a solution to the valve seat wear problem new seat and valve materials have been developed. These materials promote the formation of the protective oxide film on material surfaces. The new alloys often contain high levels of nickel (Ni) and molybdenum (Mo). [43][46].

In a conventional Diesel engine, the Diesel injector nozzle tip is cooled by the fuel flow through the injector. As the total Diesel flow is much lower in a DF engine even at high loads, the nozzle operating temperature rises. This results in problems with nozzle coking. Namely, deposits build up in the injector holes and disturb the Diesel spray. The deposits contain mainly carbon, zinc, oxygen and calcium. Nozzle coking further leads to deterioration of the combustion quality and even misfire. Nozzle coking may be reduced by increasing the heat dissipation from the nozzle to the cylinder head with different materials. A copper sleeve for the injector, for example, efficiently dissipates heat away from the nozzle. [7]

2.3 Dual-Fuel Engine Emission Formation and Causes

2.3.1 Nitrogen Oxides

Nitrogen oxides (NO_x), namely nitrous oxide (NO) and nitrogen dioxide (NO_2), favour the formation of ozone (O_3) and have the tendency to form photochemical smog. Ozone emissions are, paradoxically, responsible for destroying the stratospheric ozone layer. Furthermore, nitrogen oxides contribute to the formation of nitric acid and acid rains and may cause respiratory health issues. [40]

Four NO formation mechanisms can be identified [44]:

1) Thermal NO
2) Prompt NO
3) NO originating from the fuel nitrogen
4) NO from N_2O

The third formation mechanism may be ignored as there is no significant amount of nitrogen present in the fuel used in DF engines.

Thermal NO is formed in the hot exhaust gases after the flame front has passed and the temperature and pressure continue to rise in the combustion chamber. This type of NO is formed by the Zeldovich mechanism. The Zeldovich mechanism, later extended by Lavoie, comprises three reversible reactions: [44]

$$O + N_2 \overset{k_1}{\leftrightarrow} NO + N \tag{2}$$

$$N + O_2 \overset{k_2}{\leftrightarrow} NO + O \tag{3}$$

$$N + OH \overset{k_3}{\leftrightarrow} NO + H \tag{4}$$

Where k_i is the experimentally determined speed constant for each reaction.

While the instantaneous NO concentration is below the equilibrium concentration at the corresponding temperature, the left side reactions of the equilibriums dominate and the concentration of NO increases. The NO concentration may momentarily increase above the equilibrium concentration so that the reverse reactions govern. However, the reverse reactions are more likely to occur at the end of the expansion stroke when the temperature is significantly lower and thus the reaction speed is slow. Because thermal NO is formed in very high temperatures which are available for very short durations during the combustion process, the equilibrium is not reached before the reactions freeze. [40]

The first reaction of the Zeldovich mechanism requires high activation energy in order to break the bonds of the stable N_2 molecule. This reaction is very temperature dependent and the rate (constant k_1) increases exponentially as the temperature increases. Reactions (3) and (4) progress several orders of magnitude faster than the first one. The disintegration of molecular nitrogen in reaction (2) is therefore the rate-limiting step in the formation of NO. [40]

Prompt NO is formed in the narrow propagating flame front. The formation of prompt NO is dependent on the formation of the CH radical that can take part in several different reactions. For this reason, the formation of prompt NO is much more complicated than that of thermal NO. Prompt NO formation requires substantially less energy than the thermal NO and thus the reaction progresses already at relatively low temperatures of approximately 1000 K. There are many theories concerning the formation of prompt NO but the exact formation path is not known. [44]

The NO formation via N_2O is only significant when the formation of thermal NO is stifled due to low temperatures and if the CH radical is repressed due to a diluted mixture. The N_2O molecule is produced in a similar reaction as (2) and is further oxidized into two NO molecules. N_2O is particularly present in lean burn exhaust gases. [40]

NO_2 is formed via three different reactions [44]:

$$NO + HO_2 \leftrightarrow NO_2 + OH \quad (5)$$

$$NO + OH \leftrightarrow NO_2 + H \quad (6)$$

$$NO + O_2 \leftrightarrow NO_2 + O \quad (7)$$

The primary formation method is (5) at relatively low flame temperatures when high concentrations of HO_2 is present. There is generally significantly lower concentration of NO_2 than NO emissions present in the exhaust gases [19]. However, in lean operated gas engines much higher NO_2 emissions have been recorded [8]. One explanation for this could be the increased activity of reaction (7) at low temperatures whereas the reverse reaction is suppressed due to poor mixing and slow combustion [47].

The ignition of CH_4 is a 24-step process and some of the reactions contribute to the formation of intermediate products needed for the formation of NO_2. This may contribute to the NO_2 formation. For example the first step of the ignition can be written as follows [48]:

$$CH_4 + O_2 \leftrightarrow HO_2 + CH_3 \quad (8)$$

Reaction (8) shows how the HO_2 radical is formed as an intermediate oxidation product of CH_4.

Dual-fuel operation generally reduces the NO_x emissions compared with a similar Diesel engine. One reason for the reduced NO_x emissions is the lower peak in-cylinder temperature and pressure caused by the premixed Diesel combustion. Another reason is the reduced oxygen concentration in the mixture due to the presence of gaseous fuel. [8][41]

2.3.2 Unburned Hydrocarbons

Unburned hydrocarbons are a consequence of incomplete combustion. HC emissions in gasoline-powered engines can be categorized into four categories: paraffins, olefins, acetylene and aromatics. All these components have different reactivity and tendency to form photochemical smog and effect on human health [44]. However, as the fuel used in DF engines is mostly CH_4, it is more convenient to use a simpler categorization of HC emissions into methane and non-methane hydrocarbons (NMHC). CH_4 emissions in gas engines are also termed the methane slip. Some of the other categories may exist as products from the burning lubrication oil and Diesel but these usually exist in insignificant concentrations [22].

The HC formation in DF combustion resembles that of spark-ignited Otto-cycle engines. At least six formation mechanisms are listed in literature [22][40][44]:

1) Flame quenching at the combustion chamber walls.
2) Combustion chamber crevices, top-land volume and carbon deposits
3) Absorption of fuel vapour into the oil film covering the cylinder walls
4) Flame bulk quenching, incomplete combustion or complete misfire.
5) Slip of fresh mixture to the exhaust during in the beginning of the inlet stroke.

The cold cylinder and combustion chamber walls form a thin boundary layer in the vicinity of the surface. As the flame reaches this boundary layer it quenches and some of the mixture is left unburned. However, most of the unburned HC in the quench layer diffuse and oxidize rapidly promoted by the in-cylinder gas motion. Deposit build-ups and rough surfaces increase the methane slip originating from flame quenching. [44]

The HC particulates that enter the crevices or so called dead volumes form a major part of the HC emissions. As the cylinder pressure rises, some of the unburned mixture escapes into crevices where the flame cannot penetrate. The amount of mixture in the crevices may account for up to 10 % of the total charge. Most of this mixture is released back into the combustion chamber and oxidized as the pressure decreases and the piston moves downwards. However, a substantial part of the gas trapped in the crevices is released later in the exhaust stroke when the temperature is too low for oxidizing the hydrocarbons. The volume formed by the clearance of the piston and the liner is the largest single crevice that promotes the HC formation. This formation method is illustrated in Figure 2.10. Other crevices contributing to the HC emissions are the volume between the cylinder head and the gasket and the small volumes in the vicinity of the valves and the injector. [22][44]

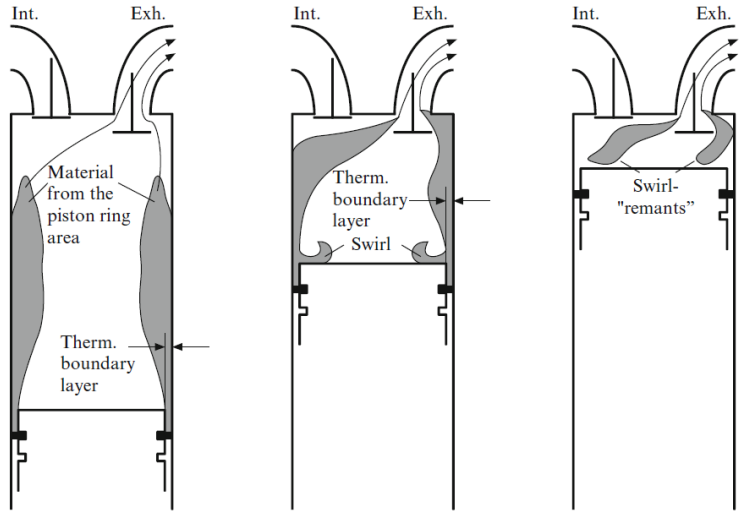

Figure 2.10. The formation of HC emissions originating from the volume between the piston and the cylinder liner. [40]

During the inlet and compression strokes any oil film present on the cylinder walls absorb fuel in the mixture. The absorption further increases with increasing pressure during the late compression stroke even beyond saturation. As the bulk mixture burns, the concentration of the fuel in the mixture decreases and the fuel absorbed in the oil is desorbed into the gaseous combustion products. Some of this desorbed fuel is oxidized but some are seen as increased HC emissions in the exhaust stream. The significance of this HC formation mechanism depends on the solubility of the fuel in the oil. [40]

Flame bulk quenching or extinction is a result of poor combustion quality of a lean mixture. As the temperature and cylinder pressure decrease during the expansion stroke, also the burning rate decreases and if this fall is very rapid, the flame extinguishes and unburned fuel is left in the cylinder. Moreover, an excessively lean mixture or a weak ignition source may cause a complete misfire. The remaining fuel from partial and complete misfires translates directly into HC emissions. Bulk quenching and misfires are

more likely to occur at idle and at light load operation with lean mixtures or mixtures diluted by EGR. [22]

Finally, a substantial methane slip source may be identified as fresh mixture literally slipping from the inlet port to the exhaust during the valve overlap period if the charge air pressure exceeds the pressure in the exhaust port. The HC emissions originating from the fresh charge slip may be rather easily avoided if the gas is admitted into the inlet only when the exhaust valve is fully closed. However, the gas valve or injector must be located close to the inlet valve so that the fuel in the inlet ports between cycles is minimised. Any gas remaining in the inlet ports will increase the methane slip during the subsequent stroke. [22]

A small amount of DF hydrocarbon emissions originate from the Diesel fuel. The Diesel HC formation methods may be divided into overleaning and undermixing. Overleaning occurs when the Diesel spray is mixed leaner than the combustion limit during the ignition delay. Undermixing, in turn, may exist in those parts of the Diesel spray that leave the nozzle at low velocity late in the combustion process. This leads to locally rich regions in the mixture [40]. Nonetheless, the HC emissions originating from the Diesel fuel are considered insignificant in comparison with the methane emissions and are not a concern in DF engines [7].

Lean operation promotes the first four mechanisms of the methane slip. In the diluted charge the cylinder wall quench layer will increase in thickness as the temperature in the bulk gas decreases. Furthermore, lower temperature results in reduced oxidation rate of the fuel desorbing and diffusing into the bulk gas from the boundary layers and crevices. On the contrary, a larger Diesel fuel amount extends the lean limit resulting in lower HC emissions at lean operation. [7]

2.3.3 Carbon Monoxide

Carbon monoxide (CO) is an intermediate product in hydrocarbon oxidation. CO emissions are produced in fuel-rich conditions when the oxygen supply is limited. Therefore CO emissions are traditionally seen significant only in spark-ignited engines which operate close to stoichiometric at part load and fuel-rich at full load. Diesel engines operate on lean mixtures and the formation of CO is often insignificant. However, the dual-fuel engine may produce substantial amounts of CO even with lean mixtures. [41]

CO is always a product of incomplete combustion. This may be a result of the lack of oxygen in the vicinity of the flame or low local temperatures. CO formation is a part of the hydrocarbon combustion reaction and can be summarized as follows: [44]

$$RH \rightarrow R \rightarrow RO_2 \rightarrow RCHO \rightarrow RCO \rightarrow CO \tag{9}$$

Where R is a hydrocarbon radical.

The oxidation reactions of CO to CO_2 are written as follows: [40, 44]

$$CO + OH \leftrightarrow CO_2 + H \tag{10}$$

$$CO + HO_2 \leftrightarrow CO_2 + OH \tag{11}$$

Reaction (10) is the dominant one of the oxidation reactions. Reaction (11) mainly occurs during auto-ignition due to the high concentration of HO_2. Reaction (10) is dependent on the concentration of OH radicals. However, as the reaction rate between OH and hydrocarbons is considerably higher than that of reaction (11), the oxidation of CO is often inhibited until the hydrocarbons are oxidized. [19]

CO emissions may also be produced in lean mixtures due to low temperatures and incomplete combustion near the combustion chamber walls. Reaction (11) is highly dependent on combustion temperature and thus the complete oxidation of CO is hindered in low combustion temperatures. Another source of CO emissions in lean mixtures is suspected to be the partial oxidation of unburned hydrocarbons emerging from the crevices and oil layers during the expansion and exhaust strokes. [44]

DF combustion is reported to produce significantly higher CO emissions than the conventional Diesel engine. This occurs mostly due to low combustion temperature in the lean premixed charge. However, even though CO is toxic to humans and may cause nausea and even death, these emissions are rather easily removed from the exhaust gases. As shown previously in Figure 2.1, CO oxidizes already in low temperatures when a catalytic converter is used. [8][40][41]

2.3.4 Particulate Matter

Particulate matter (PM) or soot consists of particulates that are considerably larger than single molecules [40]. PM emissions are a problem particularly in Diesel engines but also spark-ignited engines produce some amounts of PM. DF engines tend to emit substantially less PM than comparable Diesel engines. The formation of PM emissions can be roughly divided into two phases: 1) nuclei formation in the molecular zone and 2) particulate growth in the particulate zone. This is illustrated in Figure 2.11. [49]

1) The nuclei or kernels of soot particulates are formed as the polycyclic aromatic hydrocarbons (PAHs) or polyacetylene molecules from fuel molecule pyrolysis collide and attach to each other via van der Waals forces. The formed soot nuclei in this manner have a diameter of approximately 1…2 nm. The nuclei make only a small contribution to the total soot volume and mass due to their small size but they have an indisputable effect on the total soot formation. [44]

2) The main part of PM emissions volume and mass is formed during the particulate growth phase. Three particulate growth methods have been distinguished. Surface growth occurs between the gaseous components which adhere to the particulate surface resulting in larger particulates. Furthermore, particulates may grow via coagulation, i.e. the collision of two relatively small particulates merging together. Finally, larger particulates collide and attach to each other while keeping their size and shape. This is referred to as agglomeration. [44]

During the whole particulate formation and growth process, oxidation of particulates also occurs. The soot particulates are constantly oxidized into gaseous CO and CO_2 and the engine-out emissions depend on the balance between soot formation and oxidation. Further mass is added to the particulates during as they traverse through the exhaust system. This is a result of the condensation and adsorption of gaseous components on the particulate surface when the gases are diluted and cooled down. [44]

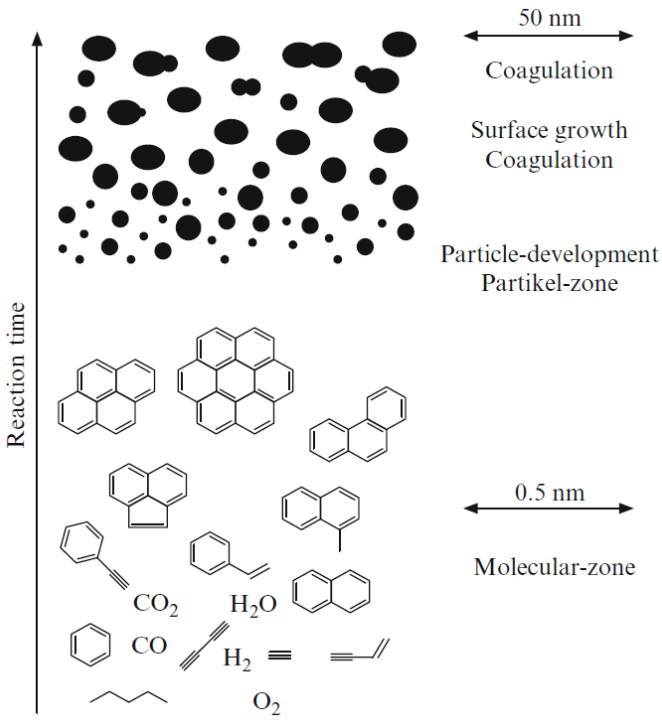

Figure 2.11. Particulate formation and growth in exhaust gases [49].

The total effect of the gas temperature on soot formation is not clear as high temperatures promote both formation (pyrolysis) and consumption (oxidation) of particulates. The critical temperature for PM processes seems to be between 1500 K and 1900 K. Outside this temperature region, the soot reactions rarely occur. [40]

The gaseous methane in dual-fuel engines effectively hinders the formation of soot. Methane is a rather small molecule belonging to the paraffin family and does not have the tendency to form soot. Another reason for the absence of soot is the exceptional mixing of the gaseous methane in the surrounding mixture. In addition, methane contributes to the oxidation of soot originating from the liquid fuel and hence the PM emissions from dual-fuel engines are rarely considered problematic. [7][8]

2.4 Variable Valve Actuation Strategies

2.4.1 Variable Valve Actuation

Variable valve actuation (VVA) is an advanced engine control technique which obliterates the restrictions created by a fixed valve timing and lift. Varied valve parameters may include lift, valve profile and opening and closing timings. VVA systems are used to improve or implement the following engine characteristics or functions [50][51][52]:

- achieve a wider powerband
- increase power and torque output
- reduce fuel consumption
- improve engine warm-up
- decrease cold start emissions

- load or lambda control without a throttle valve
- implement Miller timing
- implement internal EGR
- cylinder deactivation

VVA is mainly used in passenger car engines whereas heavy duty implementation is less common. VVA systems can be classified into camshaft based and camless systems. Camshaft based systems can be further divided into discrete and continuous. Camshaft based systems are simple and robust whereas camless systems provide more degrees of freedom to the control of the valve events. Present VVA systems in production engines are usually camshaft based systems due to costs and the simplicity of implementation on the existing valve trains. In addition to the control flexibility, VVA systems can be evaluated by their response time, power consumption, position accuracy and repeatability. [50]

There are three commonly used actuation strategies for continuously variable VVA systems: electro-hydraulically actuated (EHVA), electro-magnetically actuated (EMAVA) and electro-mechanically actuated (EMVA). However, these systems are relatively complex, costly and they require more space than less sophisticated systems. For these reasons, discrete VVA systems are often used in high-volume production engines. Discrete VVA systems provide two or more alternative valve timing and lift profiles. [52]

Some valve inlet valve control strategies are presented in Figure 2.12. Usually only the inlet valve is controlled as it provides more control over the combustion process than the exhaust valve control [53]. The simplest form of VVA is cam phasing which is illustrated on the top right side of Figure 2.12. Cam phasing changes the timing of the whole valve lobe so that both the opening and closing timing of the valve change while the lift profile is constant. The top left and the bottom left configurations are cam switching strategies which vary between different lobe profiles. This control strategy is also referred to as the variable valve event (VVE). The bottom right graph shows a variable valve lift (VVL) strategy, where the opening and closing timings are constant but the valve lift changes [51].

While the VVA systems provide undisputable benefits, there are also problems that need to be addressed. The different valve lift profiles cause variations in the gas motion flowing into the cylinder. Especially the tumble flow is sensitive to the valve lift. The degradation of gas motion may lead to poor mixing and variations in combustion quality. In addition, any variation in the system operation increases the possibility of cycle-to-cycle variation in the combustion events. [51]

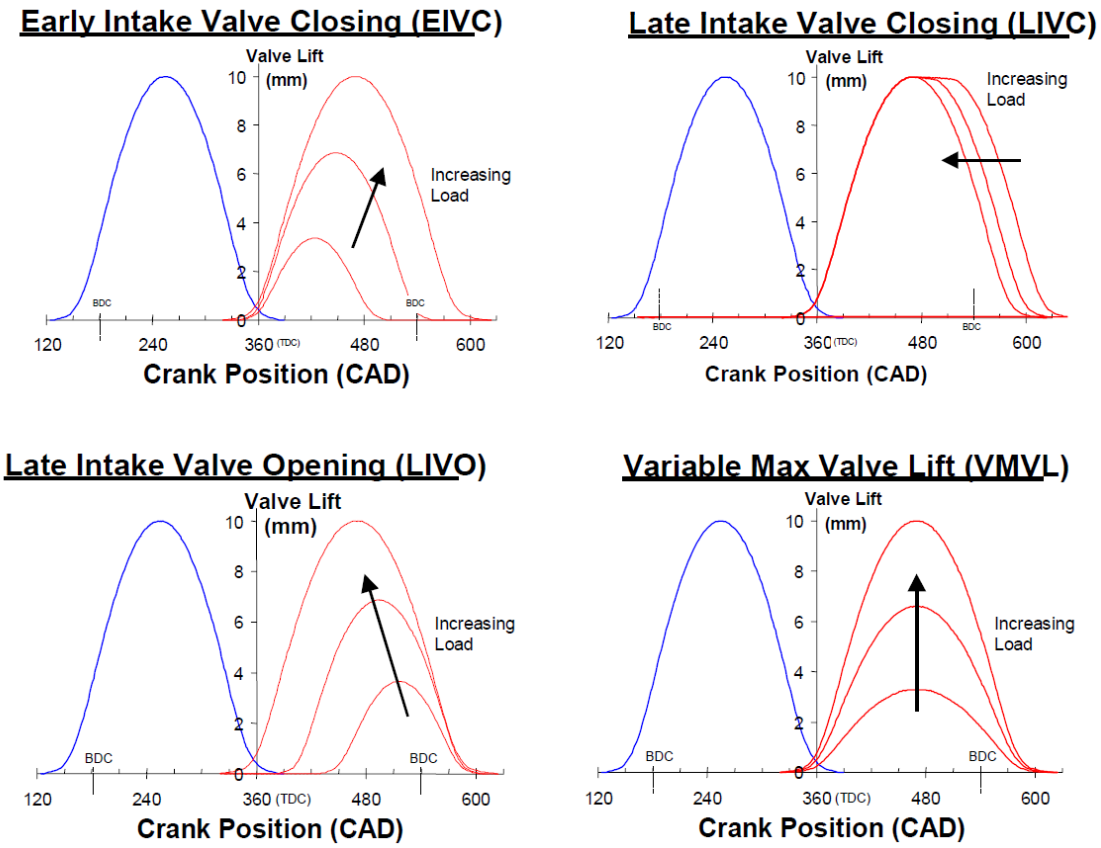

Figure 2.12. Discrete VVA strategies. Top left: VVE with fixed opening. Top right: extended inlet duration. Bottom right: VVE with fixed closing. Bottom left: VVL. [52]

2.4.2 Miller Cycle

The Miller cycle is an over-expanded engine cycle that was first presented by R. H. Miller in 1947. The goal of over-expanded cycles is to further utilize the pressure of the expanding gases beyond the conventional cycles. In addition, the Miller cycle is used to reduce pumping losses, compression work and the compression end temperature [44]. The Miller cycle is implemented by either retarding or advancing the inlet valve closing timing or by changing the effective valve lift. Advancing the closing timing is more common and applicable to heavy duty engines [5]. The valve timing strategies that were shown in Figure 2.12 can be used to implement the Miller cycle.

A pressure-volume-diagram of an over-expanded Otto-cycle is shown in Figure 2.13. The extended part of the cycle is presented as a hatched area. The gas exchange processes occur at constant pressure p_i.

The standard cycle runs as follows:

- (1) → (2): compression from p_i to p_j and from V_b to V_a
- (2) → (3): combustion from p_j to p_k at constant V_a
- (3) → (4): expansion from V_a to V_b
- (4) → (1): blowdown to p_i at constant volume V_b

The Miller cycle extends the expansion to (5) whereas the blowdown occurs from (5) to (6).

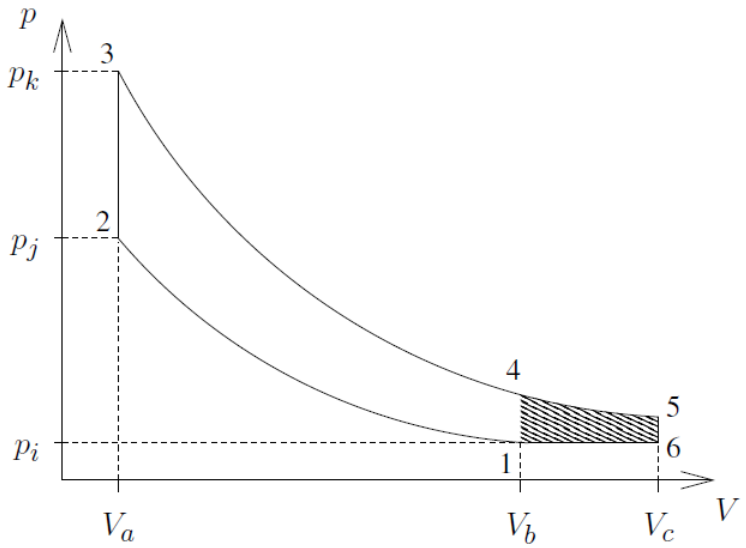

Figure 2.13. A comparison of the standard Otto-cycle and the Miller cycle pV-diagrams. [54]

The fuel conversion efficiency for an ideal constant-volume cycle may be expressed as follows [54]:

$$\eta_f = 1 - \frac{1}{r_c^{\gamma-1}} \tag{12}$$

Where r_c is the compression ratio and γ is the ratio of specific heats c_p/c_v.

Equation (12) applies to a cycle where the compression ratio is close to the expansion ratio ($r_c \approx r_e$). This indicates that the engine efficiency increases when the compression ratio (expansion ratio) is increased. However, the desired compression ratio varies as a function of load and specifically to DF engines, as a function of substitution rate. As the compression ratio is increased, the charge temperature rises which leads to rapid pressure rise and autoignition. In order to prevent this, the start of combustion must be delayed. This, in turn, leads to the reduction of the degree of constant volume combustion and nullifies the effect of the increased compression ratio on the cycle efficiency. [53]

The Miller cycle can be used to attain the efficiency increase of a high expansion ratio while keeping the compression ratio at a desired level and thus avoiding the aforementioned problems. The inlet valve closing is advanced in order to reduce the effective compression ratio while the exhaust valve opening is kept constant. This increases the expansion ratio relative to the compression ratio. The charge temperature at the end of the compression stroke is thus lower than it would be with the conventional cycle and problems with autoignition can be avoided. [53]

The use of the Miller cycle with constant charge air pressure results in reduced power density in the engine. This may be compensated by increasing the inlet pressure so that the air mass flow is equal to that of the standard cycle. Hence, the compression work done by the piston in the standard cycle can be produced by the exhaust gases in the turbocharger. Furthermore, the pre-compressed air can be cooled in a charge air cooler so that the charge air temperature is lower than it would be in the conventional cycle. [54]

The use of Miller cycle in DF engines can be seen particularly useful. A high compression ratio would result in shorter ignition delay of the Diesel pilot and thus enhance low-load operation in dual-fuel mode. Moreover, high compression ratio increases the combustion efficiency of lean CH4 mixtures. At high load, the effective compression ratio could be lowered to avoid pre-ignition and knock. [7]

2.4.3 Valve Overlap and Exhaust Valve Actuation

The exhaust gases are never fully scavenged from the engine during the exhaust stroke. In order to reduce the amount of residual gases in the cylinder from the previous cycle, the exhaust valve is generally kept open for some time after the TDC. The simultaneous open time of the inlet and exhaust valves is referred to as valve overlap. The inlet valve is usually opened well before the TDC so that the overlap period is located on either side of the TDC. In addition to reducing the residual gas fraction, overlap aids inducting the fresh charge from the inlet port provided that the inlet pressure is higher than the exhaust pressure. [40]

Valve overlap is problematic in engines where the fuel is premixed with the inlet air prior to entering the cylinder. A small part of the fresh charge may slip from the inlet to the exhaust port during the overlap period, particularly if the overlap period is long. Long overlap promotes high-speed operation as the scavenging improves but at low speed the combustion quality deteriorates and cyclic variation increases. Furthermore, HC emissions substantially increase if unburned fuel slips into the exhaust. [55]

In some cases, instead of valve overlap, negative valve overlap (NVO) is used. NVO is a valve timing strategy where the exhaust valve has been closed when the inlet valve opens. Using NVO is a strategy for avoiding the problems caused by the valve overlap. However, the residual exhaust gas fraction from the previous cycle increases with NVO as the scavenging is left incomplete. [56]

The residual gas fraction with NVO is referred to as internal exhaust gas recirculation (IEGR). IEGR in DF engines is used to dilute the mixture as well as to increase the mixture temperature. The increasing temperature reduces the ignition delay of the high-cetane fuel and improves the combustion of the gaseous methane. The improved combustion results in reduced HC and CO emissions and enhanced fuel conversion efficiency while maintaining relatively low NO_x levels. The maximum rate of IEGR in a DF engine is limited by the onset of pre-ignition and knock. Therefore, IEGR should be favoured at low loads where the HC emissions are the highest and cyclic variation is significant. [56]

3 Research System and Methods

3.1 System Overview and Measurements

3.1.1 General Overview of the Research System

The research system including the engine and the associated hardware is shown in Figure 3.1. The inlet air is pressurized in an external screw-type compressor and is led through long pipes to a flow and pressure control valve. This valve is pneumatically actuated and is PID controlled via the engine control system. The incoming air mass is measured after the control valve with a Coriolis-type flow sensor. Because the inlet piping is very long between the compressor and the engine, the compressed air is cooled down without an in-line charge cooler. Instead, a charge air heater is needed in order to simulate the losses and heat dissipation of a turbocharger. This heater is positioned just before the engine and the inlet temperature and pressure is measured after the heater. To minimize the inlet flow pulsation, a pulse absorber is installed parallel to the inlet pipe with a T-junction.

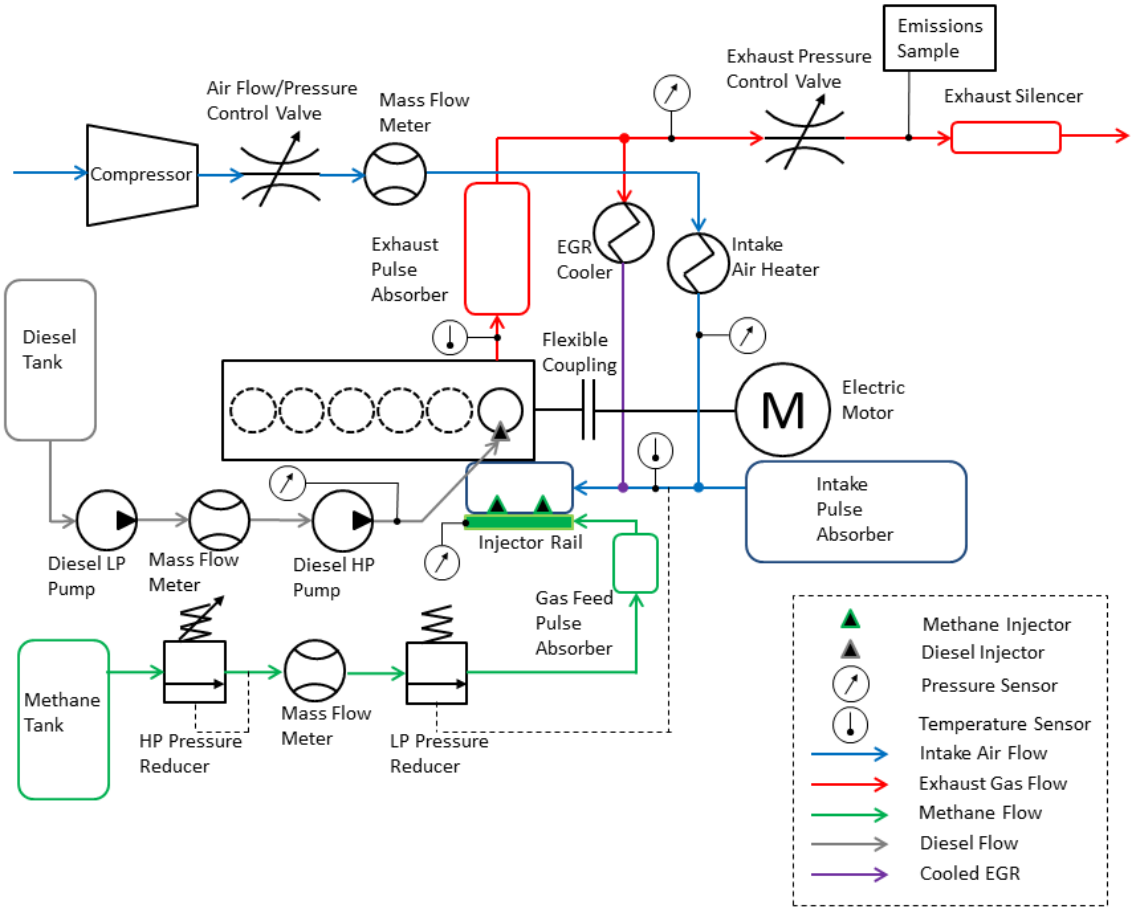

Figure 3.1. Research engine flow system overview.

The exhaust gas system consists of an exhaust manifold, pulse absorber, pressure control valve, silencer and sensors for gas pressure and temperature. The exhaust manifold is a simple straight pipe that is connected to an exhaust pulse absorber which, in turn, is connected in series with the exhaust pipe. The exhaust pressure can be varied with the pneumatically operated control valve. The valve is also PID controlled via the control

system. The exhaust silencer is installed in an upright position outside the test chamber. The exhaust system was constructed specifically for gas operation which denotes that the pipe should not run downwards but horizontally or upwards. Should the engine misfire or leak fuel gas, there is no risk that the methane, being lighter than air, forms an explosive mixture in the exhaust pipe.

The methane is fed to the engine from a high-pressure tank with a capacity of 50 litres and pressure of 200 bar. There are two pressure regulators in-line. The first one is connected directly to the methane tank to reduce the pressure to a safer level of approximately 20 bar. The other regulator is controlled by charge air pressure to maintain the gas feed pressure at constant 2.4 bar above the charge air pressure. This is important to ensure the constant mass flow of methane at different charge air pressures. In between the regulators, there is a Coriolis-type mass flow sensor. After the second pressure regulator, the methane is fed into a container for absorbing the fluctuating pulses in the gas line. Moreover, the container provides a sufficient fuel supply for the injectors so that the injection pressure does not significantly decrease during the injection period. The pulse absorber is connected to the injector rail where the methane injectors are mounted.

The research engine is installed with an exhaust gas recirculation system (EGR). The EGR system is very simple consisting of a servomotor controlled butterfly valve and an EGR cooler. The engine coolant water is circulated through the cooler as heat absorbing media. There is no additional pressure control device in the EGR-system so the exhaust gas pressure must be kept higher than the inlet pressure in order to prevent reverse flow of charge air into the exhaust. The EGR system was constructed but not used in the experiments for this thesis.

The engine is connected to an electric motor with a flexible viscoelastic coupling. The electric motor rotational speed is controlled by a frequency converter via the control system. In addition, the torque generated by the electric motor or to the motor is measured. The motor acts also as a brake to maintain the requested rotational speed when the research engine is producing torque.

The research engine is based on an off-road six cylinder direct injection Diesel engine SisuDiesel 84 CTA 4V. The standard 84 CTA 4V engine general data is presented in table 3.1.

Table 3.1. SisuDiesel 84 CTA 4V standard engine data.

Number of cylinders	6
Valves per cylinder	4
Displacement (litres)	8.4
Cylinder bore (mm)	111
Stroke (mm)	145
Compression ratio	16.5
Maximum rated charge pressure (bar)	4.5
Fuel	Diesel EN590

The engine has been modified so that only one cylinder is active. The remaining pistons and connection rods exist only for balance purposes. In addition, the camshaft has been replaced with an electro-hydraulic valve actuator (EHVA) for controlling the four poppet valves. The EHVA allows adjusting valve timing freely, the only limiting factor being the piston to valve clearance near the TDC. Moreover, high accelerations and decelerations of the valves must be avoided in order to ensure adequate precision in the valve control and proper closure of the valves.

3.1.2 Simulink Model and dSpace

Simulink is a MATLAB-integrated block diagram environment with support to an automatic code generation. Simulink provides a rather simple graphical user interface for creating complex systems with predefined and customizable block libraries. The Simulink model is the A diagram of the total engine control system is presented in Figure 3.2. The figure shows how the software and different hardware systems are connected to the real time computer (RTC). The dSpace user-interface for the Simulink model is named ControlDesk.

The dSpace system comprises a user interface for the Simulink model and a modular RTC for signal routing and processing. The system boards and connections of the RTC are presented in Table 3.2.

Table 3.2. dSpace RTC boards used in the experimental engine.

Board name	Function	Inputs	Outputs	Signal range
DS1005	Processor board	-	-	-
DS2002	Analog input	32	-	-10V…10V
DS2004	High-speed A/D	16	-	-10V…10V
DS2103	Analog output	-	32	-10V…10V
DS4002	Digital I/O and timing	24+4+8	24+4+8	TTL (0…5V)

The Simulink model used for the control of the research engine was divided into subsystems. Henceforth, larger subsystems are referred to as sections for clarity. The use of sections and subsystems simplifies the model and makes it easier to modify and test. The Simulink model uses three main sections: Input, Control System and Output. The Input and Output sections control the incoming and outgoing signals and their processing. Processing includes for example converting a voltage signal to an absolute measure. Moreover, these sections act as a link between the software and the hardware.

The actual logic of the system is contained in the Control System section. This section is divided into nine subsystems which, in turn, may contain more subsystems. For example, there is a subsystem for injection control which includes internal subsystems for Diesel injection pulses and methane injection. The Control System uses input signals as input values, processes them and outputs desired signals to the Output section.

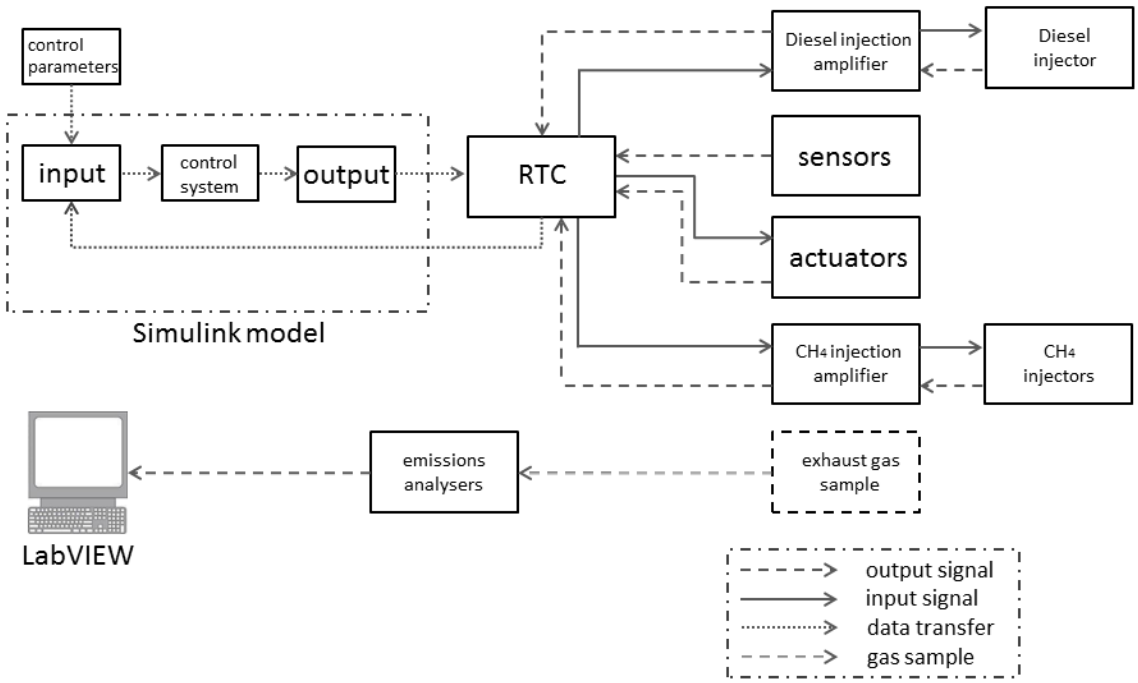

Figure 3.2. Control and measurement system overview.

Some functions needed in controlling the engine processes cannot be realized with predefined Simulink blocks. However, dSpace offers several special Simulink blocks for more complex functions for engine management. The Diesel injection timing, for example, is controlled by a mono-flop block which directly accesses one digital output channel. In addition, it is possible to code customized function blocks in C programming language. These blocks are called S-functions.

A parameter for controlling the execution time of a single simulation run is defined in Simulink as the turnaround time. The shorter the turnaround time, the more calculations are made at each time instant. Thus the measurement time resolution (more data points per time unit) increases when the turnaround time decreases. On the other hand, the disadvantage of a short turnaround time is the increased need for computational power. The lack of computational power, or rather, the heavy simulation became a problem when the methane injection control and new sensors were introduced to the system. Thus the turnaround time had to be increased in order to avoid excessive overruns.

There is also a special valve testing mode embedded in the user interface. This is used to test the correct operation of the EHVA prior to running the engine. The valve test mode is very useful when implementing new valve opening curves. Moreover, the cylinder pressure curve can be monitored on screen during the experiments. This is useful in order to avoid excessive pressure levels and high pressure rise rate.

3.1.3 Measurement Tools and Sensors

The sensors of the system can be divided into low- and high-frequency types. The cylinder pressure and crank angle measurement are of high-frequency and all the rest are of low frequency type. The read interval of the sensors is defined as 80 µs for the high-frequency and 160 µs for the low-frequency sensors. The low-frequency read interval is unnecessarily short for most sensors but it was impossible to reduce the read interval of these sensors without affecting essential parts of the Simulink model. A compromise for

smooth running and measurement frequency was adopted. The high-frequency sensors provide data at an interval of 0.72 crank angle degrees (CAD) when the engine is running at 1500 rpm.

All temperatures are measured with K-type thermocouples. The exhaust emissions are measured in a separate gas analyser. The measured gas components are O2, CO, CO2, THC, NO, NO2 and total NOx. The analyser is calibrated with precision calibration gases every day before the measurements and the emissions measurements and calibrations are done on LabView software. The mass flows are measured in Coriolis-type mass flow meters with measurement range from 0.5 to 300 kg/h.

The hydrocarbon emissions are measured in a Flame Ionisation Detector (FID) analyser. The FID analyser consists of a flame chamber where hydrogen flame is burned. The sample gas travels through a capillary pipe and is burned in the hydrogen flame. As there is no oxygen available in the flame chamber, HC in the sample form ions as they burn. The ions are then collected into an ion collector where the current across the collector is measured. The current is proportional to the rate of ionisation which, in turn, depends on the HC concentration in the sample. [57]

The NO_x emissions are measured as NO in a chemiluminescence detector (CLD). The sample is lead in a reaction chamber together with ozone O_3. NO and O3 create a chemiluminescence reaction which emits light. The photons of the emitted light are then measured in a photon multiplier tube which outputs voltage proportionally to the NO concentration in the sample. The NO_2 emissions are converted into NO and measured before entering the reaction chamber. [58]

The oxygen content measurement utilises the paramagnetic nature of oxygen gas O_2. The oxygen in introduced to a focused magnetic field. In the magnetic field, there are obstacles, for example nitrogen-filled spheres mounted on a rotating suspension, which the oxygen attempts to displace. Doing so, the oxygen gas exerts a force to the obstacles in an attempt to rotate the suspension and the spheres. This rotation is detected and countered with a current lead in the suspension, generating an opposing force. The current is directly proportional to the oxygen concentration in the sample. [59]

The carbon oxides CO and CO_2 are measured with an infrared gas analyser. The infrared measurement is based on the absorption of certain wavelengths of infrared radiation in CO and CO_2. Infrared light is led through a sample cell containing the exhaust gas and the amount of the specific wavelengths to carbon oxides is measured. The amount of absorption correlates with the CO and CO_2 concentration in the sample. [60]

3.2 Methane Feed System

3.2.1 Methane Injection

The methane feed system consists of the following components: methane tank, high-pressure regulator, mass flow meter, low-pressure regulator, gas filter, pulse absorber, injector rail and two injectors. The system was also illustrated in Figure 3.1. The gaseous fuel used in the experiments for this thesis was pure methane (>99 %).

The methane feed pressure is reduced gradually from 200 bar in the methane tank to the injection pressure of 2.4 bar. The constant-pressure type low-pressure regulator is manufactured by Keihin, Inc. The regulator is intended to be used as the primary pressure regulator but in this case the pressure was first reduced to approximately 30 bar in a reducer connected to the methane tank due to safety reasons. The Keihin regulator is equipped with connections to the engine coolant circuit in order to prevent icing.

After the Keihin pressure regulator, the methane is filtered in a high-capacity filter through which it is lead into the pulse absorber that acts as a pressure reserve in addition to absorbing the pulses generated by the injector opening. From the pulse absorber, the methane flows to the injector rail through a 16 mm diameter hose. The gas feed pressure is measured at the injector rail. The Keihin regulator adjusts the injection pressure to 2.4 bar relative to the charge air pressure.

The methane is injected to the inlet manifold with two injectors simultaneously. A 3D-model of the inlet manifold and the location of the methane injectors are shown in Figure 3.3

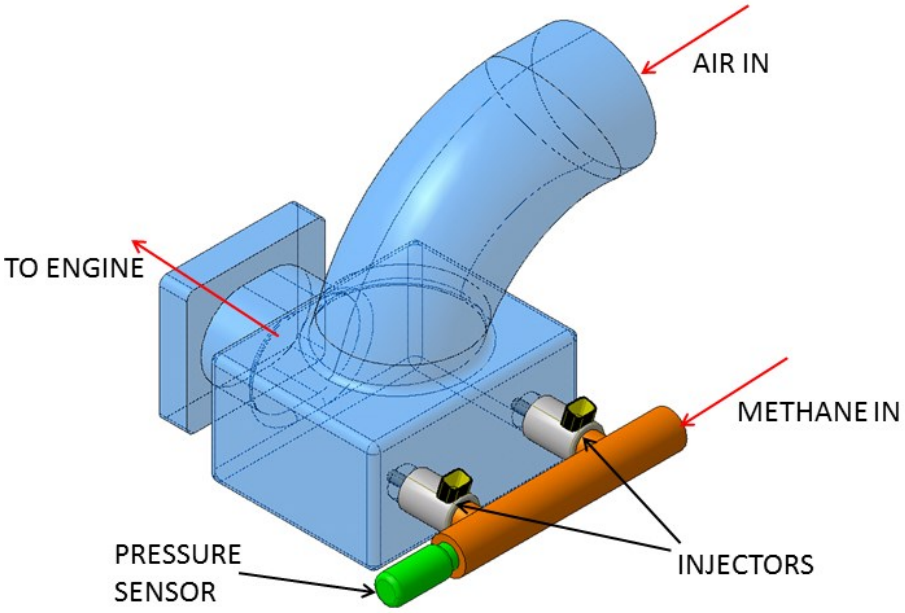

Figure 3.3. Inlet manifold and methane injection layout.

The structure of the injectors is presented in Figure 3.4. The main components of the injector are the coil, spring loaded needle and the flow tubes. As the draw current is led through the coil, the needle is drawn open by the magnetic field induced by the coil. The needle is held open as long as the hold current flows through the coil and gas is fed through the feed tubes. When the current stops, the spring closes the needle and the gas flow ceases. The injector specifications are listed in Table 3.3.

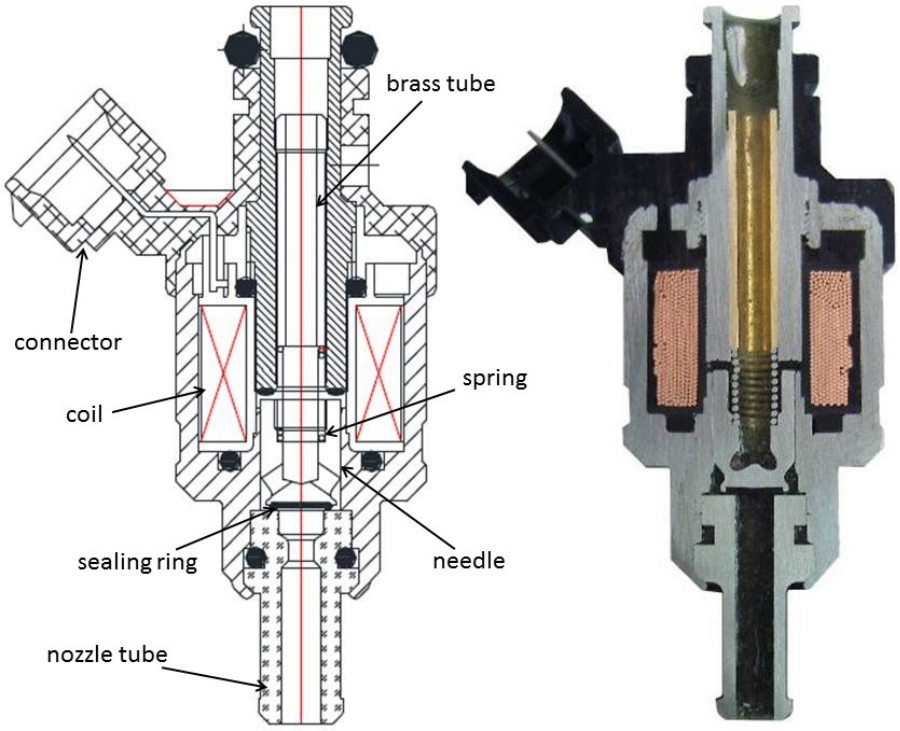

Figure 3.4. Cross-sectional views of the methane injectors. The nozzle tube inner diameter is 4,5 mm.

Table 3.3. Injector specifications.

Manufacturer	Hana Engineering, Inc
Model	H2000
Voltage	DC 12 V
Impedance	1.3 Ω
Operating Pressure	2.4 bar (relative)
Maximum Gas Pressure	5.8 bar (relative)
Flow Rate	130 l/min (at 1.2 bar)
Opening Time	2.2 ms
Closing Time	1.2 ms
Draw Current	4 A
Hold Current	2 A

3.2.2 Methane Injection Control

The methane injection signal is determined in the Simulink model in a separate subsystem. The injection duration and injection start timing can be adjusted in ControlDesk. In addition, it is possible to disable the methane injection completely. The timing is given in crank angle degrees before the top dead centre during the exhaust

stroke. The duration, in turn, is given in milliseconds. At a constant speed of 1500 rpm, one millisecond corresponds to approximately 9 °CAD. At a maximum duration of 13 ms used in this study, the methane injection lasts for approximately 117 °CAD.

The injector voltage signal sent from the dSpace real time computer is amplified in a signal amplifier. The amplifier used was an electronic control unit (ECU) of a Prins Autogas sequential vapour injection (VSI) system. The VSI ECU is normally used in bi-fuel passenger cars and it features injector control logic according to sensor data. However, as the gas injection was completely controlled in ControlDesk, these features were disabled and the VSI ECU was only used to amplify the injector signal. The complete wiring diagram of the VSI ECU is shown in Appendix 1. The temperature and pressure sensors in the wiring diagram were substituted with potentiometers with desired values in order to prevent the ECU from using any correction factors for the gas injections.

The amplifier and the injectors are supplied by a 12 volt external power source. The amplifier feeds constant 12 V voltage to one of the two injector leads in each injector. When the signal is sent from the real time computer to the amplifier, the other injector lead is grounded and current passes through the solenoid valve. The injectors need a very stable power source in order to maintain satisfactory operation. In the first test runs with the engine, it was noted, that the used power source was not capable of stable and rapid power generation for the injectors and the injector signal was distorted. The power source was replaced which solved the problem. The injector signals are presented in Figure 3.5.

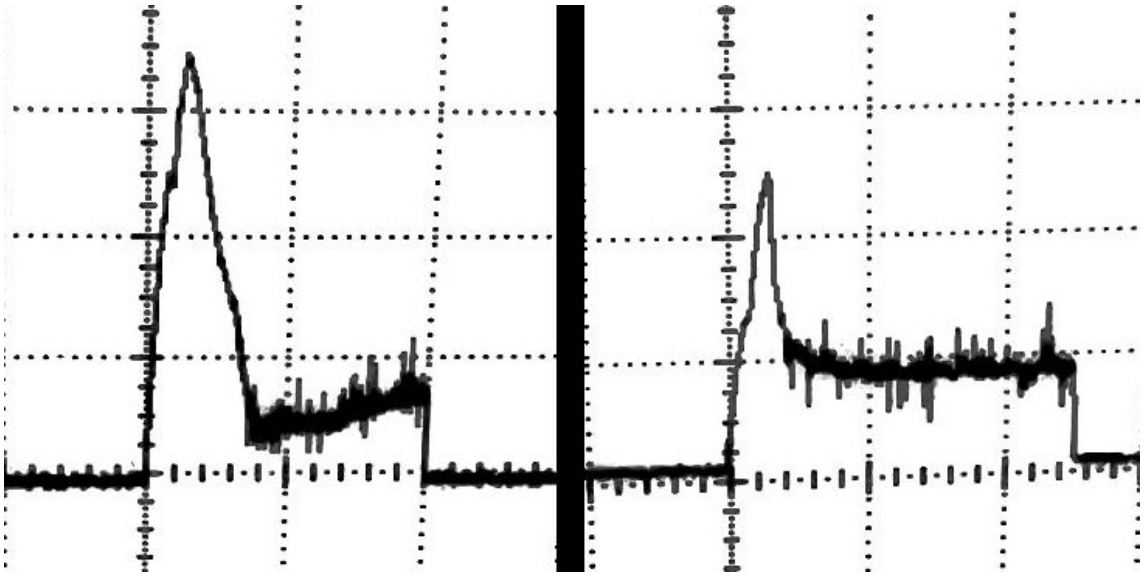

Figure 3.5. Left: 20 ms injector opening with distorted signal. Right: 25 ms injector opening with the new power source.

Insufficient current supplied to the injectors caused the solenoid valves of the injectors to close too early after the draw current dropped. This resulted in poor gas flow control. In addition, the draw current was unnecessarily high. The correct signal is shown on the right side of the figure.

3.2.3 Methane Feed Problems

The pressure pulses in the methane supply line due to injector opening resulted in varying injection pressure and high fluctuations in the mass flow readings. As the injectors opened, the pressure in the fuel rail rapidly dropped until the injectors were closed again. The combined volume in the injector rail and the hose supplying the rail was rather small and the available fuel quickly depleted.

The problem was solved with a methane container, previously referred to as the pulse absorber, on the low-pressure side of the fuel line just before the injector rail. The purpose of the pulse absorber was to reflect back the pressure pulses originating from the injectors and further to act as a methane reservoir in order to avoid fuel depletion in the injector rail. The fuel line pressures during several injection cycles with and without the pulse absorber are shown in Figure 3.6.

The graph on the left shows the methane injector rail pressure without the pulse absorber installed. The pressure in the rail decreases steeply and nearly constantly during the whole injection period. This signifies that the system cannot supply enough fuel for the injectors. The graph on the right shows the same pressure with the pulse absorber installed. The volume of the pulse absorber is roughly 4.5 litres and it is connected to the injector rail with a 16 mm hose (inner diameter). The distance from the first injector to the pulse absorber is approximately 320 mm and 400 mm from the second.

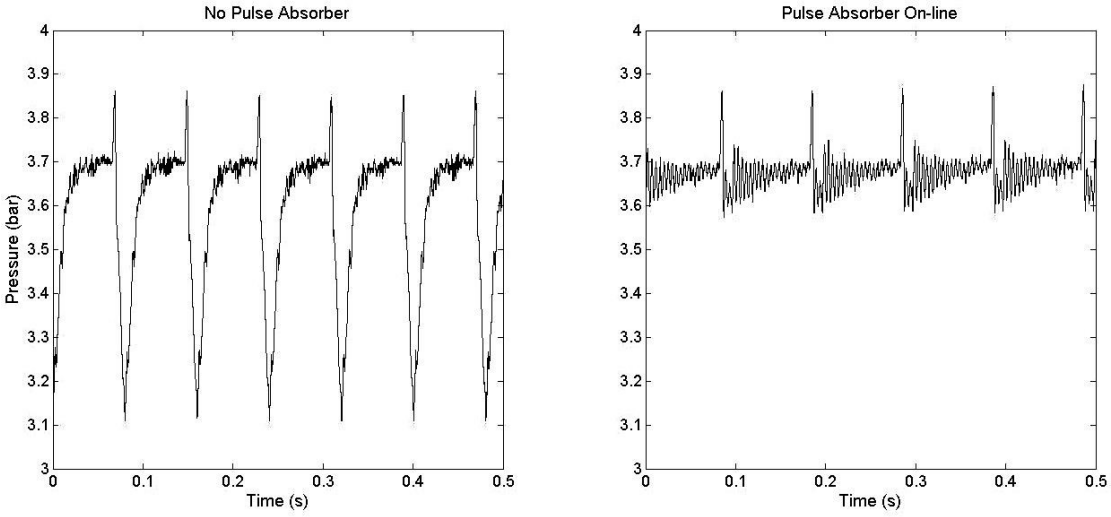

Figure 3.6. Left: Methane injector rail pressure without the pulse absorber. Right: Injector rail pressure with pulse absorber installed. The injector opening can be observed as a high peak in the pressure. Injection duration 13 ms.

In addition to stabilizing the injection pressure, the pulse absorber filtered a major part of the fluctuations in the methane mass flow readings. The mass flow meter readings at constant methane injection duration during several injection cycles with and without the pulse absorber are shown in Figure 3.7. It is probable that the pulse absorber increases the measurement accuracy of the methane mass flow as the reading is more stable.

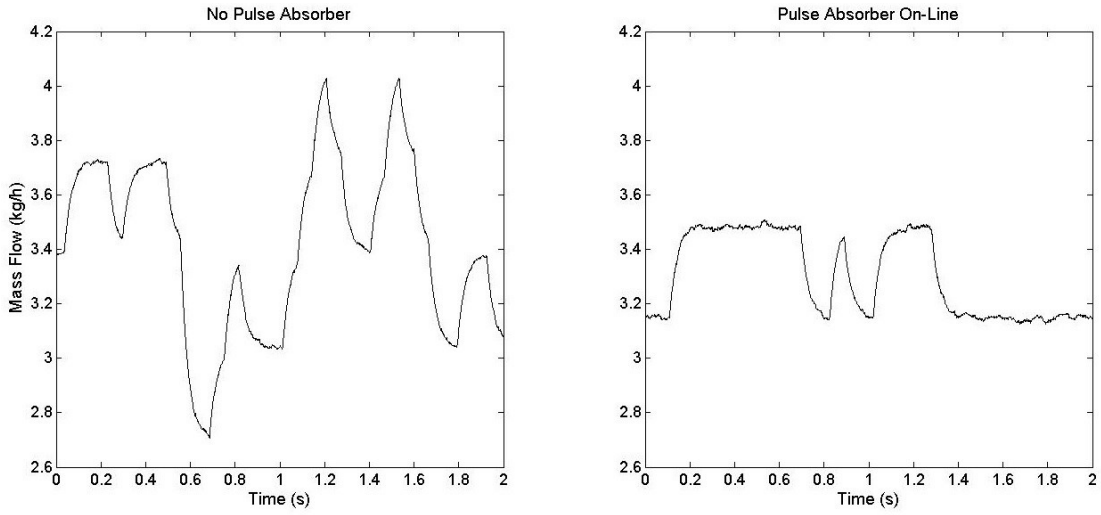

Figure 3.7. Left: Methane mass flow readings over time without the pulse absorber. Right: Similar mass flow with the absorber installed.

3.3 Research Parameters and Data Handling

3.3.1 Research Parameters and Design of Experiments

The purpose of this thesis was not to create a complete dual-fuel engine parameter mapping for all situations. Nor was the purpose to conduct extensive parameter research. Instead, the goal was to study the effects and trends in exhaust emissions and combustion phenomena relative to the substitution rate and variable valve actuation. Due to restricted time available for this thesis and in order to keep the scope of this study at a reasonable level, no simulations were carried out to find out the most interesting operating points for the study.

The experiments were divided into two phases. In the first phase one goal was to discover the Diesel injection timing that would function with different substitution rates. Another goal was to reach the upper limit of the substitution rate for the measurements while maintaining stable and safe combustion. The boundary for safe combustion was determined by the cylinder pressure rise rate limiting it to a maximum of 10 bar/°CAD. On the other hand, the stable combustion boundary was determined by the torque generated by the engine. The torque was kept at ±3 Nm from the reference Diesel engine value.

The initial operating parameters in the first phase were obtained from a comparable Diesel production engine at two load levels: 50% and 100%. The operating parameters at these load levels are listed in Tables 3.4 and 3.5, respectively. The maximum substitution rates that resulted in stable combustion were 64 E% at 50% load and 55 E% at 100% load.

One-factor-at-a-time method (OFAT) was used for all measurements. While there are disadvantages and limitations related to the OFAT method, this was seen as the best possible approach. In some cases compromises had to be made so that two parameters were changed. For example, in order to maintain the lambda constant with different valve configurations, it was necessary to increase the charge air pressure in addition to valve timing.

Table 3.4. Engine parameters at 50% load in phase 1 of the experiments.

Substitution rate (E%) →	0	29	46	54	64
Methane Injection Duration (°CAD)	-	46	52	63	69
Start of Methane Injection (°BTDC)	120				
Diesel Injection Duration (µs)	835	720	670	570	510
Diesel Injection Advance (°BTDC)	11				
Diesel Injection Pressure (MPa)	106				
Methane Injection Pressure, Relative (bar)	2.4				
Charge Air Temperature (°C)	25				
Target Charge Air Pressure (bar)	1.36				
Target Exhaust Gas Pressure (bar)	1.34				

In the second phase, the VVA was implemented. Three different substitution rates were used with associated parameters from the first phase. The substitution rates were 0 E% (Diesel reference), 46 E% and 64 E% at part load and 0 E%, 29 E% and 55 E% at full load operation. Three substitution rates, two load levels and a total of five different valve configurations signify 30 measurement points. In addition to these, some extra tests were run in order to rule out certain factors contributing to the measurement results and to support elaborate analysis.

Table 3.5. Engine parameters at 100% load in phase 1 of the experiments.

Substitution rate (E%) →	0	18	29	40	55
Methane Injection Duration (°CAD)	-	45	58	73	86
Start of Methane Injection (°BTDC)	120				
Diesel Injection Duration (µs)	2200	1500	1200	820	620
Diesel Injection Advance (°BTDC)	10				
Diesel Injection Pressure (MPa)	166				
Methane Injection Pressure, Relative (bar)	2.4				
Charge Air Temperature (°C)	34				
Target Charge Air Pressure (bar)	2.55				
Target Exhaust Gas Pressure (bar)	2.30				

3.3.2 Valve Timing Configurations

A total of five different valve actuation configurations were used, including the standard timing (STD Timing). The VVA strategies used were the Miller cycle and early exhaust valve closing (EVC). Both strategies were used with a rather conservative configuration and a more radical set-up. The VVA parameters are presented in Table 3.6. The conservative Miller and EVC strategies are referred to as M30 or Miller 30 and EVC 30, respectively. The more radical configurations, in turn, are referred to as M60 or

Miller 60 and EVC 60. Miller 60 and EVC 60 feature shorter valve openings and reduced valve lift.

As the Miller cycle is implemented, there is less time and space available for the inlet air to flow into the cylinder. In order to maintain the air-fuel-ratio constant according to the OFAT principle, it was necessary to increase the charge air pressure to a level at which the inlet air mass flow was at the same level as with the standard inlet valve timing (IVT). However, increasing the charge air pressure may increase the flow of the fresh charge from the inlet port to the exhaust during the valve overlap period.

Additional tests were carried out in order to observe the magnitude of the possible fresh charge slip during the overlap period. The 60° Miller curve was used as the reference starting point for the IVT. The reference Miller curve was retarded with two different timings both with reduced overlap. The standard Miller 60 curve was simply moved 30 and 60 degrees away from the top dead centre shortening the overlap period. In addition, tests with increased boost pressure with STD Timing were needed to further study the fresh charge slip.

Table 3.6. Valve opening and closing timings at 1 mm lift and manifold pressures at 50% load.

Valve timing configuration →	**STD**	**M30**	**M60**	**EVC 30**	**EVC 60**
Inlet valve opening (°BTDC)	6				
Inlet valve closing (°ABDC)	20	9	-15	20	
Exhaust valve opening (°BBDC)	40			32	30
Exhaust valve closing (°ATDC)	7			-7	-35
Inlet valve open duration (°CAD)	206	195	171	206	
Valve overlap duration (°CAD)	13			-1	-29
Maximum inlet valve lift (mm)	10.3	10.0	9.4	10.3	
Maximum exhaust valve lift (mm)	9.7				
Exhaust valve open duration (°CAD)	227			177	207
Target charge air pressure, 50% load (bar)	1.36	1.55	1.80	1.36	1.36
Target exhaust gas pressure, 50% load (bar)	1.34				
Target charge air pressure, 100% load (bar)	2.55	2.70	3.15	2.5	
Target exhaust gas pressure, 100% load (bar)	2.30				

The valve opening durations and the length of the overlap period can be calculated by considering a valve timing circle presented in Figure 3.8. The crank angle degrees for valve opening and closing shown in Table 3.6 are simply added to semi-circle (180 °CAD). For example with STD Timing the inlet valve opening duration becomes 6+20+180 = 206 (°CAD). The overlap period length can also be calculated in this manner but without adding the semi-circle. It is rather difficult to determine the exact valve opening because of the opening and closing ramps of the valves. Generally a constant value, for example 1 mm as in this case, of lift is used as the opening and closing boundary. Even though the flow through the valve below this limit is rather insignificant when considering the total charge flow, some of the premixed charge may already slip from the inlet channels to the exhaust during this period.

The exhaust valve timing was altered for two reasons: firstly to reduce the overlap period and secondly to implement IEGR. EVC 30 is rather conservative and its purpose was to

shorten the overlap period and to delay the blowdown of the exhaust gases. On the other hand, EVC 60 is rather radical as the exhaust valve closes 35 °BTDC and thus the amount of residual gases in the cylinder at the start of the inlet stroke is substantial. The overlap period is negative in both EVC strategies if the 1 mm boundary is considered. However, the ramps may still introduce some valve overlap.

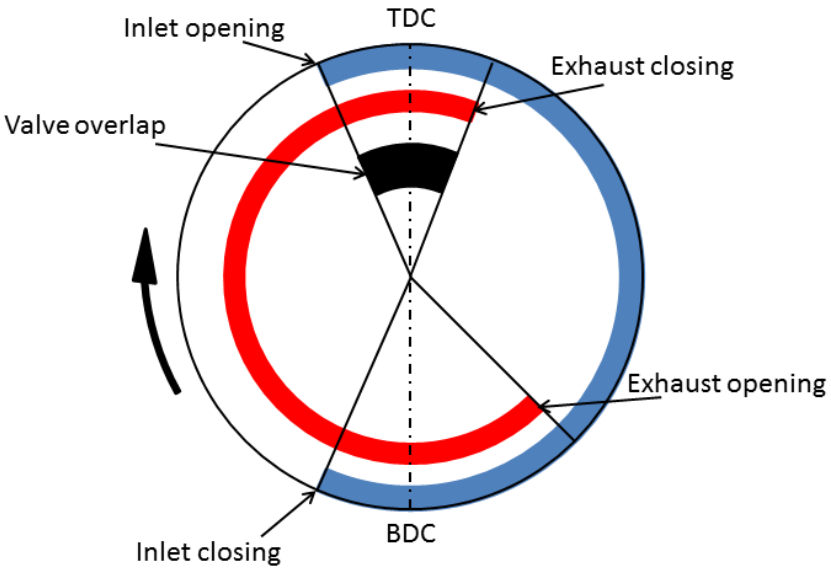

Figure 3.8. Valve timing circle.

3.3.3 Data Processing and Calculations

The raw measurement data was processed in MATLAB. A script from previous studies on the same research engine was modified and used. MATLAB is an efficient tool for extracting data from structures, arrays and matrices but also for creating coherent graphs. The cylinder pressure data is averaged over 24 work cycles and filtered with a low-pass 10^{th} order Butterworth filter.

The heat release rate is calculated from the cylinder pressure data with equations based on the first law of thermodynamics. The cylinder and its contents are assumed to be a single open system when the valves are closed. The only mass flows across the system are the fuel and crevice flows. However, the crevice flow is considered insignificant and is therefore omitted from the heat release calculations for simplicity.

The first law for the system described above can be expressed as follows [46]:

$$\frac{dQ}{dt} - p\frac{dV}{dt} + \dot{m}_f h_f = \frac{dU}{dt} \tag{3.1}$$

Where dQ/dt is the heat transfer across the system boundary, $p(dV/dt)$ is the rate of work done by the gas expansion, $\dot{m}_f$ and h_f are the mass flow and enthalpy of the fuel flux entering the cylinder and dU/dt is the change in internal energy of the substances in the cylinder.

The net heat release rate *dQn/dt* can be expressed as the difference between the fuel chemical energy and the system heat transfer [46]:

$$\frac{dQ_n}{dt} = \frac{dQ_{ch}}{dt} - \frac{dQ_{ht}}{dt} = p\frac{dV}{dt} + \frac{dU_s}{t} \tag{3.2}$$

Assuming that the in-cylinder mixture can be regarded as ideal gas, the net heat release can finally be written in form:

$$\frac{dQ_n}{dt} = \frac{\gamma}{\gamma - 1} p\frac{dV}{dt} + \frac{1}{\gamma - 1} V\frac{dp}{dt} \tag{3.3}$$

Where γ is the ratio of specific heats c_p/c_v.

As the cylinder pressure is measured as a function of the crank angle, it is more appropriate to express equation 3.3 relative to the crank angle too:

$$\frac{dQ_n}{d\varphi} = \frac{\gamma}{\gamma - 1} p\frac{dV}{d\varphi} + \frac{1}{\gamma - 1} V\frac{dp}{d\varphi} \tag{3.4}$$

The energy flows from both fuels are calculated from the metered mass flows and from the lower heating values of the fuels. Consequently, the substitution rate can be calculated from the energy flows of the fuels. These as expressed as:

$$\dot{E} = \dot{m} \times LHV \tag{3.5}$$

$$SR = \frac{\dot{E}_{CH4}}{\dot{E}_{CH4} + \dot{E}_{DI}} \times 100\% \tag{3.6}$$

Where $\dot{m}$ is the mass flow of a fuel and LHV is the lower heating value.

The stoichiometric AFR of methane and Diesel are different and hence the total stoichiometric AFR has to be calculated:

$$AFR_{DF,st} = AFR_{CH4,st} \times m\%_{CH4} + AFR_{DI} \times (1 - m\%_{CH4}) \tag{3.7}$$

Where $AFR_{CH4,stoich}$ is the stoichiometric AFR for methane, $AFR_{DI,stoich}$is the stoichiometric AFR for Diesel and $m\%_{CH4}$ represents the CH4 mass relative to the total fuel mass.

And consequently the total lambda of the mixture can be expressed as

$$\lambda_{DF} = \frac{AFR_{DF}}{AFR_{DF,st}} \tag{3.8}$$

Where AFR_{DF} is calculated from the fuel mass flows.

The cycle-to-cycle variation was evaluated with the coefficient of variation (COV) of the maximum cylinder pressure P_{max}. This was calculated from the standard deviation of the maximum pressure values of 25 consecutive cycles.

Mean P_{max} can be written as:

$$\overline{P}_{max} = \frac{1}{n}\sum_{i=1}^{n} P_{max} \tag{3.9}$$

Where *n* is the number or cycles.

Standard deviation of P_{max}:

$$\sigma_{P_{max}} = \sqrt{\frac{\sum_{i=1}^{n}(\overline{P}_{max} - P_{max,i})^2}{n-1}} \tag{3.10}$$

And finally the coefficient of variation for P_{max}:

$$COV_{P_{max}} = \frac{\sigma_{P_{max}}}{\overline{P}_{max}} \tag{3.11}$$

COV can further be calculated for the pressure rise rate and indicated mean effective pressure (IMEP) in a similar manner.

3.3.4 Uncertainties Related to Measurements and Calculations

It is impossible to avoid errors and uncertainties in experimental research. Therefore it is vital to understand and analyse the sources of error and if possible, prevent some errors by additional tests. Three error types can be distinguished in this study: calculation errors, device and control errors and conjunction errors. The calculation errors originate from the approximations made in the equations used. However, the equations used for the calculations are generally accepted and proven and possible errors are negligible. Therefore, this error type is not considered further.

The device and control errors can, in turn, be divided into errors originating on one hand from the physical sensors and on the other hand from the control system. Each sensor has an absolute error value often given in percentage of the measured value. For example, the Coriolis mass flow sensor for methane has an error of approximately 0.5 % of the measured value with the rather low mass flows present in the experiments. In addition, many of the sensors have a certain frequency at which they renew their state. This is also referred to as the sample rate. Should the sample rate be insufficient for rapid measurements, such as the cylinder pressure, the resolution of the measurements deteriorates.

The dSpace- and Simulink-based control system is used to read and capture the sensor data. The simulation turnaround time determines at which rate the sensor outputs are read. This denotes that if the turnaround frequency of the control system is lower than the sensor sample rate, the control system becomes the limiting factor for high-resolution measurements. The control system turnaround time was set to 80 µs which equals a

frequency of 12.5 kHz and approximately 0.7 °Cad at 1500 rpm. Very fast measurements are needed with two sensors: the crankshaft position sensor controlling injection and valve timing and the cylinder pressure sensor. The turnaround time is adequate for the crankshaft position sensor, but for the cylinder pressure measurements the frequency is regrettably low.

If the sensor or control system sample rate is too low, it may be impossible to capture the measured phenomenon accurately. This is referred to as aliasing in signal processing. According to the Nyquist Theorem, the sample rate must be at least twice the frequency of the measured phenomenon in order to avoid aliasing [61]. The cylinder pressure can undoubtedly be measured accurately even with a 12,5 kHz measuring frequency but problems may arise with very high frequency in-cylinder phenomena, such as knock. Knock-related phenomena often occur at a frequency of approximately 10 kHz and thus aliasing will occur ($f_S < 2f_N$) and these phenomena cannot be reliably captured. However, knock-related phenomena are not essential for this study and hence, the sample rate may be considered adequate for the cylinder pressure measurements.

The digital signal processing boards of the real time computer feature 16-bit resolution. This signifies that the analogue voltage signal is divided into 2^{16} = 65 536 discrete packages. With a voltage range from 0 to 10 V, the smallest detectable voltage change is approximately 0.00015 V. With the cylinder pressure measurements, for example, this corresponds to approximately 0.0035 bar which can be considered more than adequate. Hence, it is safe to assume that the A/D resolution does not provide a significant error for the measurements.

A conjunction error does not directly affect the measurement data but rather the analysis of the data. This error type originates from the lack of supportive simulations and from the OFAT research method. A conjunction error may occur when an engine parameter change results in major changes in the engine performance. This may lead to a conclusion that the parameter that was changed caused the phenomenon. However, the actual cause for the performance change may derive from a collateral change of some other parameter, rather than the one controlled. An example of such a case would be a Miller cycle with increased boost pressure in order to keep the air mass flow constant. If an increase in THC emissions is measured, the cause might not necessarily be the valve timing change and related events but rather the increased boost pressure and charge slip during the overlap period. However, conjunction errors can be diminished or completely avoided by additional tests.

As important as it is to identify and be conscious of possible errors, it can be stated that the nature of this research is not very prone to errors originating from the experimental apparatus. The figures are only compared with other figures obtained from the same engine in similar tests. Therefore, systematic errors are present in all measurements thus having little impact on the relative results of different measurement points. Moreover, the values are only used to research engine phenomena in general and trends rather than to validate the engine emissions or performance. However, conjunction errors are more probable.

4 Experiment Results and Analysis

4.1 Boundary Conditions

4.1.1 Engine Parameters

The engine was run with different substitution rates (SR) at 50% and 100% loads. The goal was to maintain the total energy content of the fuel constant and study the emissions and in-cylinder phenomena. The energy content of the fuels was rather constant between all cases except in full Diesel mode at 50% load.

Some of the parameters listed as target values in Chapter 3.4.1 were rather difficult to achieve. Namely the charge air pressure was difficult to control at part load due to the small charge air valve opening. Moreover, the total fuel mass flow varied slightly when the substitution rate was changed. The measured pressure levels, lambda ratios and fuel mass flows in the standard valve timing measurements are presented in Table 4.1 (50% load) and Table 4.2 (100% load).

Table 4.1. Operating parameters at 50% load and standard valve timing.

Substitution rate (E%) →	**0**	**29**	**46**	**54**	**64**
Charge Air Pressure (bar)	1.35	1.30	1.36	1.29	1.40
Exhaust Gas Pressure (bar)	1.34	1.34	1.36	1.35	1.37
Air mass flow (kg/h)	89.3	82.6	85.8	83.4	92.7
Diesel mass flow (kg/h)	2.4	2.1	1.9	1.7	1.3
Methane mass flow (kg/h)	-	0.9	1.4	1.7	2.0
Total Lambda	2.5	2.2	1.9	1.5	1.8
Methane Lambda	-	4.1	3.3	2.8	2.7

Table 4.2. Operating parameters at 100% load and standard valve timing.

Substitution rate (E%) →	**0**	**18**	**31**	**40**	**55**
Charge Air Pressure (bar)	2.46	2.51	2.51	2.45	2.52
Exhaust Gas Pressure (bar)	2.27	2.33	2.28	2.28	2.35
Air mass flow (kg/h)	131.4	132.1	129.3	125.6	129.2
Diesel mass flow (kg/h)	7.3	5.5	4.7	4.0	3.2
Methane mass flow (kg/h)	-	1.0	1.6	2.3	3.1
Total Lambda	1.2	1.3	1.3	1.3	1.3
Methane Lambda	-	7.3	4.6	3.2	2.6

The fuel flows with different valve configurations were very similar to those listed in Tables 4.1 and 4.2 with equivalent substitution rates. However, the air mass flow was substantially affected by the valve actuation and charge valve control. Differences in air mass flow will also affect the lambda ratio of the mixture. The air mass flow, methane-

air mixture lambda and the total lambda of the combustion (Diesel+methane) in all VVA cases are presented in Figure 4.1 (50% load) and Figure 4.2 (100%) load.

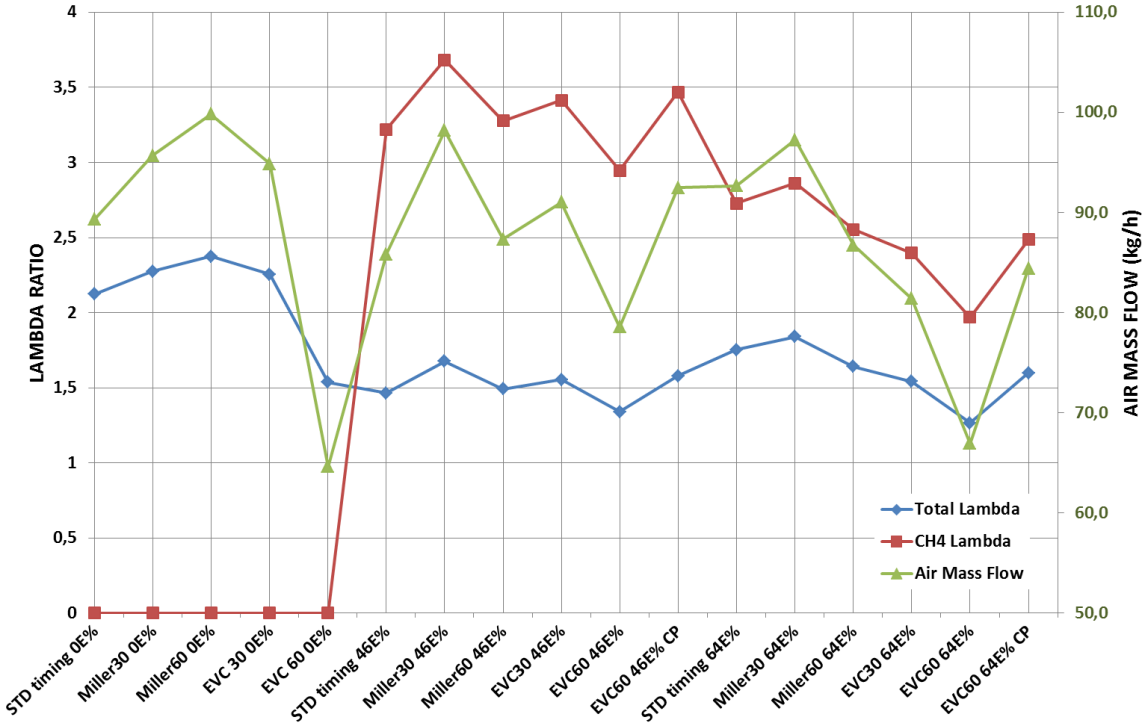

Figure 4.1. Air mass flow and the resulting lambdas with different valve configurations at 50% load.

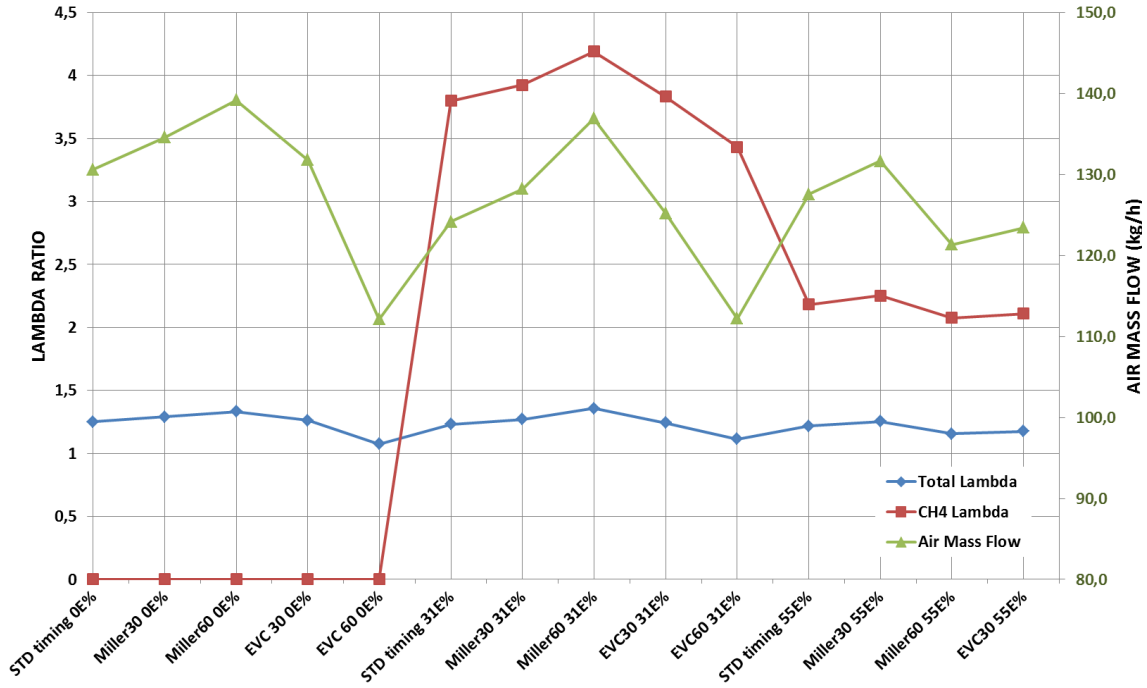

Figure 4.2. Air mass flow and the resulting lambdas with different valve configurations at 50% load.

The EVC 60 seemed to have a substantial effect on the mass air flow and thus two additional tests were run at 50% load with increased charge air pressure. These are referred to as EVC 60 46E% CP and EVC 60 64E% CP.

The methane lambda is the most interesting of the listed parameters as it directly affects the flammability of the premixed methane-air mixture. A very lean mixture is prone to flame quenching and even to complete misfire (see Figure 2.5) whereas a rich mixture may lead to very rapid combustion and knock.

The Diesel injection timing at 100% load was 10 °BTDC for the substitution rate measurements (Table 3.5). However, it was necessary to retard the injection timing to 5 °BTDC for the VVA measurements at 100% load in order to implement the EVC valve configurations without exceeding the safety cylinder pressure limit. Nevertheless, the cylinder pressure with EVC 60 at 100% load with of 55 E% SR was not measured due to very early preignition and high cylinder pressure.

4.1.2 Variable Valve Actuation Curves

The valve opening curves in the VVA measurements with the Miller and EVC cycles according to Table 3.6 are presented in Figures 4.3 and 4.4. Moreover, two retarded Miller cycle curves that were used in overlap measurements are presented in Figure 4.5. The curves are more or less similar to the Miller 60 curve but 30 °CAD and 60 °CAD retarded.

There is some unwanted deviation in the valve curves especially in the opening and closing ramps between different curves due to the hydraulic system behaviour. However, the deviations occur mostly between different curves, not between cycles and are thus acceptable. Moreover, some valve bounce can be observed with some curves. The exhaust valve bounce at closing may have a slight effect on the methane slip.

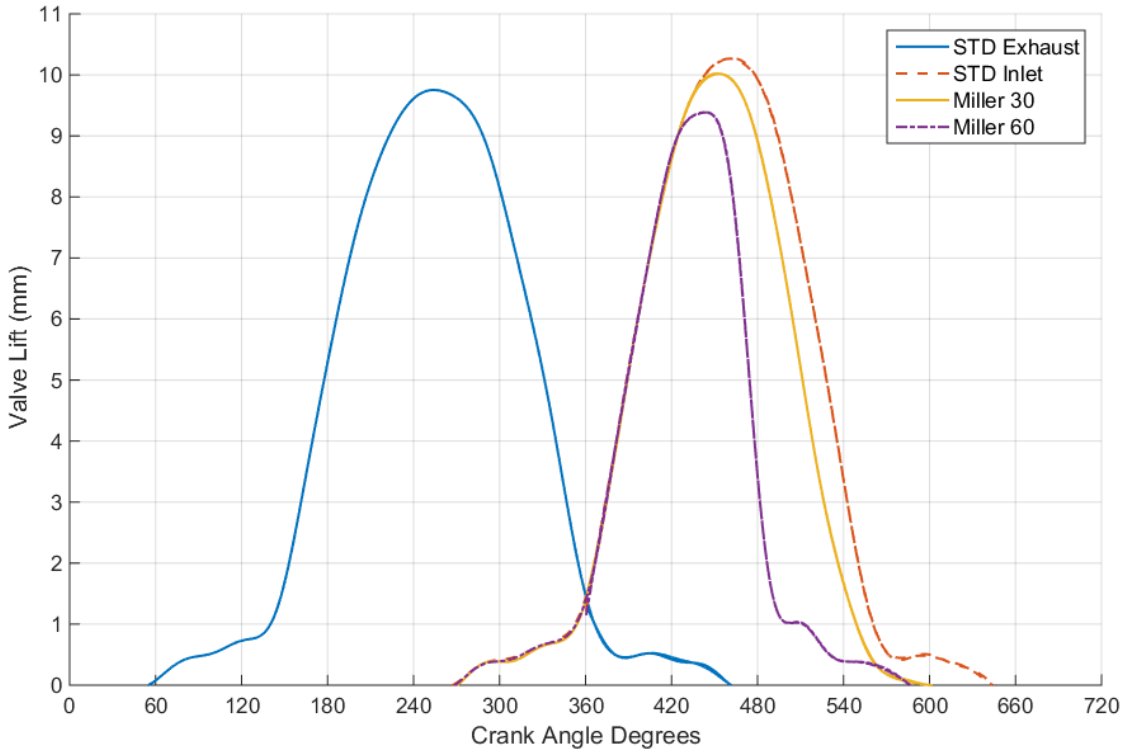

Figure 4.3. Miller cycle valve curves.

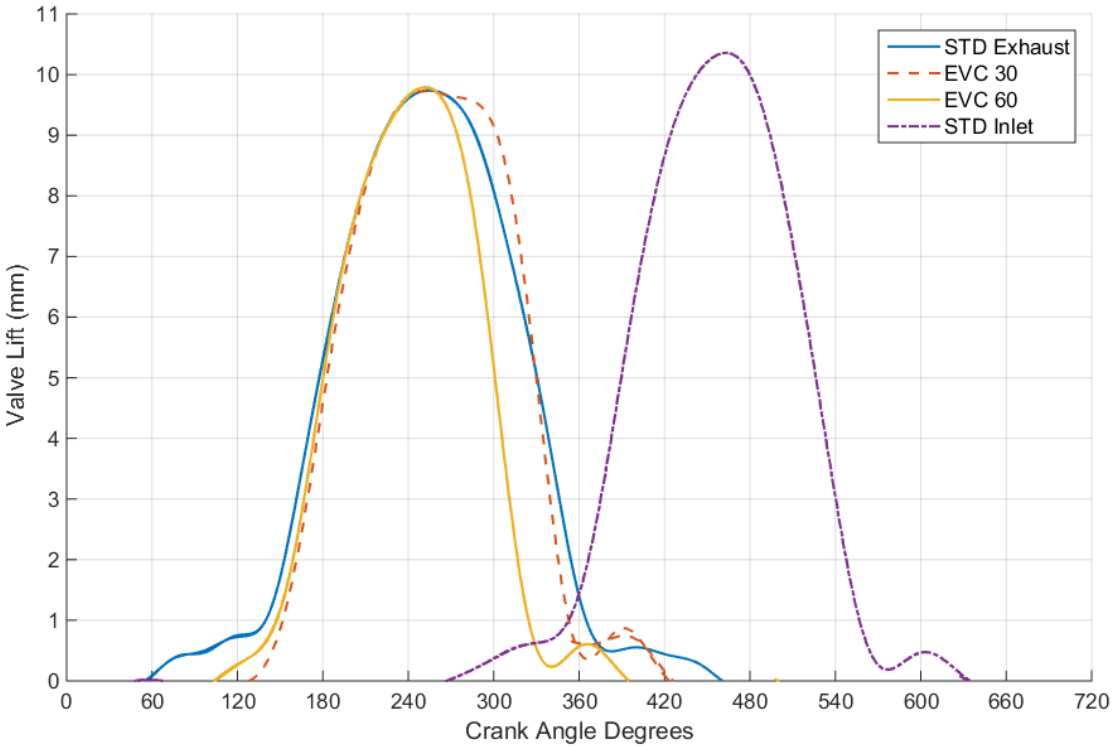

Figure 4.4. EVC valve curves.

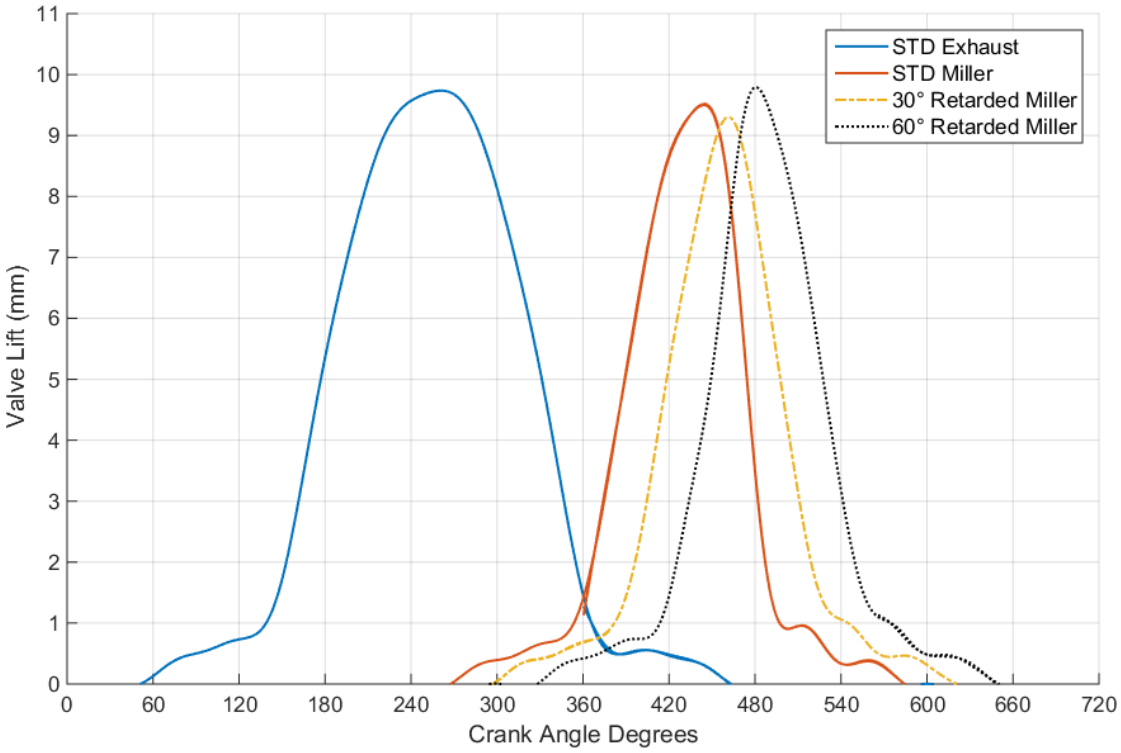

Figure 4.5. Retarded Miller cycle curves. The STD Miller is similar to Miller 60.

4.2 Cylinder Pressures

4.2.1 Cylinder Pressures at 50% Load

The cylinder pressure curves with different substitution rates at 50% load are presented in Figure 4.6. The deviations in maximum pressure values are partly a coincidence from slightly different charge air pressures. All peak pressure values occur between 123 and 129 bar. The pressure peak timing is slightly advanced with higher substitution rates of 54 E% and 64 E%. The effect of the substitution rate on the cylinder pressure behaviour at 50% load seems to be small.

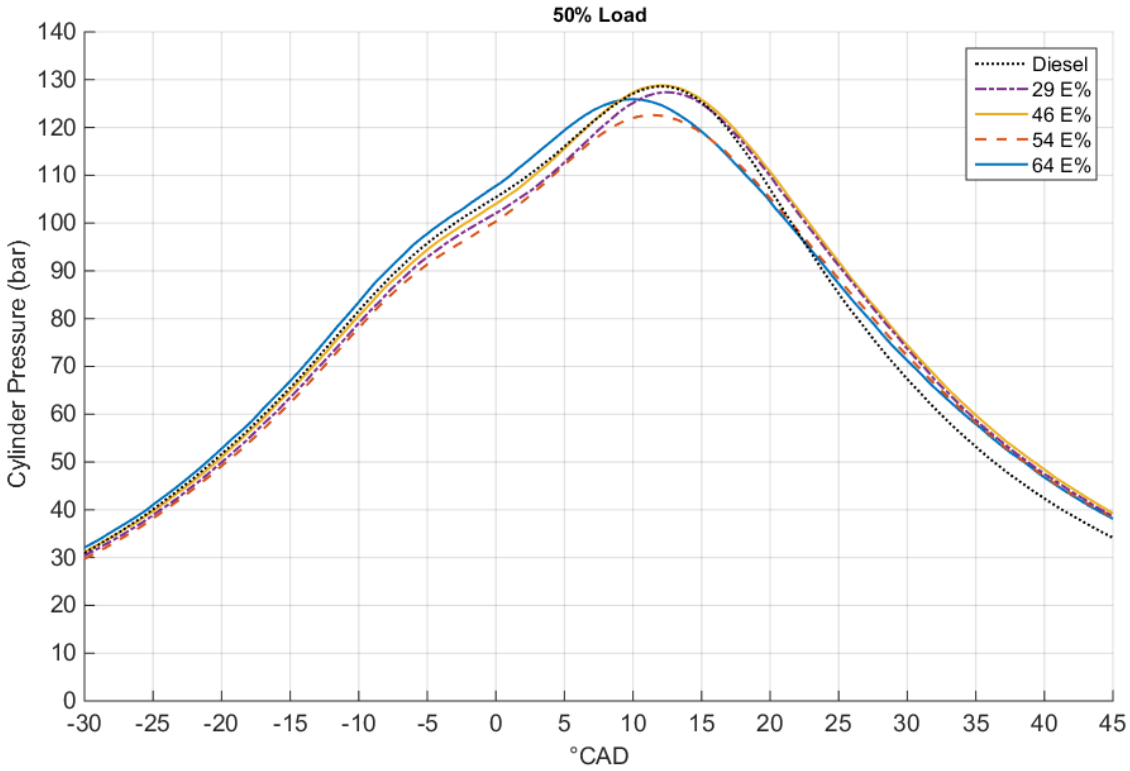

Figure 4.6. Averaged cylinder pressure with different substitution rates at 50% load.

The cylinder pressure graphs with different VVA configurations at 50% load in Diesel operation and with 46 E% SR and 64 E% SR are presented in Figures 4.7, 4.8 and 4.9, respectively. The differences in peak pressure values in Diesel operation seem to originate from the slightly different charge air pressures and compression end pressures. Overall, there are no substantial changes in the cylinder pressure behavior between different valve configurations in Diesel mode. The cylinder pressure varies from approximately 135 bar with Miller 60 to 150 bar with Miller 30 and EVC 30. The compression end pressures are also highest in these two measurements.

The differences in compression end pressures with 46 E% SR, especially with Miller 60, are partially caused by the different compression end temperatures and partially by the slightly different air mass flow rates. The most distinctive features in the graph are the very high peak cylinder pressures and rapid pressure rise rates with EVC 60 and with EVC 60 CP. EVC 60 peaks at approximately 174 bar and EVC 60 CP at 192 bar. The increase in cylinder pressure in the CP case is mostly due to the higher charge air pressure.

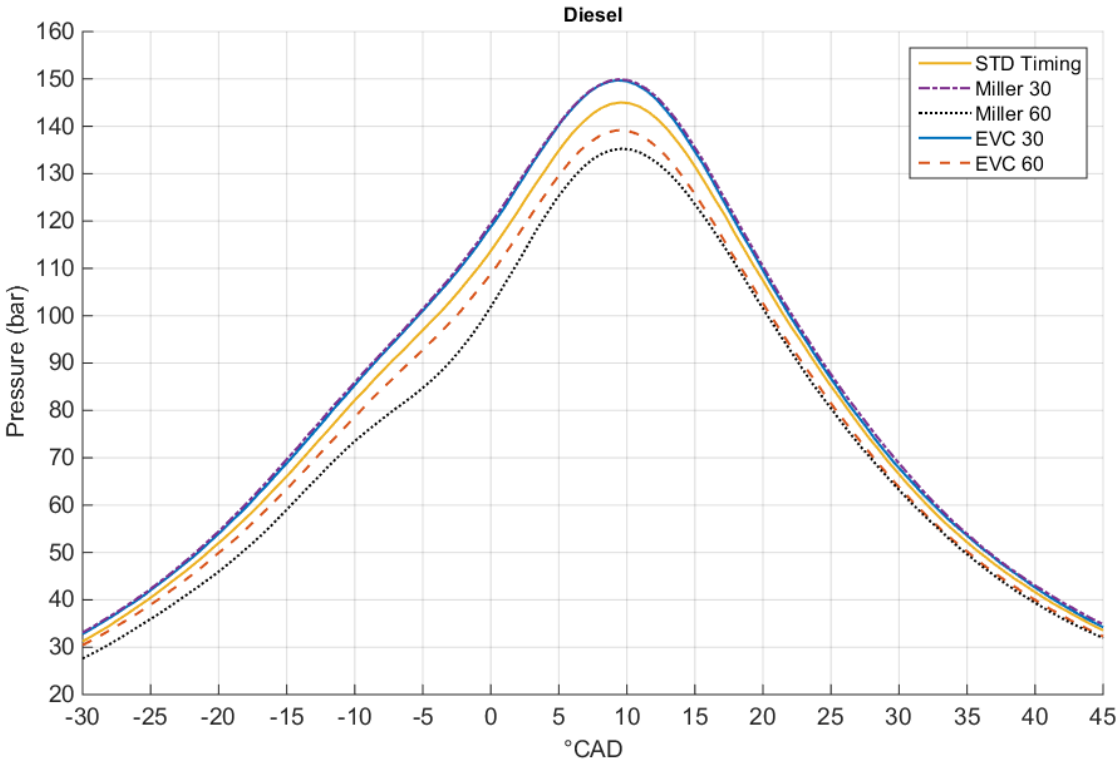

Figure 4.7. Averaged cylinder pressure curves with different valve configurations in Diesel operation at 50% load.

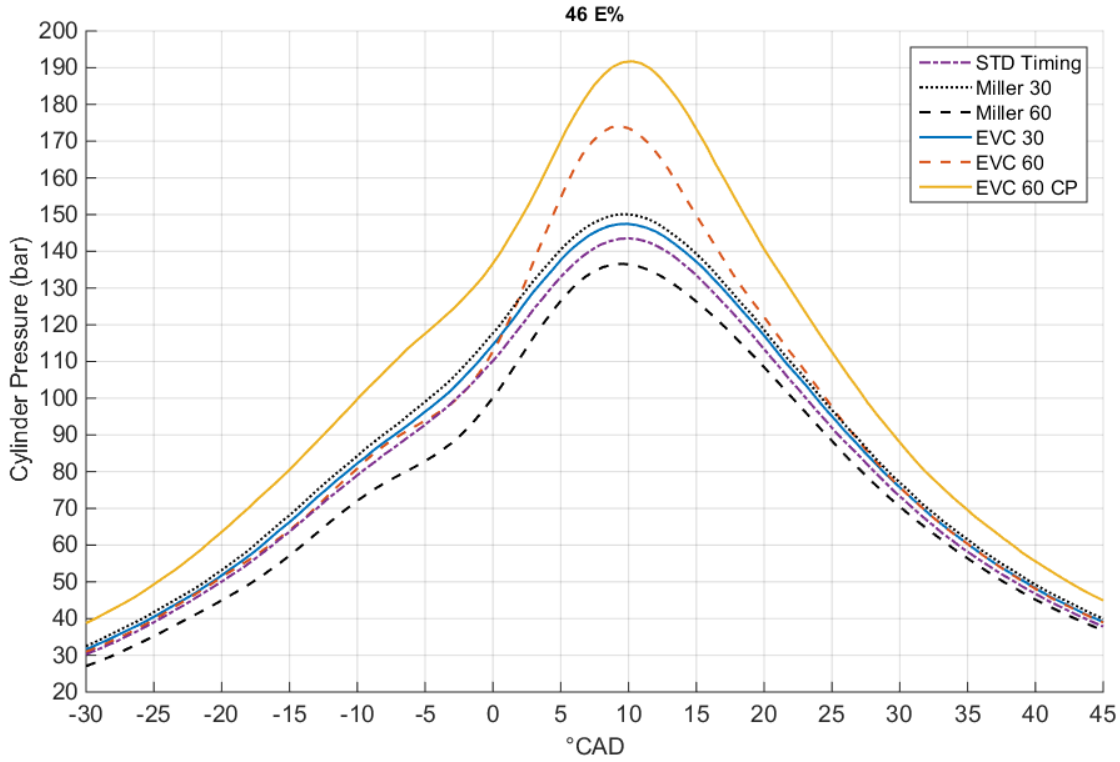

Figure 4.8. Averaged cylinder pressure curves with different valve configurations in with 46 E% substitution rate at 50% load

Moreover, the pressure peak is retarded by approximately 2 °CAD as a result of leaner methane-air mixture and decreasing mixture temperature. The other peak cylinder pressures are substantially lower from approximately 137 bar with Miller 60 to 150 bar with Miller 30. The pressure peak is slightly advanced with both EVC 60 and Miller 60 occurring at approximately 8 °ATDC.

The cylinder pressures with 64 E% SR are presented in Figure 4.9 are rather different from those in Figure 4.8. Only the EVC 60 and EVC 60 CP curves appear to be quite similar. Interestingly, the peak pressure timing is advanced with Miller 30 (8 °ATDC), Miller 60 (8 °ATDC) and EVC 30 (9 °ATDC) compared with the STD Timing (10 °ATDC). The Miller 60 pressure also peaks slightly higher (127 bar) than the STD Timing pressure (125 bar).

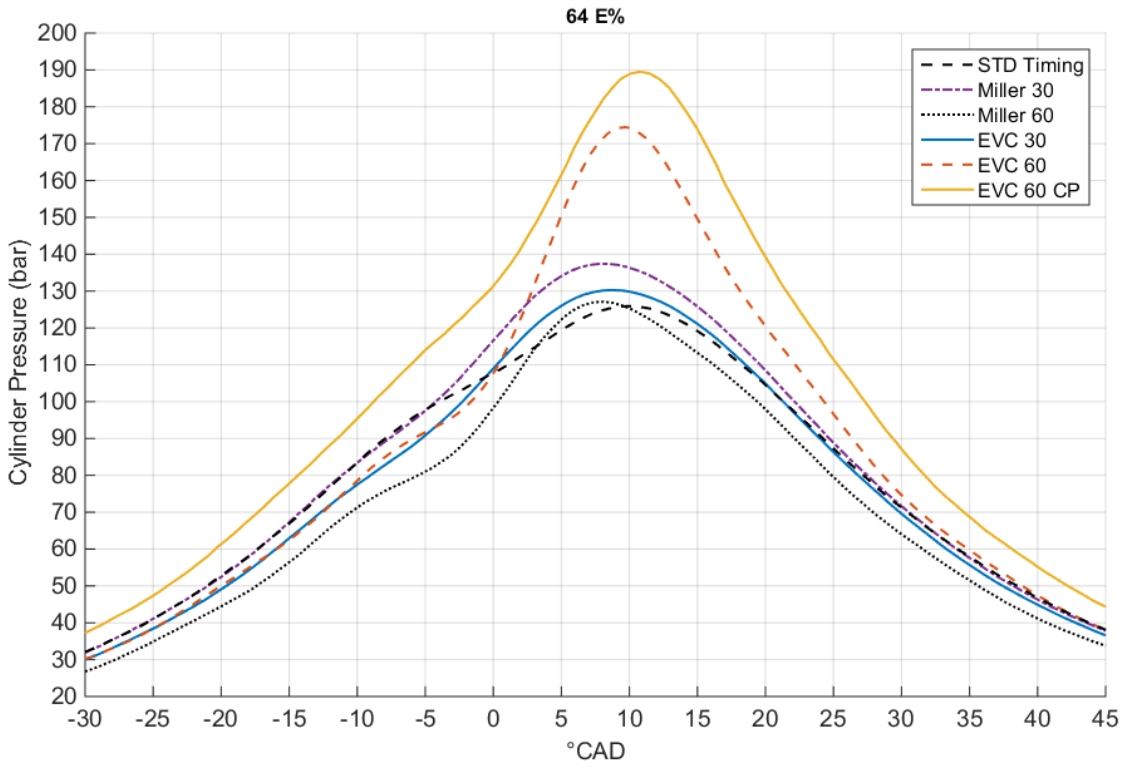

Figure 4.9. Averaged cylinder pressure curves with different valve configurations with 64E% substitution rate at 50% load.

4.2.2 Cylinder Pressures at 100% Load

The averaged cylinder pressures with different substitution rates at 100% load are presented in Figure 4.10. A clear trend can be observed in the cylinder pressures: The peak pressure increases significantly from 221 bar in Diesel operation to approximately 232 bar with only 18 E% SR. The peak pressure continues to rise up to 237 bar with 29 E% SR but any further increase in the substitution rate does not seem to affect the peak pressure value. Another noticeable trend is the retardation of the pressure peak with an increasing substitution rate.

The difference between peak pressure timings in the Diesel reference measurement and the first dual-fuel measurement with 18 E% SR is substantial. The Diesel mode pressure peak occurs at approximately 10,5 °ATDC whereas in the latter case the peak occurs at

13 °ATDC. The pressure peak is gradually retarded as the substitution rate increases. With 55 E% SR the pressure peak is reached just after 15 °ATDC. A probable reason for the pressure peak not rising over 237 bar with higher substitution rates is the retardation of the pressure peak. The available space for expansion increases more rapidly as the piston recedes from the TDC and thus mitigates the rise in pressure due to the heat release.

Figure 4.11 presents the cylinder pressure curves with VVA in Diesel operation. The only noticeable differences in the curves occur with Miller 60 and EVC 60. Miller 60 substantially reduces the cylinder pressure whereas EVC 60 causes the cylinder pressure to drop slightly faster. The effect of Miller 60 on the cylinder pressure is mostly due to lower compression end temperature which signifies that the Miller cycle functions as intended. This effect cannot be observed with Miller 30.

The cylinder pressures with 31 E% SR are shown in Figure 4.12. The most distinctive curve is the EVC 60 one which peaks very high at approximately 246 bar and early at 7 °ATDC. A clear pre-ignition occurs as the compression end pressure rises dramatically even before the Diesel injection. The cylinder pressure curves of the STD Timing, Miller 30 and EVC 30 are quite similar to each other. The pressure peak in all cases is reached at approximately 16 °ATDC. STD Timing peaks slightly higher at 210 bar than Miller 30 and EVC 30 which both reach roughly 204 bar. The Miller 60 pressure peak is the lowest at 185 bar, as was expected.

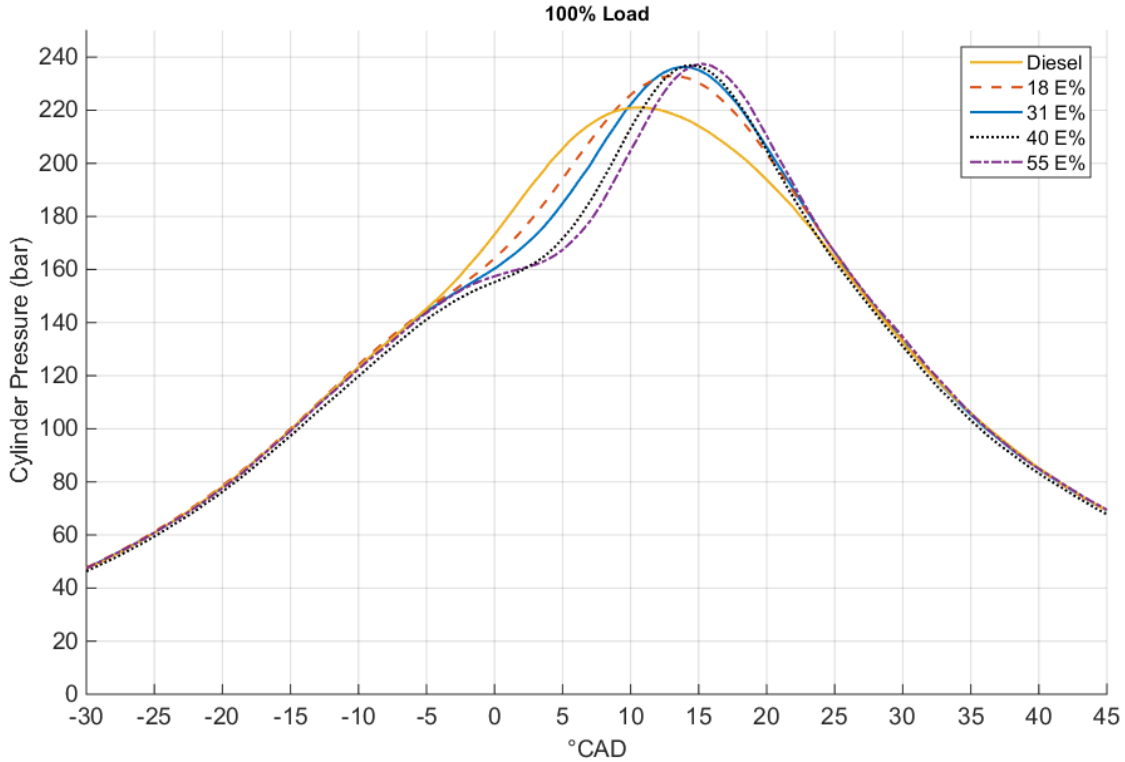

Figure 4.10. Averaged cylinder pressure curves with different substitution rates at 100% load.

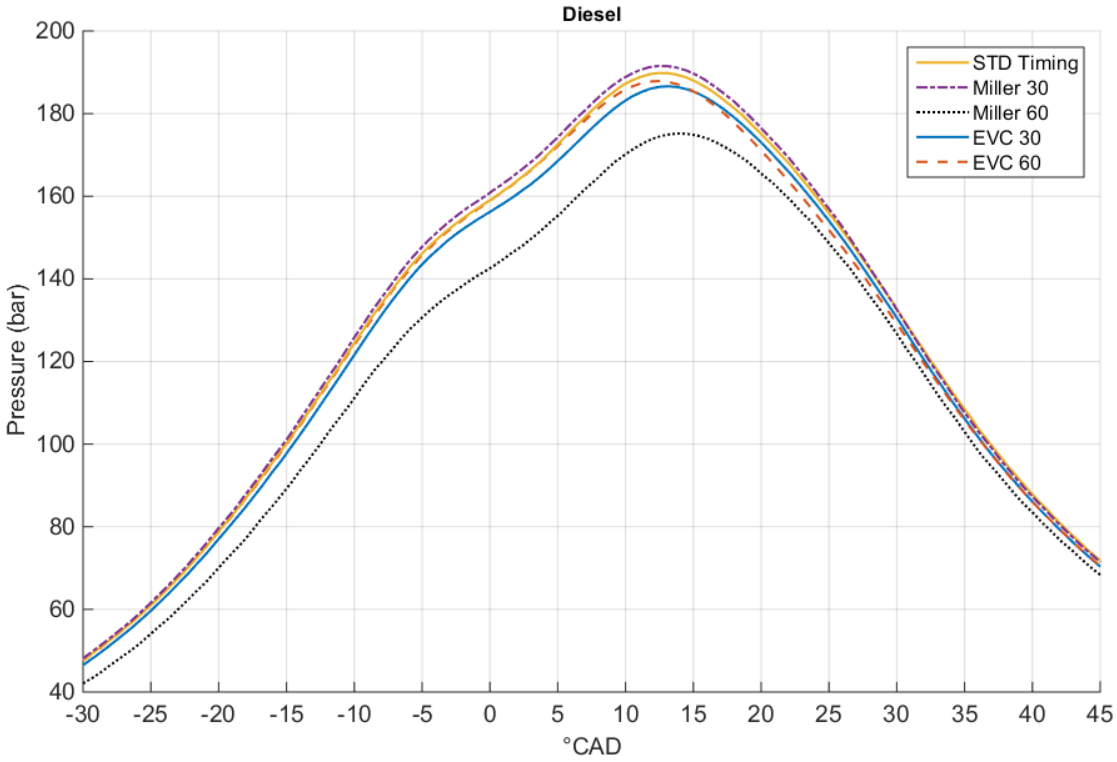

Figure 4.11. Averaged cylinder pressure curves in Diesel operation with different VVA configurations at 100% load.

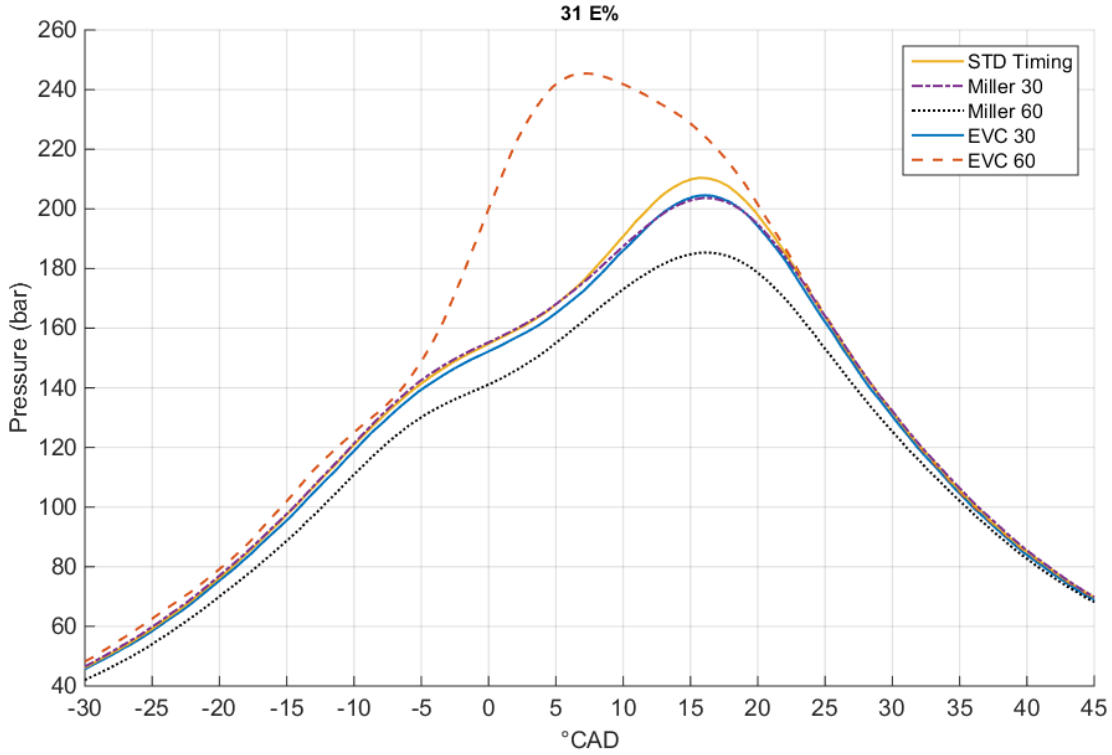

Figure 4.12. Averaged cylinder pressure curves with 31 E% substitution rate with different VVA configurations at 100% load.

The cylinder pressures with 55 E% SR are plotted in Figure 4.13. The figure presents only four curves as the EVC 60 case was not measured. The cylinder pressure with STD Timing is slightly lower than with 31 E% at 203 bar whereas EVC 30 peaks somewhat higher at 213 bar although the peak timing is slightly retarded. The Miller 30 cylinder pressure peak is approximately the same with both substitution rates but the timing of the peak is slightly advanced to 15 °ATDC with 55 E%. The Miller 60 pressure peak, in turn, is lower with 55 E% and it occurs 2 degrees earlier in the cycle than with 31 E% SR.

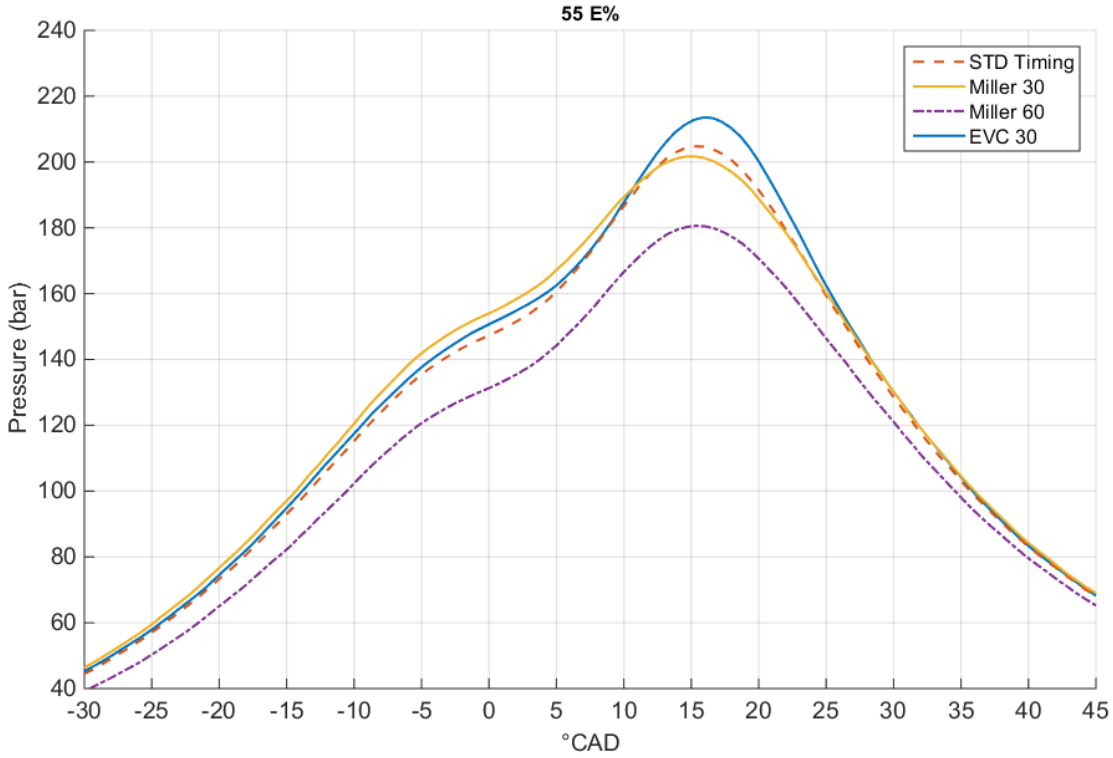

Figure 4.13. Averaged cylinder pressure curves with 55 E% substitution rate with different VVA configurations at 100% load.

4.3 Heat Release

4.3.1 Heat Release at 50% Load

The heat release rates (HRR) and cumulative heat release (HR) curves were calculated from the averaged cylinder pressures using Equation 3.4. The dual-fuel HRR was divided into three overlapping phases in Chapter 2.1.3:

1) Premixed Diesel combustion
2) Partially oxidized methane combustion
3) Combustion of the lean bulk mixture

The first phase contributes to a major part of the total heat release in the early part of the combustion and commences the second phase. The second phase causes a high peak in the HRR whereas the last phase contributes mostly to the slowly propagating combustion later in the cycle.

The HRRs with different substitution rates at 50% load are plotted in Figure 4.14. The slopes of the HRR curves are nearly identical regardless of the substitution rate. The partially oxidized methane seems to replace the high premixed Diesel peak in HRR with lower substitution rates. However, with 54 E% SR and 64 E% SR the peak values are substantially lower. This signifies that a larger portion of the heat release originates from the combustion of the lean bulk mixture. The smaller amount of Diesel injected lead to lower combustion temperatures early in the expansion cycle and thus less partially oxidized methane products are formed. It must be noted that the Diesel reference case contained less fuel energy and hence the total heat release is lower.

It appears that the combustion quality degrades with higher substitution rates at 50% load which leads to lower HRRs. Bulk quenching or quenching at the combustion chamber walls are likely to occur but complete misfires were not detected during 24 consecutive cycles. The methane-air mixture is very lean at 50% load as was seen in Table 4.1. Even though it becomes richer ($\lambda \approx 2.7$ with 64 E% SR) with an increasing substitution rate, it may still linger below or very close to the lean flammability limit of methane in some parts of the combustion chamber. Moreover, as the substitution rate increases, the amount of available ignition energy in Diesel decreases in proportion. It appears that the methane-air mixture is too lean for self-sustaining combustion further away from the Diesel flame when the Diesel quantity is small.

Figure 4.15 presents the total heat release calculated from the HRRs in Figure 4.14 over crank angle degrees. The dashed lines indicate 10%, 50% and 90% fuel mass fraction burned. Henceforth the timing of each mass fraction will be referred to as x_{10}, x_{50} and x_{90}, respectively. The x_{10} is used as the reference point for the start of combustion. The x_{50} predicts the cylinder pressure peak behaviour. The x_{90}, in turn, indicates the end of bulk combustion. The mass fraction burned timings over substitution rate are plotted in Figure 4.16.

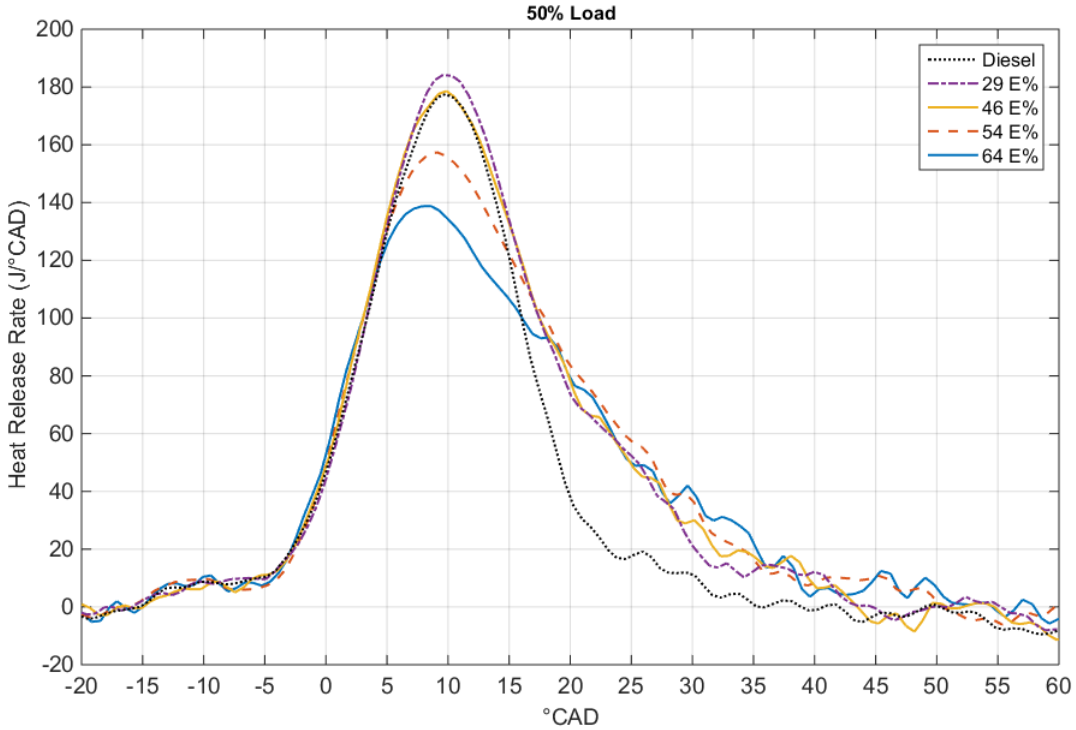

Figure 4.14. Calculated heat release rates with different substitution rates at 50% load.

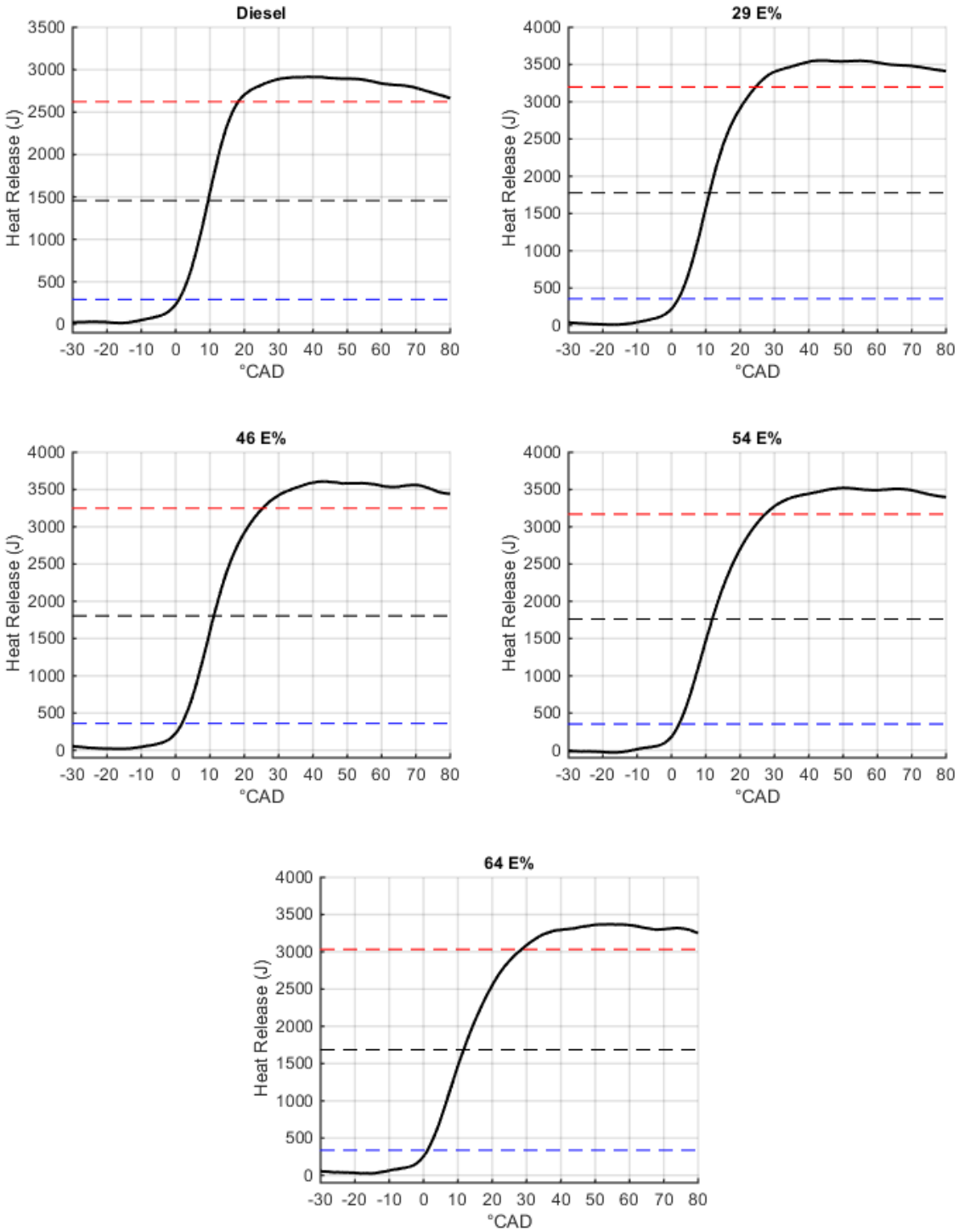

Figure 4.15. Cumulative heat release curves with different substitution rates at 50% load. The blue, black and red dashed lines indicate 10%, 50% and 90% mass fractions burned, respectively (percentage of maximum value). The substitution rate is noted above each graph.

The heat release rates with VVA in Diesel operation are plotted in Figure 4.17. VVA appears to have very little effect on the combustion event. Only Miller 60 and EVC 60 show some deviation in the heat release rate. The cumulative HRs are shown in Figure 4.18. The curves are nearly perfectly in union with the exception of EVC 60, which appears to deteriorate the combustion efficiency somewhat as the total heat released is approximately 150 J lower than in other cases even though the fuel mass flows are similar.

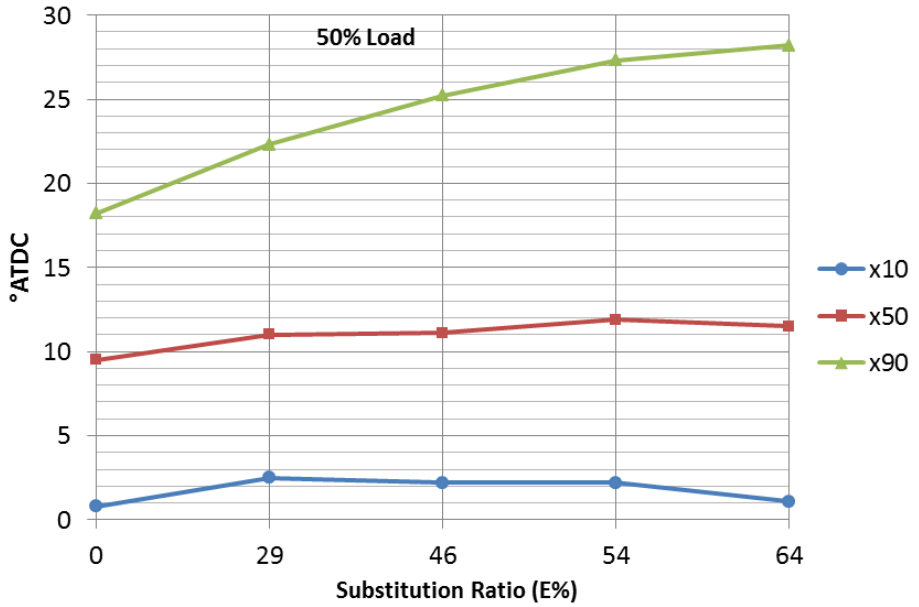

Figure 4.16. Development of mass fractions burned timing over substitution rate at 50% load.

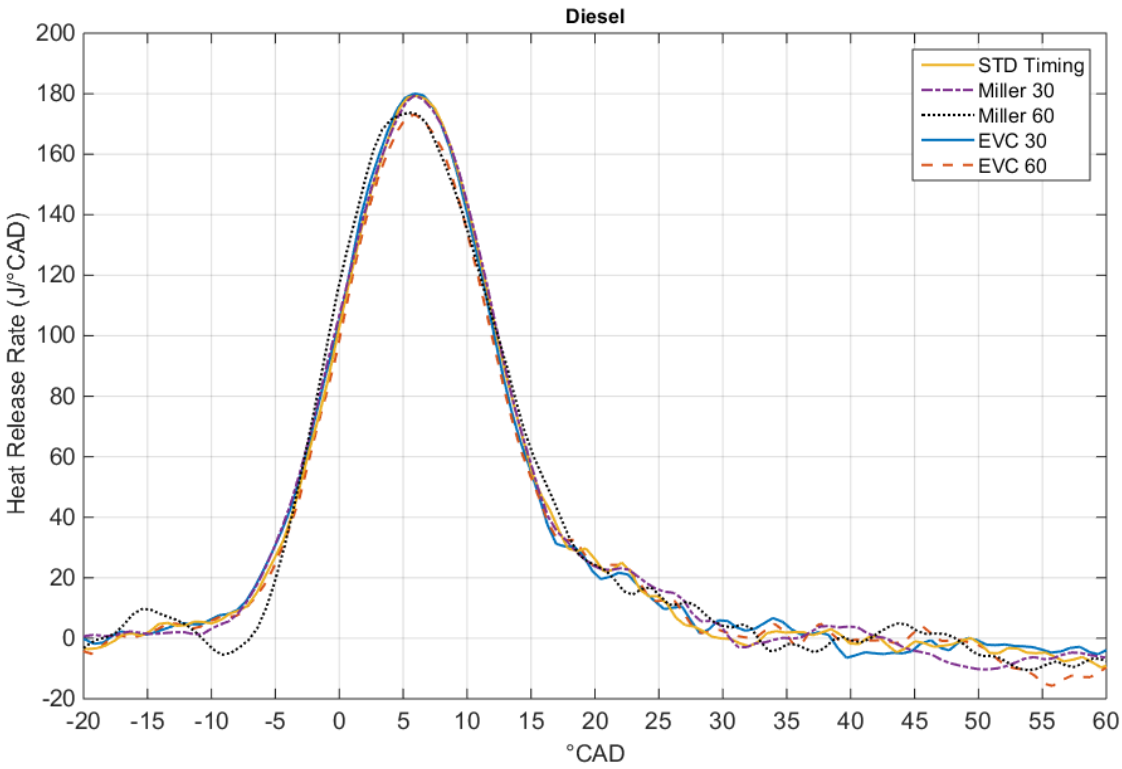

Figure 4.17. Calculated heat release rates with different valve configurations in Diesel mode at 50% load.

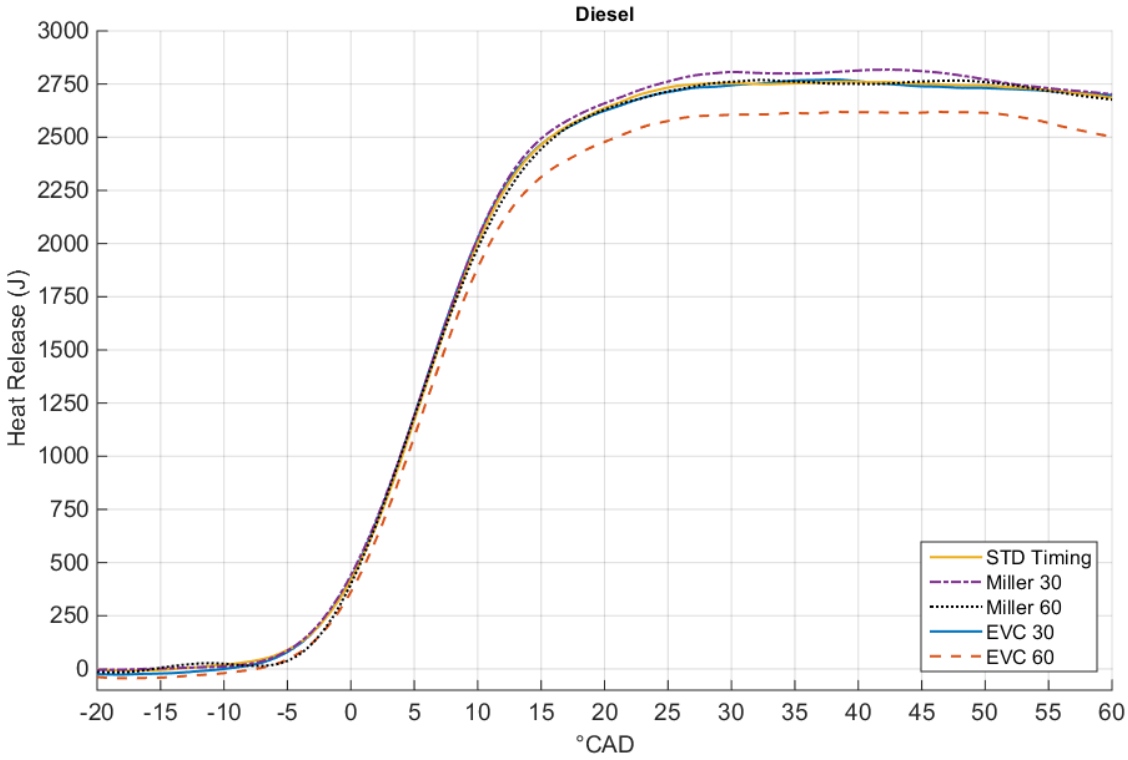

Figure 4.18. Cumulative heat release curves with different valve configurations in Diesel mode at 50% load.

The HRRs with 46 E% SR are shown in Figure 4.19. The high cylinder pressure peaks that were observed with the EVC 60 cases in Figure 4.8 is even more prominent in the corresponding HRR plot. The peak HRR occurs at approximately 300 J/°CAD. Moreover, the rise and drop are very steep. STD Timing, EVC 30 and Miller 30 all show rather similar HRR curves. They all peak at approximately 180 J/°CAD and the only notable difference is the fluctuation of HRR after 13 °ATDC. The STD Timing HRR curve does not show any fluctuation similar to those of EVC 30 and Miller 30. The Miller 60 peak is slightly higher at 185 J/°CAD and the rise is steeper towards the peak value. However, the Miller 60 HRR decreases more quickly just after the peak value.

The HRR peaks with the EVC 60 cases indicate that the contribution of the second combustion phase is substantial. It is likely that the higher mixture temperature due to IEGR promotes the formation of methane partial oxidation products which, in turn, are very quickly ignited by the Diesel flame. The increased dilution of the methane-air mixture by increasing the charge air pressure in EVC 60 CP notably delays the HRR peak but does not significantly affect the contribution of the second phase combustion. The slow lean mixture combustion is more prominent in all other cases whereas the amount of partially oxidized methane prior to combustion appears to be small.

The cumulative HR curves presented in Figure 4.20 show how all the heat releases apart from the EVC 60 cases are in union for the main part of the combustion. Only after approximately half of the charge is burned, the STD Timing and Miller 60 curves diverge from the other two. The slopes of the EVC 60 curves are very steep indicating rapid combustion. However, the start of the combustion is very similar in all cases. Another notable difference between different valve configurations is the end value of total heat

released. EVC 60 CP shows the highest heat release of approximately 3900 J whereas the lowest is detected with STD Timing and Miller 60 at 3400 J.

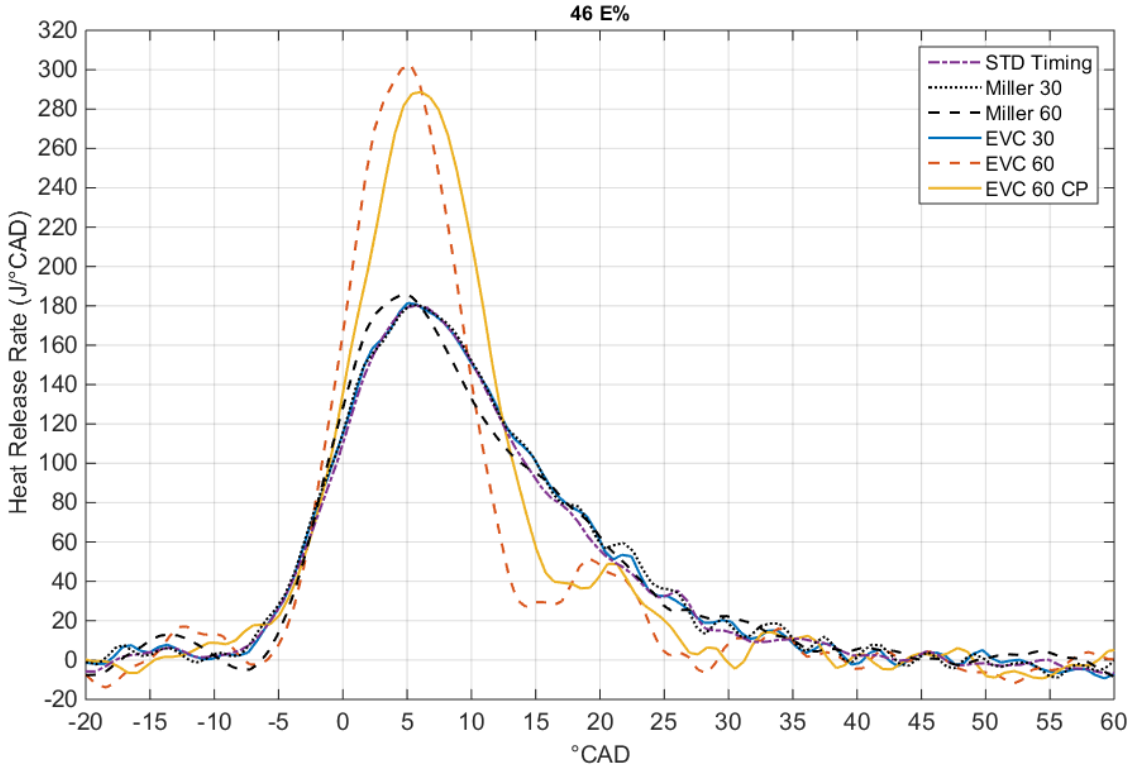

Figure 4.19. Calculated heat release rates with different valve configurations with a substitution rate of 46 E% at 50% load.

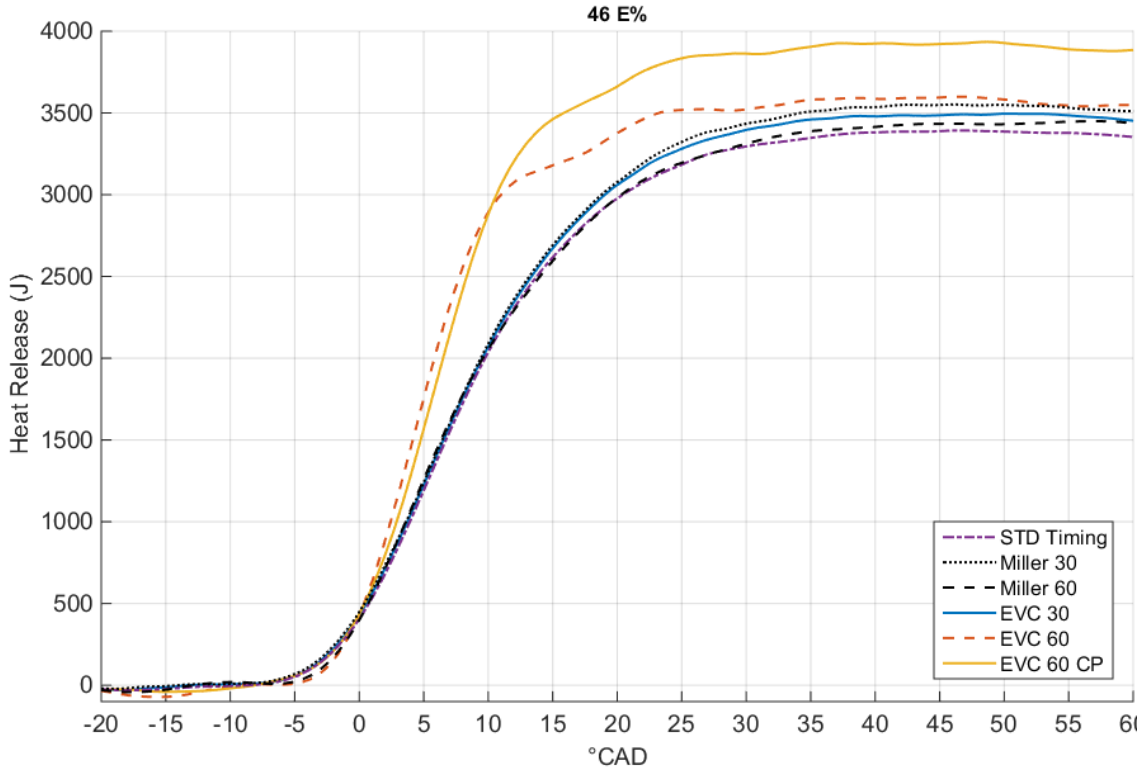

Figure 4.20. Cumulative heat release curves with different valve configurations with E% 46 at 50% load.

The total heats released indicate that the combustion efficiencies are very different as the fuel mass flows between cases are nearly identical. Particularly, the total heat released with EVC 60 CP is interesting as it is approximately 300 J higher than that of EVC 60 with the standard charge air pressure.

The HRRs with 64 E% SR with VVA are presented in Figure 2.21. The peak values are generally relatively low with the exception of the EVC 60 cases which peak at above 300 J/°CAD. This is over double the value of for example the STD Timing HRR peak (140 J/°CAD). The Miller 60 curve shape is rather interesting. The peak occurs very early at 2.5 °ATDC while the rapid rise is followed by a rapid decrease and a second peak. In addition, the similar behaviour of the EVC 30 and Miller 30 curves is notable. In both cases, the heat release starts very early while the peak is low at approximately 130 J/°CAD.

The cumulative heat release curves in Figure 4.22 show even more pronounced differences with EVC 60 and Miller 60. Particularly, the differences in the total heats released at the end of combustion are remarkable. With EVC 60 CP the total heat released reaches approximately 4100 J while with Miller 60 it climbs just above 3000 J. STD Timing, EVC 30 and Miller 30 all reach approximately 3250 J. EVC 60 CP shows again substantially higher total heat released than EVC 60. The difference between the two is approximately the same as with 46 E% SR.

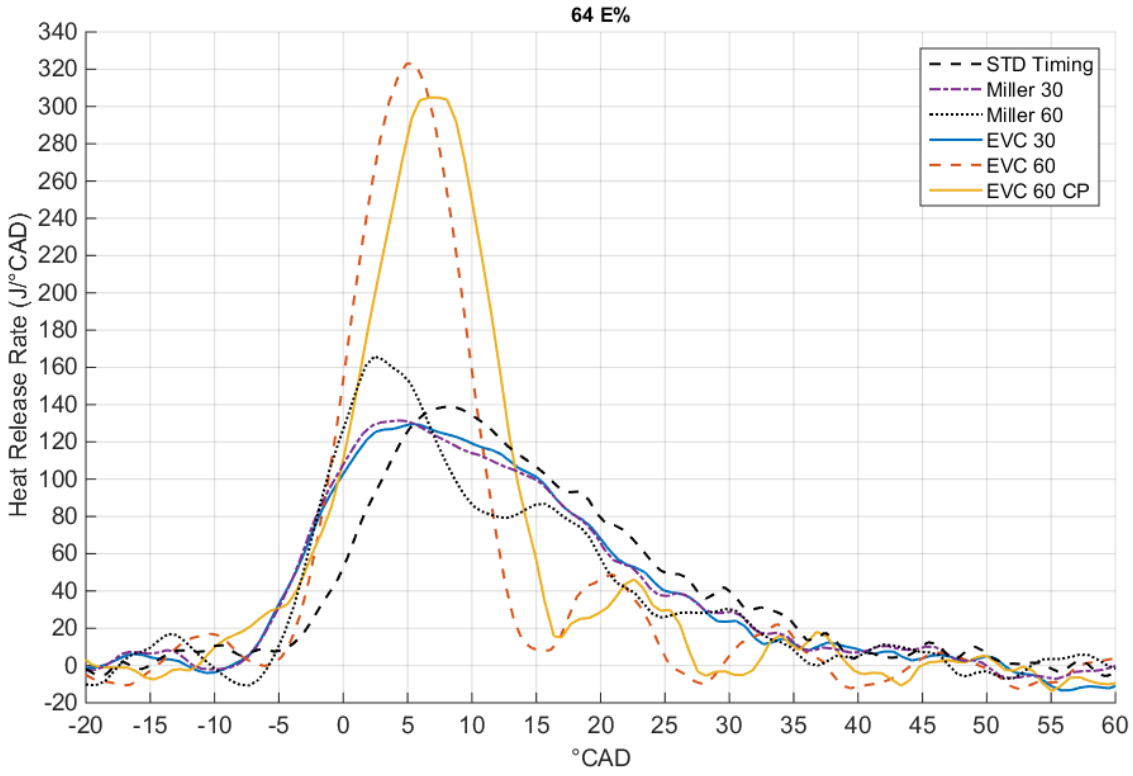

Figure 4.21. Cumulative heat release curves with different valve configurations with E% 64 at 50% load.

The combustion with the EVC 60 cases seems to behave in a similar manner than with 46 E% SR although the HRRs are slightly higher. A significant fraction of the STD Timing, Miller 30 and EVC 30 HRRs seem to originate from the bulk combustion of the lean mixture whereas the first and second combustion phases are less pronounced. The

high HRR peak with Miller 60 is rather interesting. It is unlikely that this peak is caused by the combustion of partially oxidized methane as the compression end temperature, in theory, is lower than in any of the other cases. Hence, the peak is probably caused by premixed Diesel combustion.

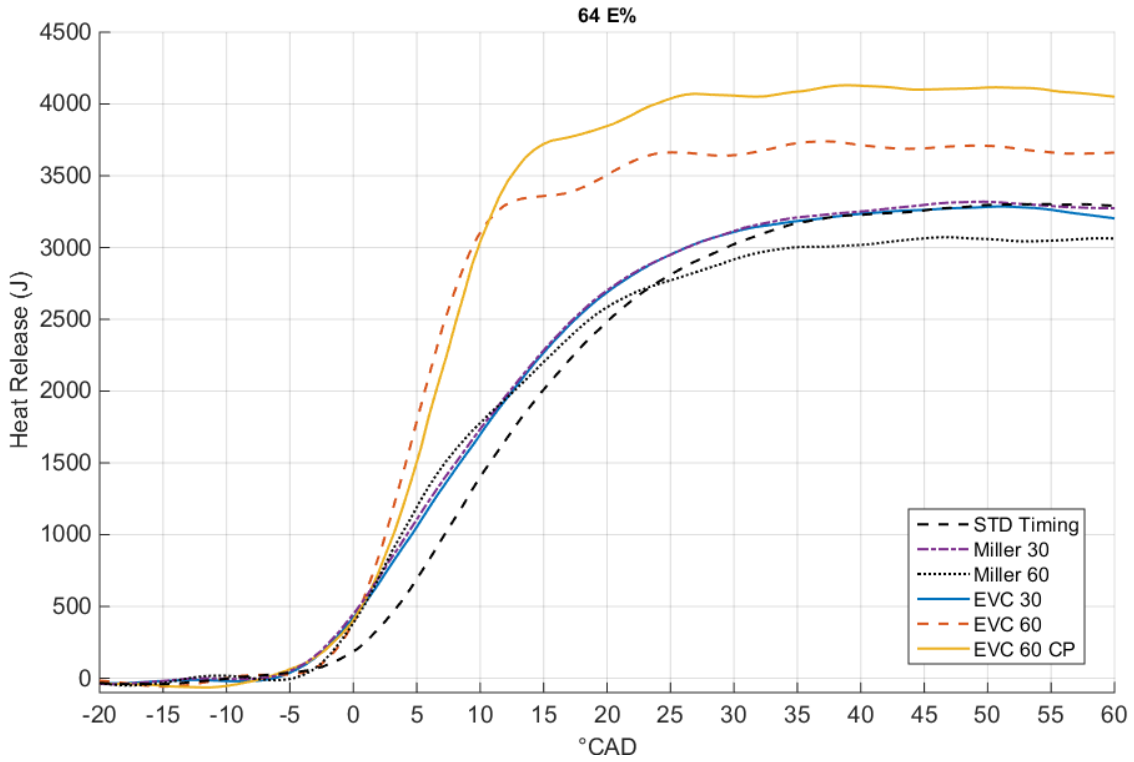

Figure 4.22. Cumulative heat release curves with different valve configurations with a substitution rate of 64 E%.

It is possible that the Diesel injector used is not performing as intended with high substitution rates and the atomization and mixing is rather poor. If this is the case, the mixing of the Diesel may be enhanced by the increased in-cylinder gas motion as the charge air pressure is increased with Miller 60. Although the combustion appears to start rather early and steadily, the HRR quickly decreases. This can be observed with both substitution rates but the phenomenon is more prominent with 64 E% SR. It seems that the combustion commences rapidly in the vicinity of the Diesel flame but then diminishes. Whether this is bulk quenching or just slow propagation of the flame in the lean methane-air mixture is difficult to conclude. However, it is probable that this rapid drop in the HRR results in high HC emissions.

4.3.2 Heat Release at 100% Load

The combustion event at full load differs substantially from the 50% load case. This can be observed in the HRR curves with different substitution rates with STD Timing in Figure 4.23. The heat release becomes substantially more rapid as the substitution rate increases whereas the 50% load case showed signs of combustion degradation with high substitution rates.

There can be a number of reasons for this phenomenon: The charge air temperature and the compression end temperature and pressure are higher, which promotes more rapid combustion. Moreover, the flow of the incoming methane-air mixture is different with

higher mass flow rates which may enhance mixing and in-cylinder turbulence. Furthermore, the amount of the ignition energy in Diesel form is much higher in all cases at 100% load. This will increase the in-cylinder temperature and thus promote the ignition of the lean methane-air mixture. In some cases, the methane lambda was also lower which, in turn, lowers the flammability temperature of the mixture.

The peak HRR gradually increases as the substitution rate is increased. The peak HRR with 55 E% SR (540 J/°CAD) is over twice the peak HRR in Diesel operation (260 J/°CAD). On the other hand, the start of combustion is also gradually retarded. This retardation can be identified as lower contribution of the premixed Diesel combustion to the HRR. This is substituted by the partially oxidized methane combustion which causes the high peak in HRR. The contribution of the third component, the slow combustion of the lean methane-air mixture, diminishes as the substitution rate increases and the methane lambda decreases.

The cumulative heat release curves plotted in Figure 4.24 and the corresponding mass fractions burned timings are shown in Figure 4.25 to further explain the combustion timing. The start of combustion, the x_{10}, is gradually retarded from the TDC in Diesel mode to approximately 4 °ATDC with 55 E% SR. Even though the ignition delay is clearly longer with high substitution rates, x_{50} occurs at approximately 10…11 °ATDC in all cases signifying that the combustion becomes more rapid with an increasing substitution rate. Moreover, there is a clear trend in advancing x_{90} as the substitution rate increases. The end of combustion is advanced from 23 °ATDC in Diesel mode to approximately 19 °ATDC with substitution rates of 40 E% and 55 E%. Overall, the combustion duration (from x_{10} to x_{90}) is decreased from nearly 25 °CAD to 15 °CAD.

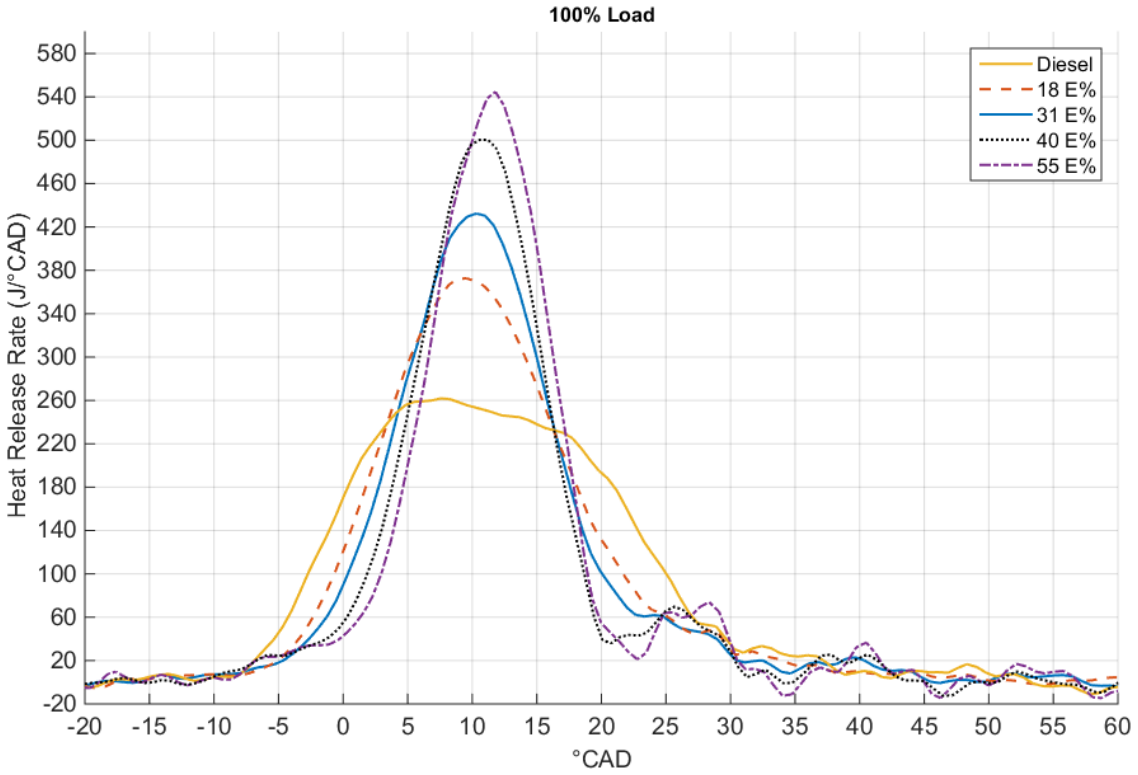

Figure 4.23. Calculated heat release rate with different substitution rates at 100% load.

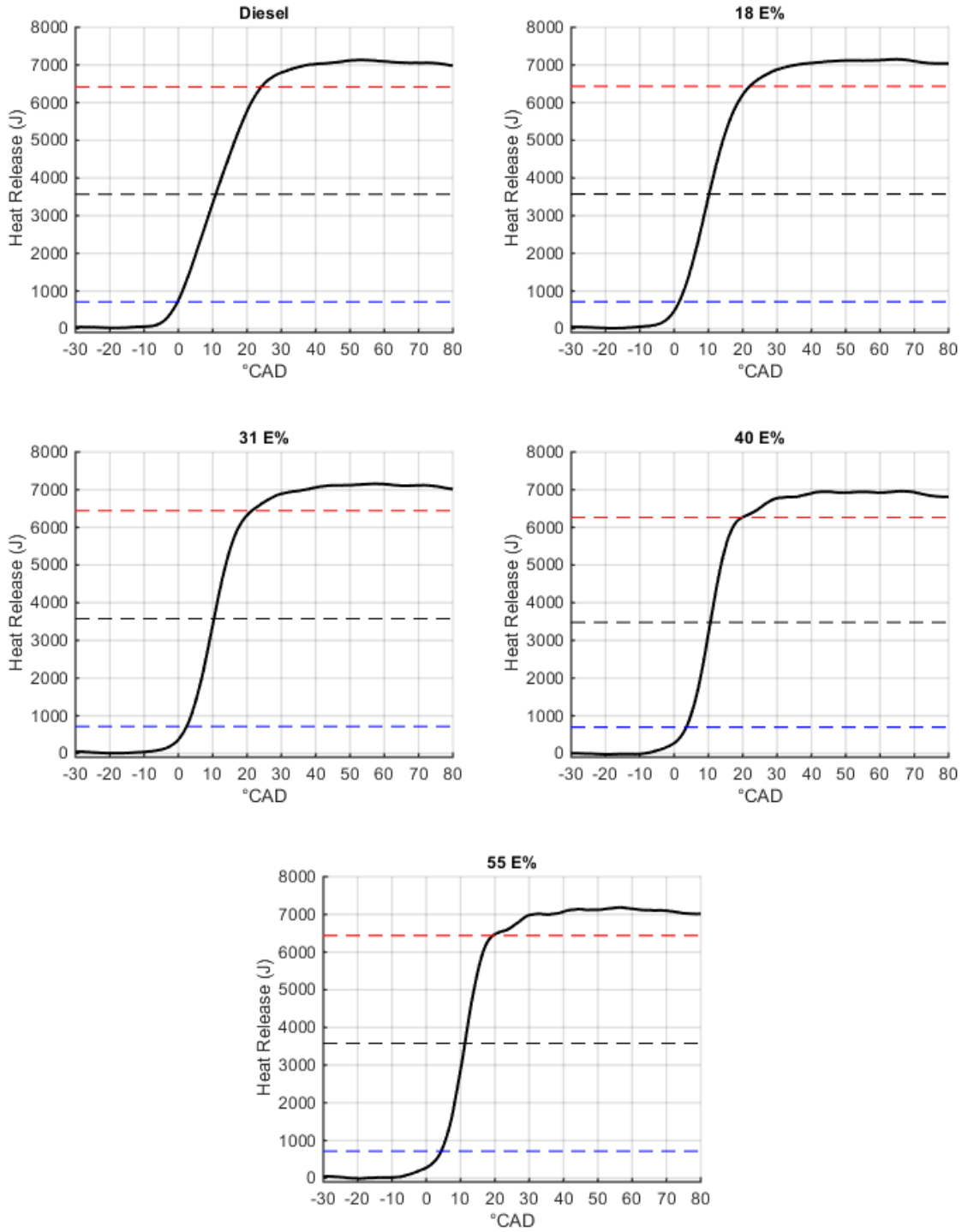

Figure 4.24. Cumulative heat release curves with different substitution rates at 100% load. The blue, black and red dashed lines indicate 10%, 50% and 90% mass fractions burned, respectively (percentage of maximum value). The substitution rate is noted above each

It is somewhat misleading to conclude that the increase in ignition delay is caused by the increasing substitution rate. The ignition delay is more likely to be affected by the lower amount of high-cetane Diesel fuel rather than by the higher amount of methane involved. With a lower Diesel amount the premixed portion of the Diesel fuel naturally decreases and thus delays the onset of the combustion. However, a part of the ignition delay is probably caused by the lower concentration of oxygen in the vicinity of the Diesel flame due to the presence of methane.

The HRRs and the cumulative HR curves in Diesel operation with the VVA strategies are plotted in Figures 4.26 and 4.27. The effect of valve timing on the heat release seems to be very small as was the case at 50% load. Only EVC 60 has a notable, adverse effect on the heat release. The figures clearly show how the IEGR introduced by EVC 60 lowers the HRR and the total HR. The other configurations seem to have little or no effect on the heat release.

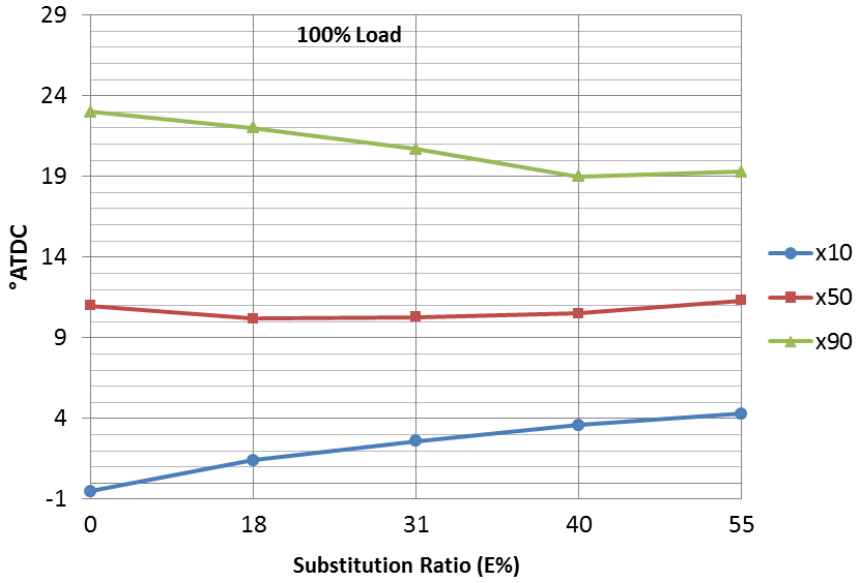

Figure 4.25. Development of mass fractions burned timing over substitution rate at 100% load.

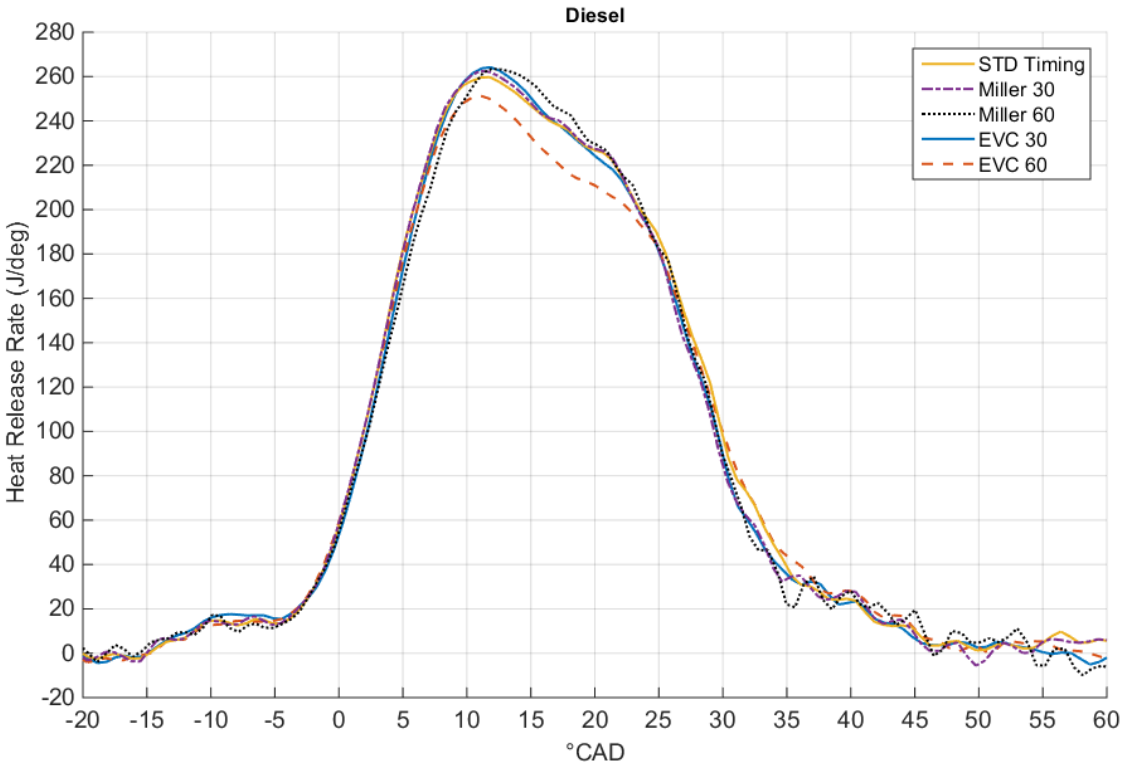

Figure 4.26. Calculated heat release rates with different valve configurations in Diesel mode at 100% load.

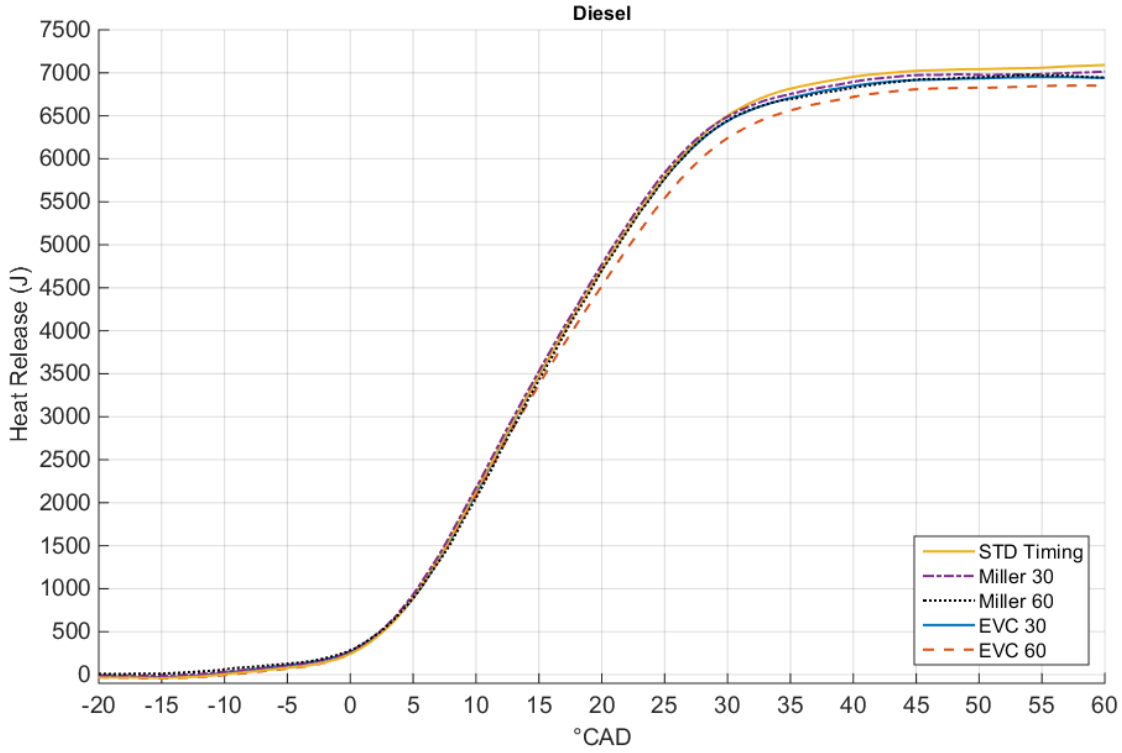

Figure 4.27. Cumulative heat release curves with different valve configurations in Diesel mode at 100% load.

The HRR curves with 31 E% SR presented in Figure 4.28 confirm the observation of EVC 60 preignition. The heat release commences already at approximately 8 °BTDC, three degrees before the start of the Diesel injection. This pre-ignition leads to a partial combustion of the mixture while the rest of the charge is ignited by the Diesel later after the TDC. The phases of the combustion may clearly be distinguished from the figure as two separate peaks. On the other hand, EVC 30 appears to have only a small effect on the total combustion event. The figure shows how the contribution of the partially oxidized methane combustion diminishes with the Miller cycles and the lean mixture combustion becomes more pronounced as the mixture temperature decreases.

The STD Timing combustion appears to be the most rapid of all cases if EVC 60 is not considered. The heat release rate reaches 400 J/°CAD while the lowest peak HRR is measured with Miller 60 at 335 J/°CAD. STD Timing, Miller 30 and EVC 30 behave in a similar manner, EVC 30 peaking slightly higher. However, only small differences may be observed in the total heats released in Figure 4.29. Miller 60 combustion is rather slow towards the end of combustion while EVC 60 is clearly distinguished. However, the total heats released are approximately the same in all cases.

The HRRs presented in Figure 4.30 with 55 E% SR show a substantially higher peak at above 440 J/°CAD with EVC 30 than was observed with 31 E% SR. On the other hand, STD Timing and Miller 30 peaks occur lower but slightly earlier in the cycle. It appears that the slight IEGR introduced by the EVC 30 combined with the lower lambda with 55 E% SR promotes the formation and combustion of partially oxidized methane and thus contributes to the second combustion phase. Miller 60 peaks at 330 J/°CAD which is approximately the same as with 31 E% SR. However, the peak is reached roughly 2 degrees earlier at 12,5 °ATDC.

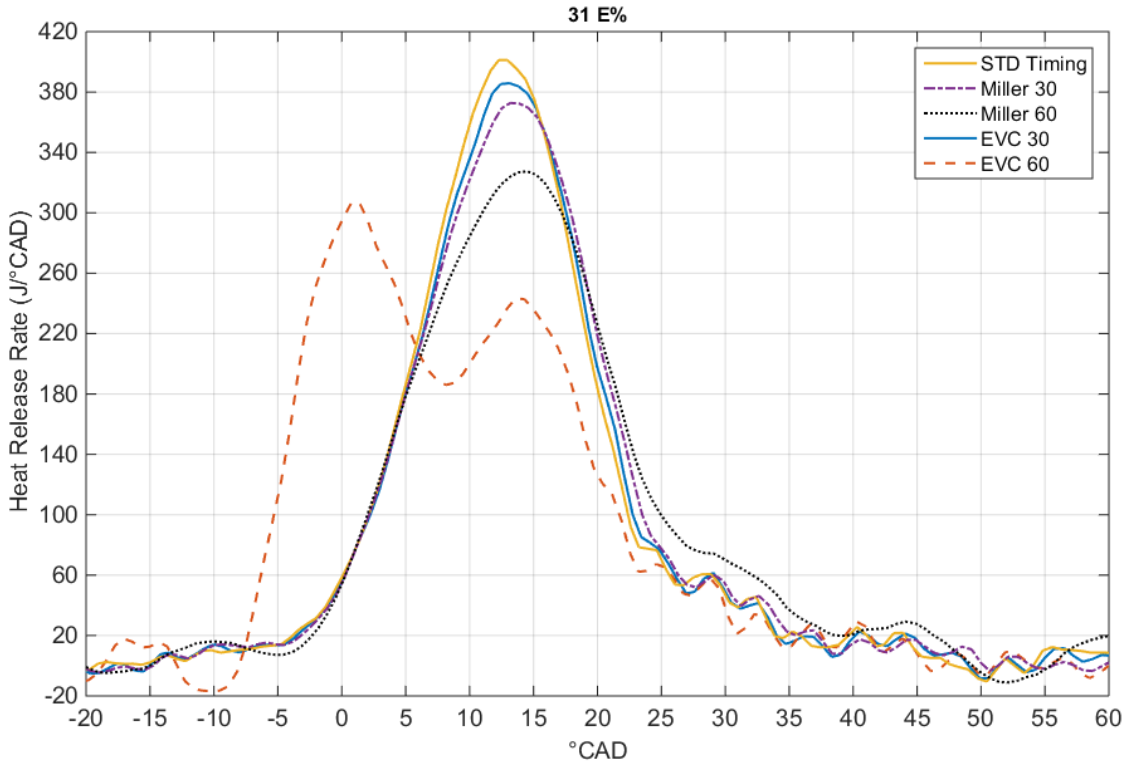

Figure 4.28. Calculated heat release rates with different valve configurations with 31 E% substitution rate at 100% load.

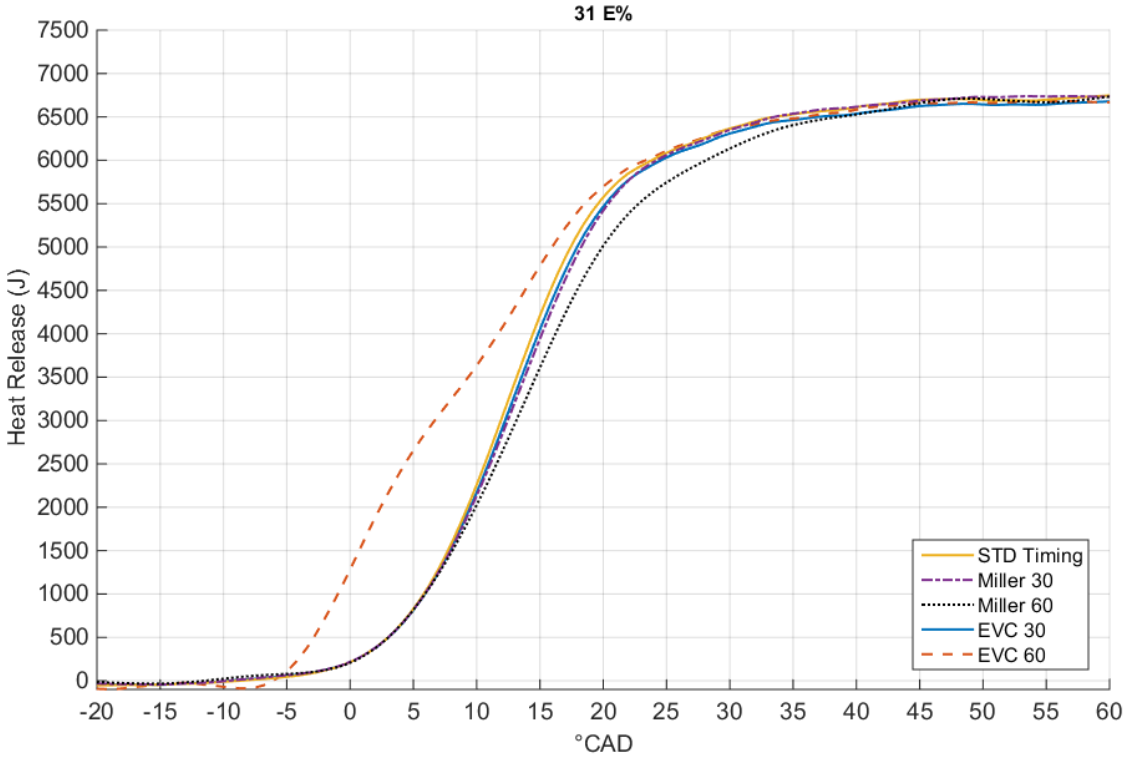

Figure 4.29. Cumulative heat release curves with different valve configurations 31 E% substitution rate at 100% load.

The cumulative HRs in Figure 4.30 with 55 E% SR show substantially more pronounced differences between valve configurations than those shown in Figure 4.29. Furthermore, the figure clearly presents how the combustion end timing is affected by the valve configuration. EVC 30 clearly promotes rapid combustion whereas the Miller timings have the opposite effect. The differences in the total heats released can be seen as a variation of the combustion efficiency. The differences are clearer than with 31 E% SR but much less prominent than at 50% load.

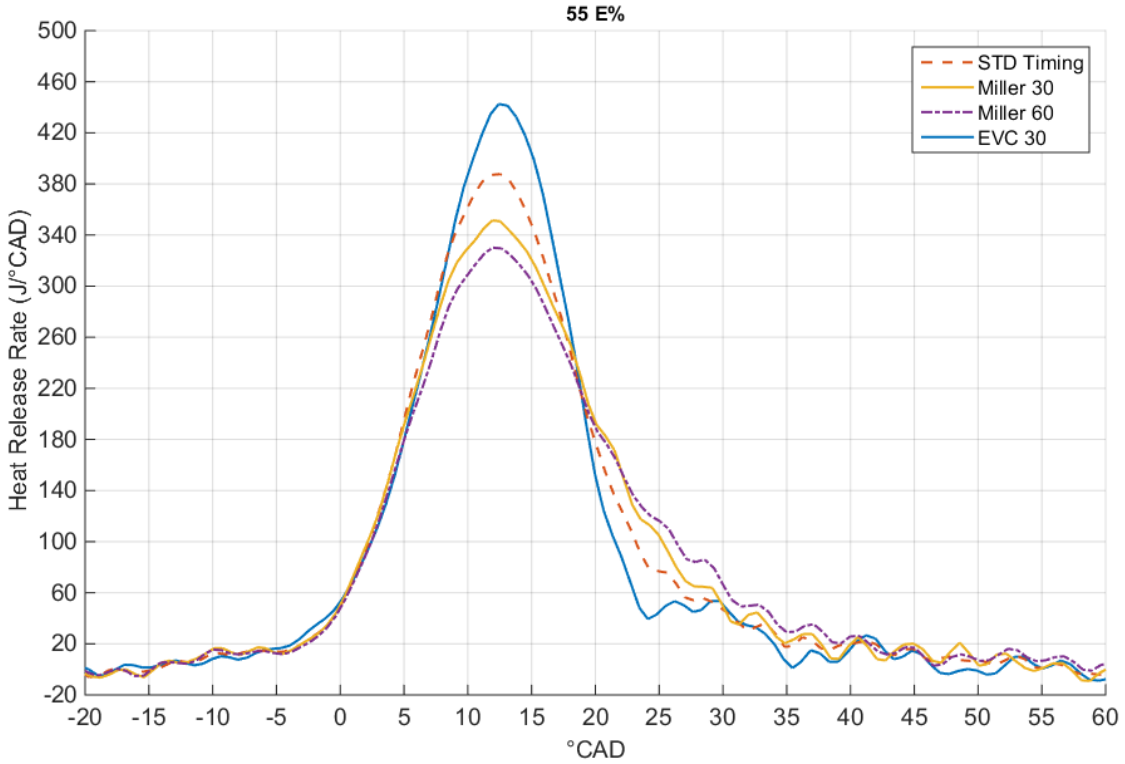

Figure 4.30. Calculated heat release rates with different valve configurations with 55 E% substitution rate at 100% load.

An interesting observation is that EVC 30 has an adverse effect on the combustion velocity with 31 E% SR whereas the combustion becomes more rapid with 55 E% SR. It is likely that the fuel-richer methane-air mixture with 55 E% SR reaches the flammability limit more quickly due to the partially oxidized methane and therefore contributes to the second combustion phase.

The full load conditions show less variation in the combustion between different valve configurations than do the 50% cases. This is most likely due to the stable ignition of the mixture as the Diesel fuel energy content is rather high even with E% 55. Moreover, the conditions are more prone to pre-ignition of the premixed charge with EVC 60. The factors that promote pre-ignition at full load are the slightly lower lambda of the methane-air mixture in some cases, the higher temperature of the residual exhaust gases and higher compression end temperature.

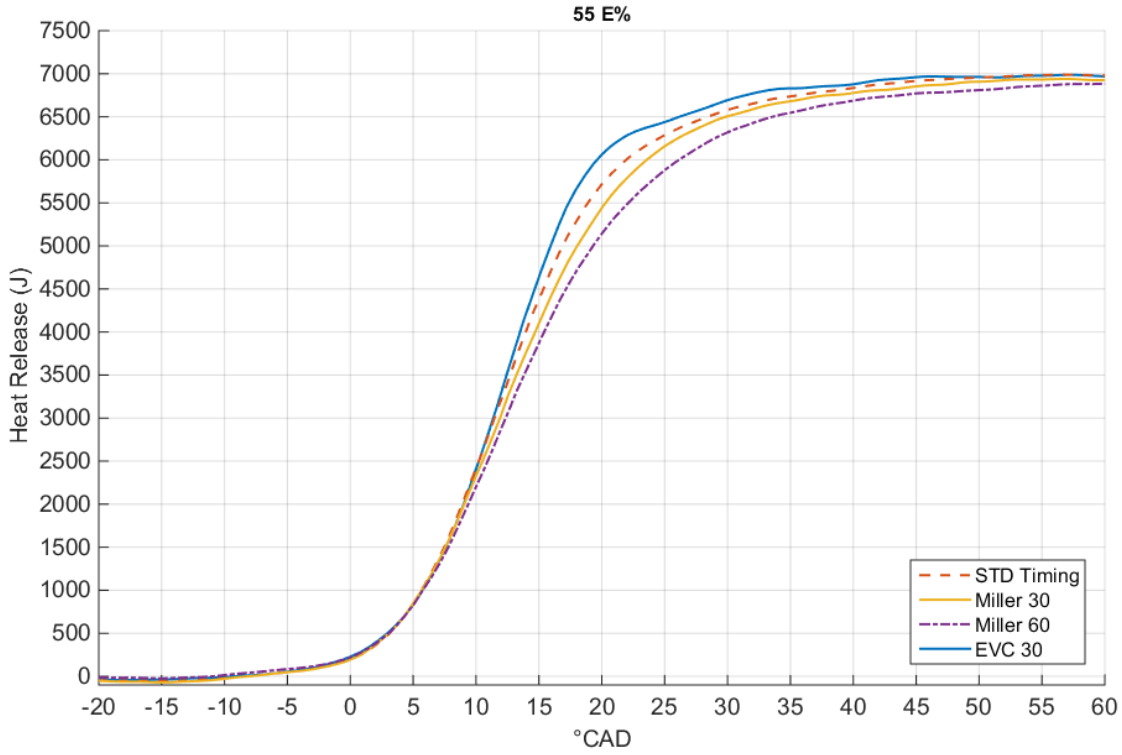

Figure 4.31. Cumulative heat release curves with different valve configurations with 55 E% substitution rate at 100% load.

4.4 Emissions

4.4.1 Hydrocarbon Emissions at 50% Load

The HC emissions at 50% load as a function of substitution rate are presented in Figure 4.32. In Diesel operation, there are little HC emissions regardless of engine load. As methane is admitted into the cylinder and the substitution rate increases, HC emissions suddenly increase a hundredfold even with relatively low substitution rates. The figure shows HC emissions of approximately 3700 ppm with 29 E% SR. Only a modest increase to 4600 ppm occurs with 46 E% SR. However, as the substitution rate is raised to 54 E%, the growth in HC emissions becomes steeper and the HC concentration climbs up to nearly 10 000 ppm as the substitution rate is increased further to 64 E%. It is evident that a combustion event producing very high HC emissions is of poor quality. Particularly the last two points with a high substitution rate are interesting due to the steep increase in the HC concentration.

The formation of HC emissions was covered in chapter 2.3. Five formation methods were identified:

1) Flame quenching at the combustion chamber walls
2) Combustion chamber crevices and top-land volume
3) Absorption of fuel vapour into the oil film covering the cylinder walls
4) Flame bulk quenching, incomplete combustion or complete misfire of a lean mixture
5) Slip of fresh mixture to the exhaust during in the beginning of the inlet stroke

The concentration of HC emissions relative to the methane mass flow rate is plotted in red in Figure 4.32. This confirms that the HC emissions per mass unit of fuel increase with the two highest substitution rates.

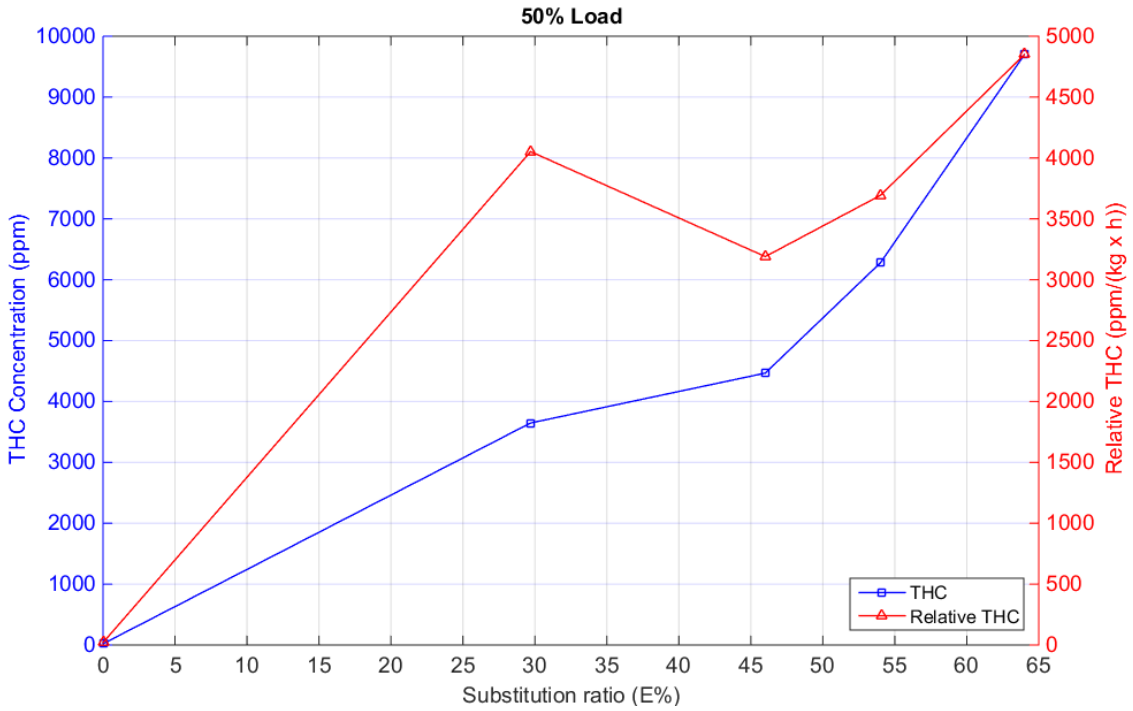

Figure 4.32. Exhaust unburned hydrocarbons (blue curve, left axis) and relative HC emissions(red curve, right axis) as a function of substitution rate at 50% load.

All five methods are possible and probable in the experimental engine. Literature suggests that the HC originating from the crevices is often the governing formation method contributing to a major part of the total HC emissions. It is logical that as the concentration of methane in the mixture increases, also the concentration of unburned methane in the exhaust gases increases proportionally. Nevertheless, the non-linear shape of the blue curve in Figure 4.26 suggests that the crevice effect is no longer the main contributor to the HC emissions with high substitution rates. HC formation methods 2), 3) and 5) may be considered to contribute more or less linearly to the HC emissions with an increasing substitution rate while methods 1) and 4) may cause a more progressive rise in HC emissions.

The HC emission measurements with different valve configuration cases at 50% load are presented in Figure 4.33. The Diesel reference case is not shown as the HC concentration was minimal at approximately 20 ppm in all cases. The HC concentration with 64 E% SR was significantly higher in all cases which was expected from the previous measurements. An exception in the trend can be seen in Miller 30 with 64 E% SR where the HC concentration slightly drops when compared with the STD Timing. However, the difference is rather small. Generally, the HC concentration increases as the Miller cycle is implemented and decreases as the EVC configuration is used.

The highest HC concentration is detected with Miller 60 with 64 E% SR at above 11 000 ppm and with 46 E% SR at approximately 5200 ppm. EVC 30 does not seem to significantly affect the HC with 46 E% compared with the STD Timing. On the other hand, with 64 E% the concentration drops to approximately 7500 ppm when it is nearly

10 000 ppm with STD Timing. The most interesting configuration is the radical EVC 60 which substantially reduces the HC emissions. Even with 64 E% SR, the concentration drops well below 2000 ppm.

Overall it appears that the formation of HC is very dependent on the mixture temperature. EVC 60 significantly increases the temperature while the Miller timing has an opposite effect. High temperature boosts the cold combustion and pre-combustion phenomena of methane. In addition, it aids in atomizing and vaporizing the Diesel fuel and thus causes a higher premixed combustion peak. However, the latter conclusion is questionable because neither a high HRR peak nor more rapid HRR can be distinguished in pure Diesel operation. Therefore it is probable that the effect of mixture temperature mainly affects the methane-related reactions. The decrease in methane lambda with EVC 60 does not explain the low HC emissions because EVC 60 CP with higher lambda produces nearly identical emissions.

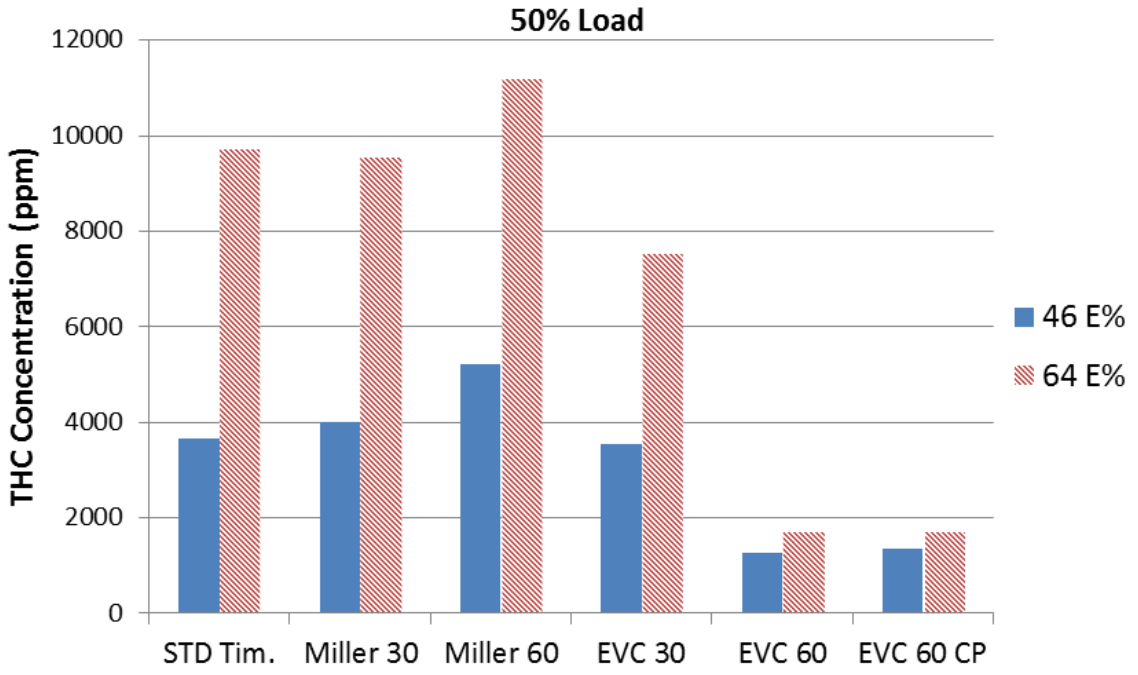

Figure 4.33. HC emissions with different valve timing configurations at 50% load. The blue columns represent a substitution rate of 46 E% and the red columns a substitution rate of 64 E%.

Another cause for high HC with the Miller timings could be the increased charge pressure or rather the increased pressure difference between the inlet and exhaust channels. More fresh charge containing methane would therefore slip during the overlap period. This effect is studied later in Chapter 4.6. Moreover, this slip could also be partly responsible for the deteriorating combustion efficiency with Miller 60 that was recorded in the cumulative HR. This is due to the loss of the energy content of the fuel escaping the combustion.

The similarities of the HRR curves with Miller 30 and EVC 30 in Figures 4.19 and 4.21 are interesting, especially as the recorded HC emissions are quite different. The mixture temperature is unlikely to substantially affect the HC emissions with Miller 30 and EVC 30 because of the similarities of the HRRs. Particularly, the blowdown of the exhaust gases is retarded with EVC 30. On the other hand, EVC 30 timing is rather conservative

which implies that only little residual gas can linger in the cylinder when the exhaust valve closes. It is therefore possible that part the HC oxidize late in the expansion cycle before the blowdown with EVC 30 as the expansion is prolonged. Furthermore, the slightly shorter valve overlap due to early exhaust valve closing decreases the HC emissions with EVC 30.

4.4.2 Hydrocarbon Emissions at 100% Load

The HC emissions at 100% load with different substitution rates are shown in Figure 4.34. There is a clear increase in HC emissions also at 100% load as the substitution rate increases. However, there is no evidence of deteriorating combustion efficiency in the heat release curves. Moreover, the HC emissions follow a rather linear curve which indicates that the emissions are most likely mainly formed by the methods 2), 3) and 5). Naturally, the formation methods 1) and 4) may exist but they seem to increase in proportion with the substitution rate.

The HC concentration starts from approximately 30 ppm in Diesel operation and rises up to 1270 ppm with 55 E% SR. The HC concentrations in all cases are generally much lower than those at 50% load. Interestingly, the relative HC emissions at 100% load decrease as the substitution rate increases. This is the contrary of what was recorded at 50% load.

The HC emissions with VVA and two different substitution rates are presented in Figure 4.35. The emissions behave as expected: the Miller cycles tend to increase the HC emissions whereas the EVC strategies decrease the emissions. EVC 30 with 55 E% substitution ratio is an exception to the rule as the HC concentration increases compared with the STD Timing. The overall HC concentrations in all valve configuration cases are substantially lower than at 50% load. This was already noticed in the first tests with the STD Timing and different substitution rates. The highest HC concentration with 31 E% SR is recorded with Miller 60 at approximately 2250 ppm. With 55 E% SR, the corresponding concentration is just above 2900 ppm. The HC emissions with 31 E% SR seem to react more dramatically to the Miller timings whereas the 55 E% SR cases are more prone to changes with the EVC timings.

It is evident that the higher HC emissions with the Miller cycles are linked to the retarded and lower HRR peaks. Especially the radical Miller 60 emits nearly twice the HC emissions with 31 E% SR when compared with the STD Timing. There are again two probable reasons for this: On one hand the lower mixture temperature deteriorates the oxidation of the HC and on the other hand the fresh charge slip from the inlet to the exhaust increases with the rising pressure difference. On the contrary, the increase in HC emissions with Miller 30 is small or nonexistent even though the combustion is rather slow particularly with 55 E% SR.

The HC emissions decrease even with E% 31 SR when EVC 30 is used even though the STD Timing combustion is more rapid. This differs from the previous observations where lower HC was generally linked to more rapid heat release. There are at least two possible causes for this: The dilution effect of the residual gases may cause the slightly lower HRR peak but the increased mixture temperature aids in HC oxidation later in the cycle. Another plausible is reason is that the retarded blowdown timing increases the oxidation time of the HC late in the expansion cycle.

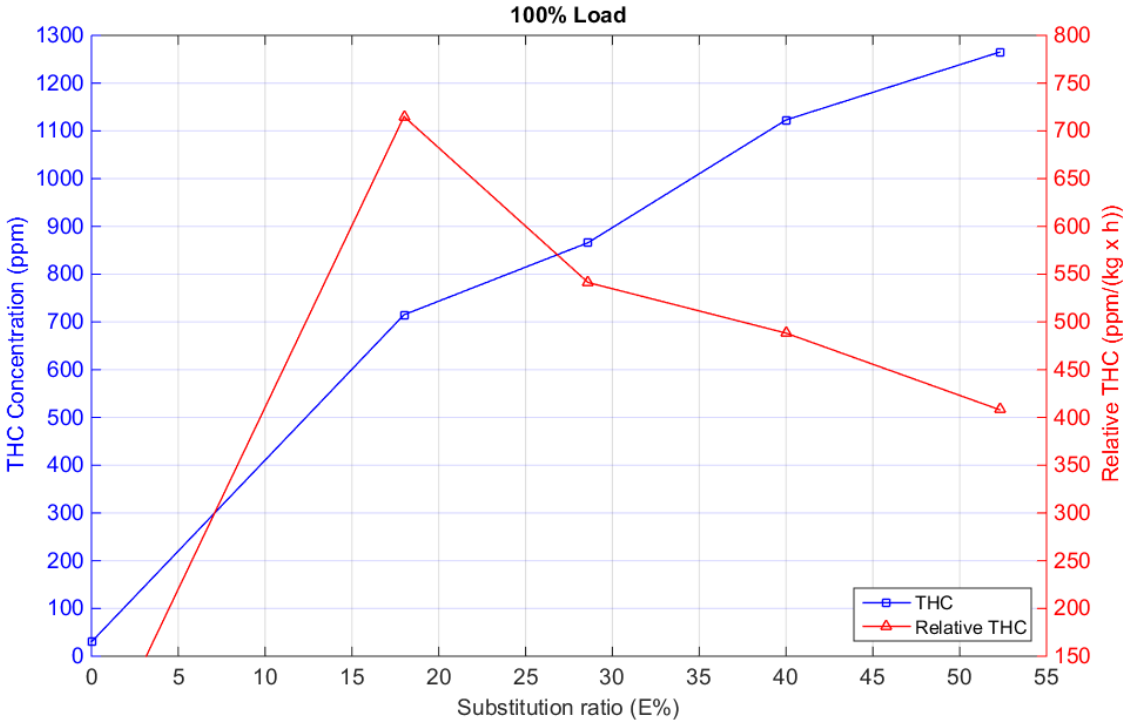

Figure 4.34. Exhaust unburned hydrocarbons (blue curve, left axis) and relative HC emissions (red curve, right axis) as a function of substitution rate at 100% load.

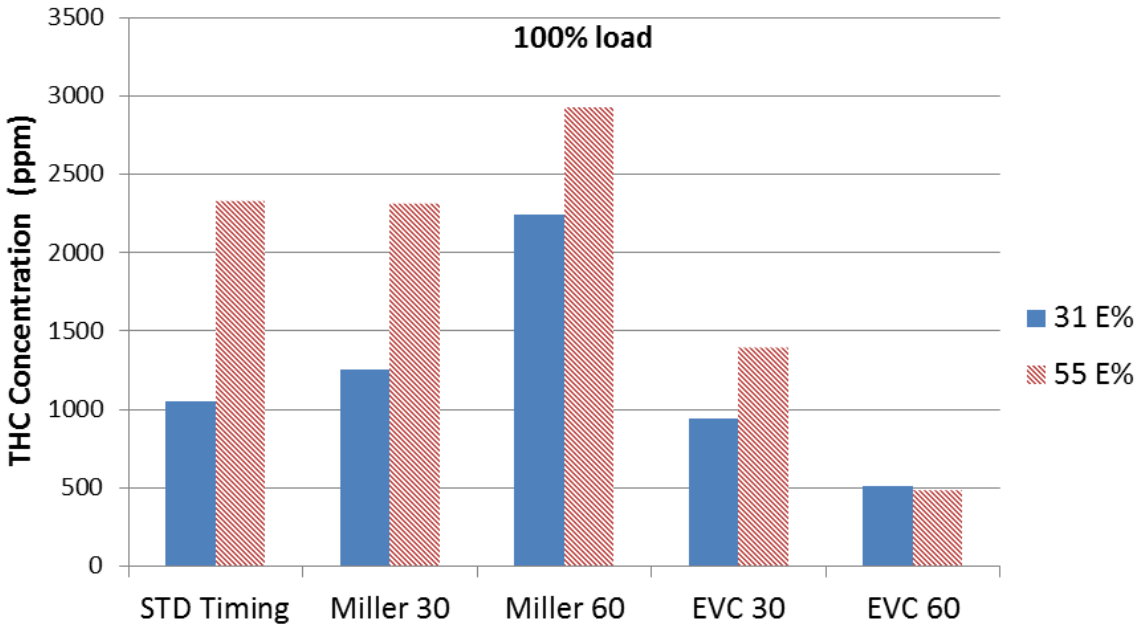

Figure 4.35. HC emissions with different valve timing configurations at 100% load. The blue columns represent a substitution rate of 31 E% and the red column a substitution rate of 55 E%.

4.4.3 Nitrogen Oxides at 50% Load

The formation of NO_x emissions was covered in Chapter 2.3. The governing NO formation type is the thermal NO which is highly dependent on peak cylinder temperature. NO_2, in turn, is formed in rapidly cooling exhaust gases and in the presence of the HO_2 radical. HO_2 is an intermediate product of methane low and moderate temperature oxidation. The measured NO_x emissions at 50% load as a function of substitution rate are presented in fractions of NO and NO_2 in Figure 4.36. The three curves represent the total NO_x (black), NO emissions (red) and NO_2 emissions (blue).

Figure 4.36 shows how the total NO_x decrease slowly at first and more rapidly with higher substitution rates. The total NO_x concentration is approximately 670 ppm in Diesel mode and it is lowered down to 410 ppm with 64 E% SR. The decrease is a result of lower NO concentration. According to literature, dual-fuel operation generally reduces the peak cylinder temperature which, in turn, leads to lower NO emissions. The peak cylinder temperature is reduced due to a lower pre-mixed Diesel HRR peak and slower combustion propagation. Furthermore, the Diesel flame front is smaller which may lead to lower prompt NO emissions.

It is important to notice the HRR curves in Figure 4.14 and the deteriorating combustion efficiency with high substitution rates. This will inevitably lower the in-cylinder temperature and thus hinder the thermal NO formation. Interestingly, the NO_2 concentration is multiplied from 60 ppm in Diesel operation to approximately 200 ppm with even modest substitution rates. Because NO_2 is formed via NO oxidation, the concentration of NO affects the reaction kinetics. Therefore it is possible that the effect of the lower combustion temperature promoting NO_2 formation is diminished by the lower NO concentration. This could explain the rather constant NO_2 concentration with an increasing substitution rate.

There are most likely two root causes for the increase in NO_2 emissions when methane is admitted into the cylinder: On one hand, the relatively low flame temperatures promote the oxidation of NO to NO_2 (equation 2.7) whereas the reverse reaction is hindered. On the other hand, the intermediate products from methane oxidation may contribute to NO_2 formation. One of such products is the HO_2 radical.

The NO_x emissions at 50% load with different valve configurations in Diesel operation and with substitution rates of 46 E% and 64 E% are presented in Figures 4.37, 4.38 and 4.39, respectively. The solid blue columns represent the NO emissions and the striped part of the column indicates the NO_2 fraction. A very expected result is seen in pure Diesel operation where the NO_x emissions decrease with the Miller timings while they increase with both EVC timings.

While the NO concentration increases with the rising temperature, it is interesting how the NO_2 concentration also increases with EVC 30 and EVC 60 even in Diesel mode. There are at least two possible reasons for this: The NO in the residual exhaust gases linger in the cylinder and hence the NO concentration of the next cycle is increased. This will shift the equilibrium towards the formation of NO_2. Another reason could be the delayed blowdown and the increased time for NO oxidation.

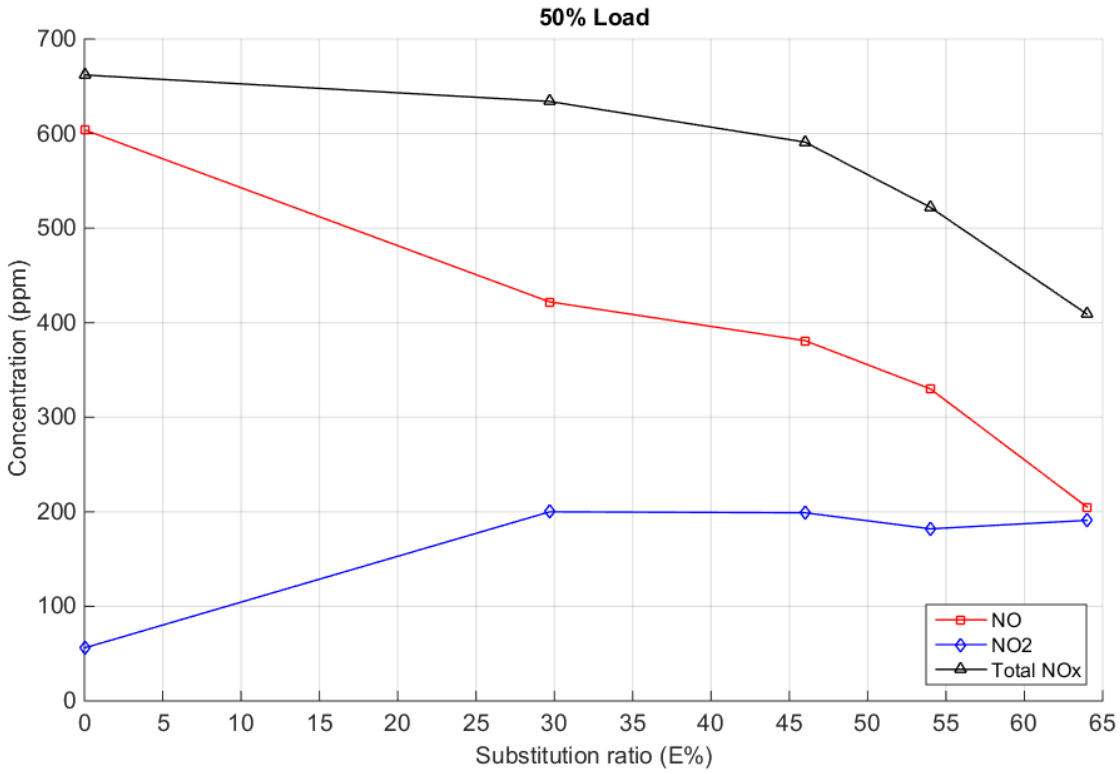

Figure 4.36. NO (red curve), NO2 (blue curve) and total NOx (black curve) concentrations as a function of substitution rate at 50% load.

The STD Timing emissions in dual-fuel mode with 46 E% SR are lower than in Diesel operation as was observed before. Surprisingly, the NO_x emissions increase from the STD Timing case with both Miller 30 and Miller 60. This increase is even more evident with 64 E% SR presented in Figure 4.39. The cause for higher NO_x emissions with Miller timings in both cases is the early HRR peak as was seen in Figures 4.19 and 4.21.

There are a number of reasons that could cause the early and more rapid heat release with the Miller timings. The increased charge pressure changes the flow characteristics of the mixture entering the cylinder. This naturally affects the in-cylinder gas motion which may enhance the mixing of the fuel. Particularly the premixed part of the Diesel fuel is important for the formation of NO_x. Moreover, the mixture temperature at the end of the compression stroke is lower which may also interfere with the fuel mixing. A more intuitive conclusion would be that lower mixture temperature would result in poorer mixing. However, it is possible that the Diesel fuel is better mixed due to the increased charge air pressure with the Miller configurations and hence leads to higher NO emissions.

The NO_x emissions also increase with the EVC timings in dual-fuel mode as was the case in the Diesel mode. The increase is modest with EVC 30 but very clear with EVC 60. This is, as stated before, a cause of the increasing peak cylinder temperature due to the hot residual gases. Both NO and NO_2 emissions are higher in the dual-fuel cases with EVC 60 than in the Diesel reference case due to the more rapid combustion. Interestingly, the NO_x emissions with Miller 60 are lower with the 64 E% substitution rate than with 46 E% SR even though the HR is more rapid with 64 E%. This may result from the slightly reduced oxygen concentration in the cylinder due to the higher amount of methane with 64 E% SR or from the lower temperature during the late expansion phase.

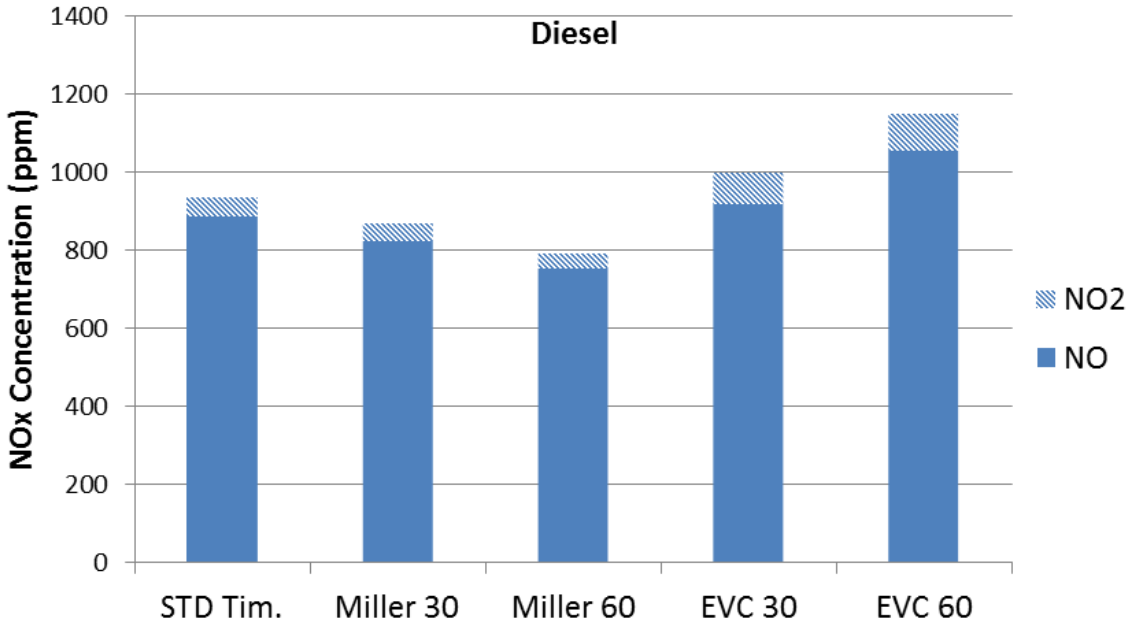

Figure 4.37. NOx emissions with different valve configurations at 50% load in Diesel mode.

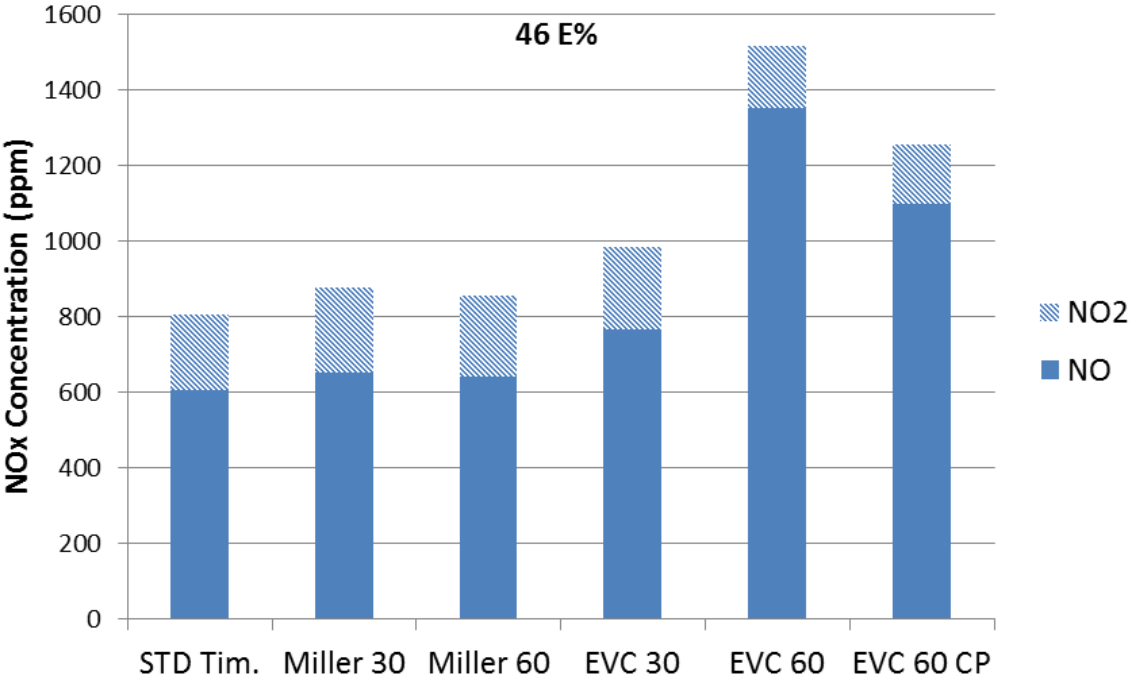

Figure 4.38. NOx emissions with different valve configurations at 50% load with 46 E% substitution rate.

The increased charge air pressure with EVC 60 CP seems to dramatically affect the NO emissions. Fundamentally, the increased charge air pressure lowers the mixture temperature and lowers the methane lambda. It is evident that the combustion peak temperature decreases but whether this is mostly caused by the lower mixture temperature or higher lambda is unclear. However, the decrease in NO with the CP case explains some

of the differences in the total heats released as the endothermic formation of NO binds some of the heat released.

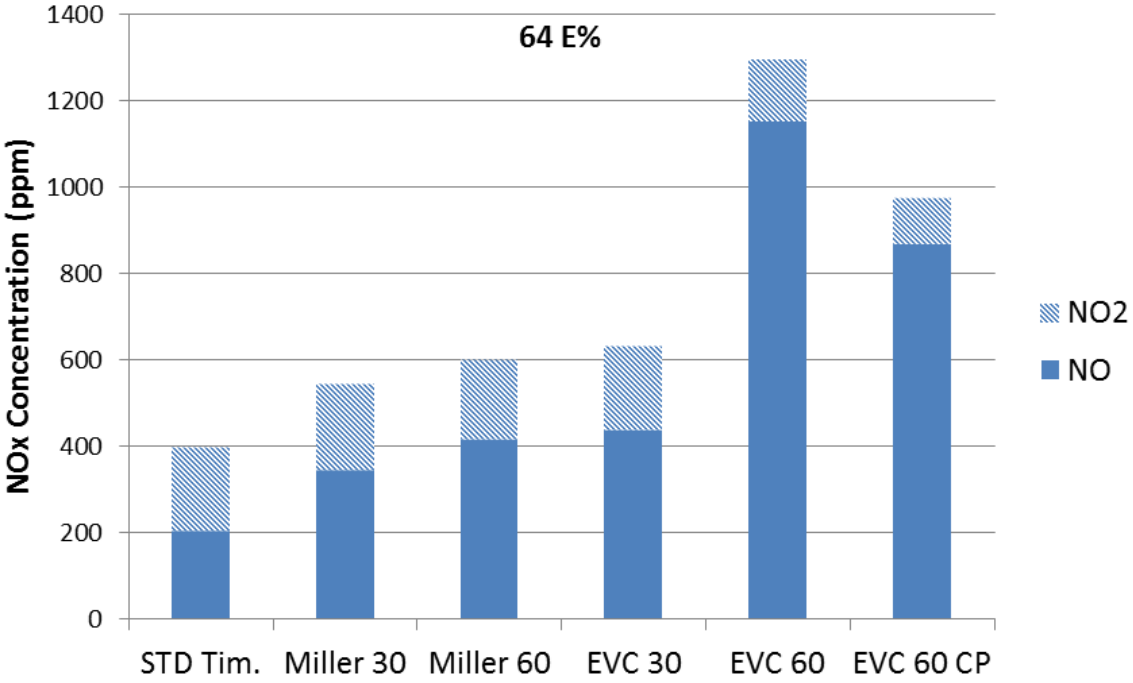

Figure 4.39. NOx emissions with different valve configurations at 50% load with 64 E% substitution rate.

It can also be observed how the NO_2 emissions decrease with EVC 60 even though the total NO_x increases substantially. As the combustion becomes more rapid and radical, the amount of intermediate temperature products that promote NO_2 formation is reduced which, in turn, reduces the concentration of NO_2. Moreover, the combustion temperature most likely favours the formation of NO over NO_2.

4.4.4 Nitrogen Oxides at 100% Load

Figure 4.40 presents the corresponding NO_x emission curves at 100% load. The concentrations linger at nearly 1900 ppm and are significantly higher than at 50% load. The NO emissions show only a slight decrease as the substitution rate increases while NO_2 increases modestly. Total NO_x concentration is nearly constant although it decreases by approximately 70 ppm with substitution ratios of 40 E% and 55 E%. This decrease is mainly NO. On the other hand, the NO_2 concentration rises by only approximately 30 ppm from the Diesel reference values.

The concentration of NO implies that the in-cylinder peak temperature does not significantly change as the substitution rate is increased at 100% load. Furthermore, the high peak temperature hinders the formation of NO_2. The slight increase in NO2 is most likely caused by the increasing formation of the intermediate products from the methane oxidation.

The NO_x emissions in Diesel operation and with substitution rates of 31 E% and 55 E% with different valve configurations at 100% load are presented in Figures 4.41, 4.42 and 4.43, respectively. In Diesel mode, only Miller 60 and EVC 60 show a notable decrease in the NO_x concentration. The decrease is most evident with EVC 60 with the expense of

slightly deteriorating combustion which was observed in the heat release graphs. On the other hand, EVC 30 seems to decrease the NO emissions while the NO_2 concentration is increased.

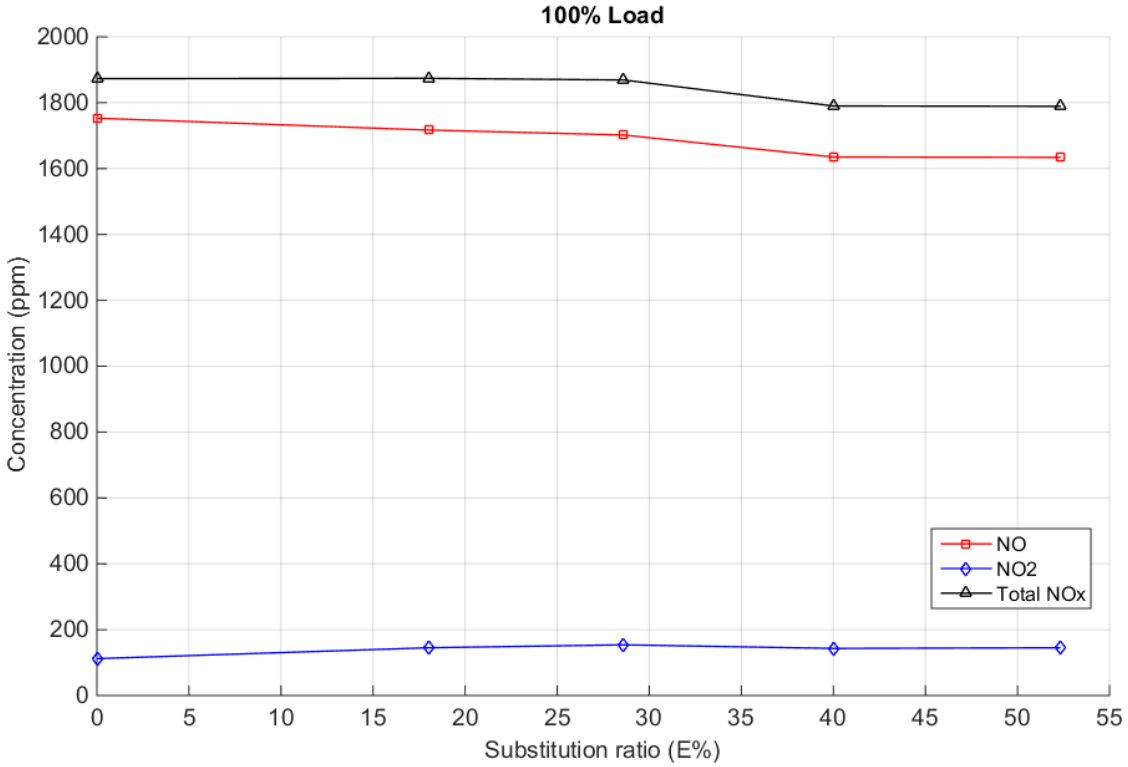

Figure 4.40. NO (red curve), NO2 (blue curve) and total NOx (black curve) concentrations as a function of substitution rate at 100% load.

The NO_x emissions with 31 E% SR are generally approximately 200 ppm higher than those in Diesel operation. This is caused by the significantly higher cylinder pressures and HRRs with 31 E% SR and the resulting rise in the in-cylinder temperature. The concentration of NO_2 is significantly increased in all cases which was also noted before with 50% load in DF operation. It seems that even a modest amount of methane in the mixture causes a substantial increase in the NO_2 concentration. With 31 E% SR, only Miller 60 shows significant reduction in the NO_x emissions down to 1100 ppm while a slight decrease was observed with Miller 30.

With 55 E% SR, the STD Timing emissions are the highest recorded in the VVA measurements. The NO_x concentration climbs up to nearly 1700 ppm. EVC 30 also shows rather high NO_x concentration of over 1500 ppm. Even though a very early pre-ignition occurred with EVC 60, the NO_x emissions are rather low at below 1200 ppm. On the contrary, the Miller timings show a significant decrease in NO_x down to approximately 1200 ppm.

The concentration of NO in the exhaust gases appears to be linked to the high HRR and pressure peaks. On the other hand, it does not seem to be affected by the presence of methane in the combustion. On the contrary, the NO_2 emissions increase significantly even with modest substitution rates as was the case with 50% load. This is evident at both load conditions and this was observed in all measurements. The concentration of NO_2 does, however, decrease when the peak pressure and HRR rise further.

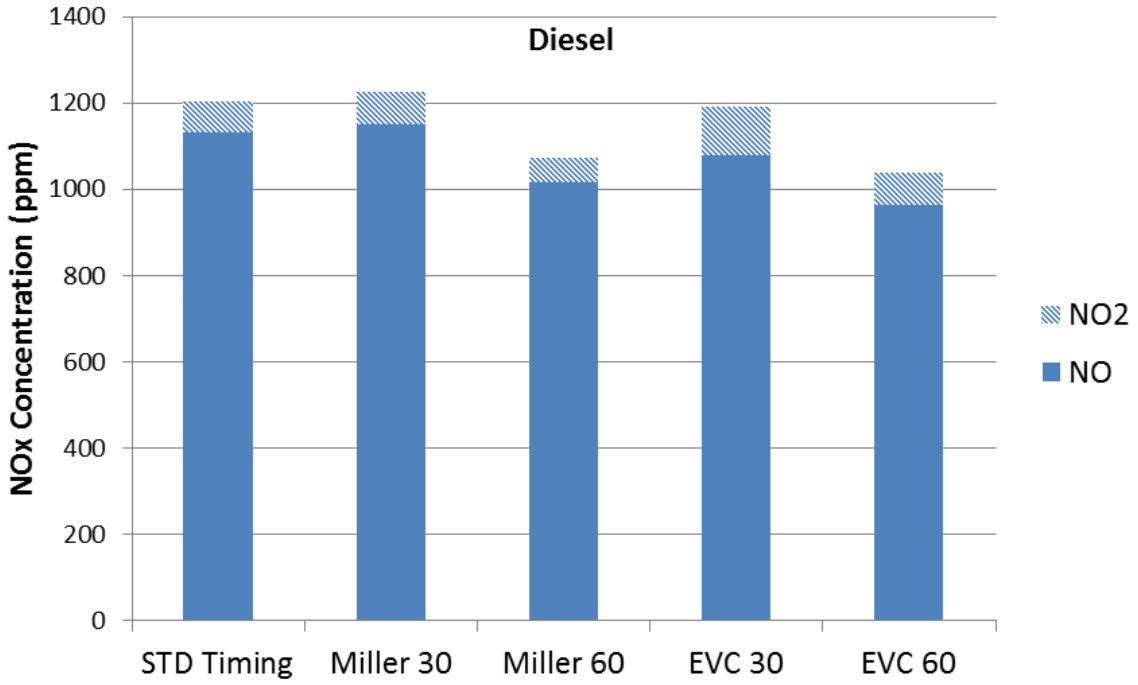

Figure 4.41. NOx emissions with different valve configurations at 100% load in Diesel mode

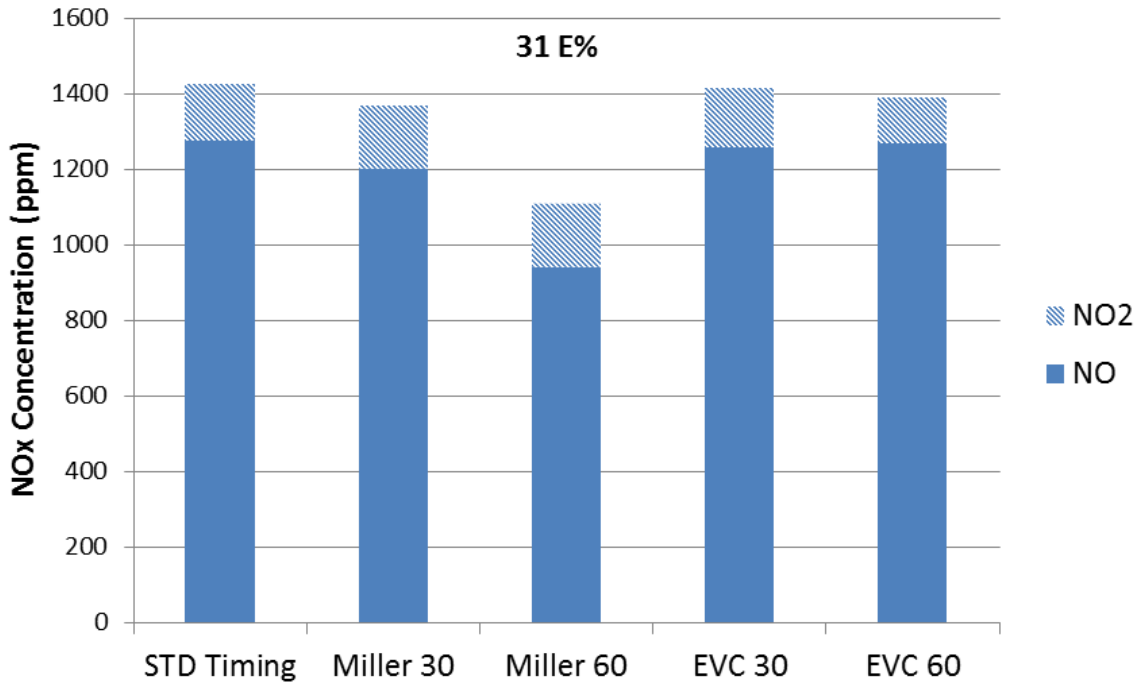

Figure 4.42. NOx emissions with different valve configurations at 100% load with 31 E% substitution rate.

It is important to notice the lower NO_x emissions with 55 E% SR with EVC 30 when compared with the STD Timing. This is interesting because also the HC emissions were lower than with the STD Timing, for example. Generally high NO_x concentration is consequently linked to the high HRR and cylinder pressure. In either case, the NO_x concentration should intuitively be higher with EVC 30. It is plausible that the dilution effect of the IEGR causes the lower NO_x emissions whereas the higher mixture temperature promotes HC oxidation. On the other hand, the lower HC may result from

the longer expansion and oxidation time as stated before. However, this shows that the HC and NO_x emissions may be reduced simultaneously with IEGR in certain conditions.

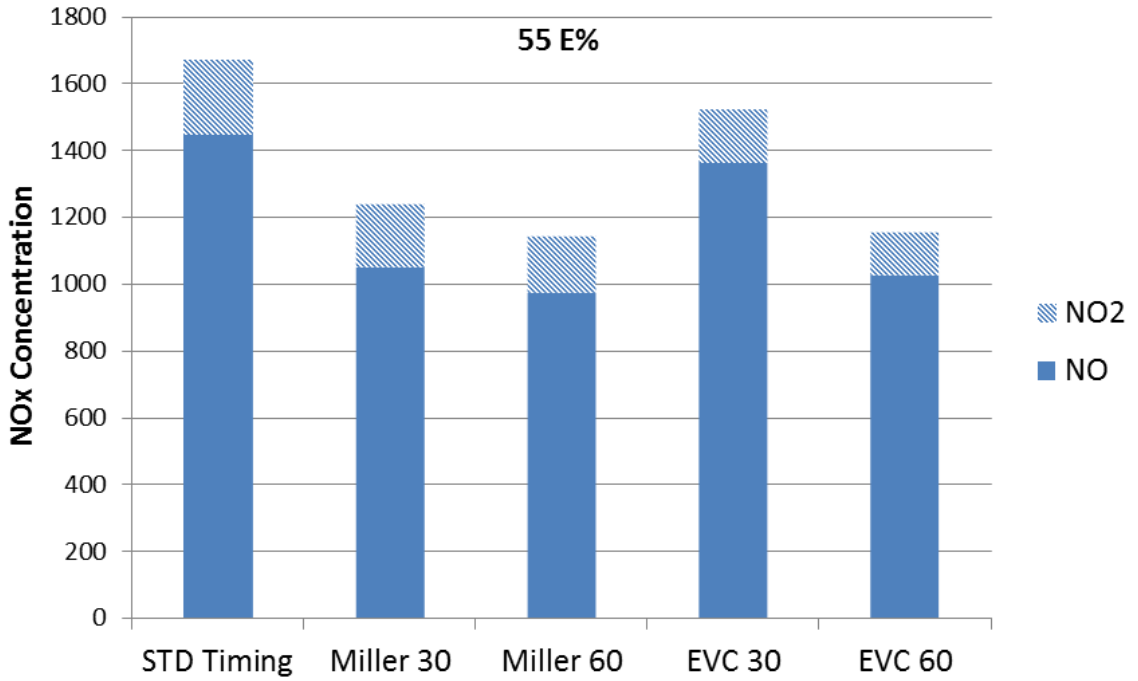

Figure 4.43. NOx emissions with different valve configurations at 100% load with 31 E% substitution rate.

4.5 The Effect of Valve Overlap on Hydrocarbon Emissions

The overlapping opening time of the inlet and exhaust valves causes a part of the mixture to slip directly in the exhaust port. This effect is more prominent when the pressure in the inlet ports is higher than the pressure in the exhaust. This is referred to as positive ∆p (pi > pe). Moreover, the pressure pulses in the ports may increase the methane slip.

In order to find out how large a portion of the measured Miller timing HC emissions originate directly from the scavenging, the 50% load case with 64 E% substitution rate was studied. The exhaust gas pressure was increased above the inlet pressure so that ∆p was negative. In such a case very little methane should slip directly from the cylinder. Moreover, another test was carried out with only Miller 60 and E% 64. In this test, the inlet valve opening was kept similar but the position of the lobe was retarded. This effectively decreases the valve overlap and should have the same effect as negative ∆p. The results of both tests are shown in Figure 4.44.

The left side of Figure 4.44 clearly shows how the HC emissions decrease by approximately 1300 ppm with Miller 60 and by 1200 ppm with Miller 30 as the ∆p is changed from positive to negative. Both Miller timings have similar valve opening curves and valve overlap periods. It is safe to conclude that at least this part of the HC emissions originate directly from the gas exchange process. The ∆p values were ±0.2 bar for Miller 30 and +0.4 and -0.1 bar for Miller 60.

The right side of the figure also shows a decrease in HC emissions as the overlap period is shortened. Miller 60_30 represents a case where the Miller 60 valve opening curve was maintained but it was shifted 30 degrees later in the cycle. Miller 60_60 shifted the curve 60 degrees later. Miller 60_30 decreased the emission approximately 950 ppm whereas Miller 60_60 showed a decrease of 1750 ppm. This experiment was carried out with positive ∆p and some unintended valve overlap is still possible due to valve bounce. Therefore it may be possible that the true methane slip is even higher. The valve profiles were presented in Figure 4.5.

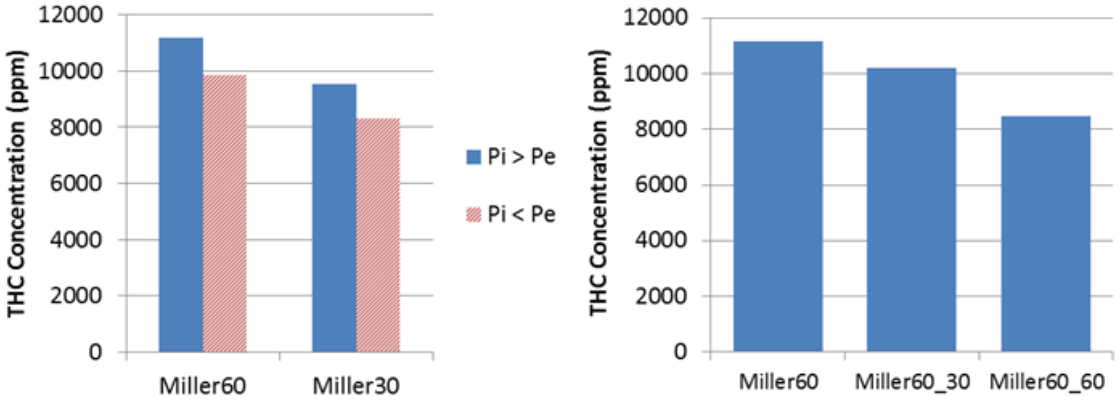

Figure 4.44. Left: HC emissions with varied ∆p. The blue columns represent the pressures used in the previous experiments (positive ∆p) whereas the red columns have increased exhaust gas pressure (negative ∆p). Right: Miller 60 HC emissions with different valve overlaps

The methane slip from the scavenging accounts for approximately 15…25 % of the total HC emissions with 64 E% SR according to these tests. The HC originating from this source can be considered to increase in proportion with the substitution rate as the methane-air mixture is considered rather homogeneous. However, ∆p has a substantial effect on the scale of the slip as is seen in Figure 4.44.

The HC emissions from scavenging could be completely avoided by better managing the methane injection timing so that the methane is injected only after the exhaust valve is fully closed. However, in order to minimize the possible residual methane in the inlet channels between cycles, the methane injector should be located close to the inlet valve. If the gas injector is capable of injecting the methane in a relatively short time, even a more remote location in the manifold can be used. In these experiments, the methane injection was complete before the TDC in all cases.

4.6 Cycle-to-Cycle Variation

Cycle-to-cycle variation is an important factor in determining the controllability of the combustion. There are several indicators that can be used to calculate the cycle-to-cycle variation. The most commonly studied parameters are the maximum cylinder pressure, HRR and IMEP. The variation of maximum cylinder pressure is studied in this chapter.

Cycle-to-cycle variation is generally caused by an inhomogeneous methane-air mixture, variation in Diesel spray dispersion and atomization and variation in mixture flow. Normally, cycle-to-cycle variation is higher in Otto cycle engines than in Diesel engines due to mixture inhomogeneity. The variation is usually measured with the coefficient of

variance (COV) that is the ratio of the standard deviation and the mean of the maximum measured pressures.

Figure 4.45 presents the coefficient of variance with different valve timing configurations and substitution rates at 50% load. The blue columns represent the Diesel mode. COV in Diesel operation seems to be generally lower than in dual-fuel mode, which was expected. However, with STD Timing and 46 E% SR the COV is lower and slightly so with EVC 60. The measurements with a substitution rate of 64 E% show the highest variations in all cases except with Miller 60. Here the COV with 46 E% is very high at 0.0225. Miller 60 causes the highest variations in all cases.

A similar graph for COV at 100% load is shown in Figure 4.46. The values are generally significantly lower than at 50% load. The differences in COV at 100% load between various valve timing configurations are smaller and the trends are less evident. A high substitution rate still appears to have the tendency to increase COV. The highest COV occurs with 55 E% SR in all cases except with Miller 30. On the other hand, the effect of the modest substitution rate of 31 E% SR is less clear as the COV in Diesel operation is higher with both Miller timings. An interesting observation is that COV with EVC 60 and 31 E% SR is very low. It seems that the occurring pre-ignition is somewhat stable and the cyclic repeatability is very good.

It is probable that high substitution rate increases the cyclic variations due to several reasons. The larger amount of methane increases the relative amount of the premixed mixture energy of the total fuel energy. This makes the combustion more prone to variations in methane-air mixture quality. Furthermore, the smaller quantity of Diesel injected results in a smaller volume of methane to be in a direct contact with the Diesel flame, which makes the ignition more unstable. In addition, the injected Diesel spray properties and atomization may deteriorate with very low injection amounts unless a special injector is used.

The more stable nature of the full load combustion is mostly due to the same phenomena. The Diesel fuel quantity even with a high substitution rate is absolutely higher while the combustion chamber volume is the same as at 50% load. Therefore the Diesel injector will function as intended while the Diesel flame is more widespread. Moreover, the methane-air mixture and the total lambda of the combustion is often lower at full load which is beneficial for the combustion of the premixed methane-air mixture. Finally the higher mass flow or air increases the in-cylinder turbulence that enhances fuel mixing.

The sample sizes for the cycle-to-cycle calculations were rather small, only 24 cycles for each column presented in the graphs. Thus it was imperative to estimate the statistical significance of the results. The confidence intervals at 95 % confidence level were calculated for each set of cycles according to the equations listed in Chapter 3.3.3. The confidence intervals are presented in Appendix A3. The intervals were rather narrow in comparison with the maximum deviations of the maximum cylinder pressures which denotes that the calculations are statistically significant.

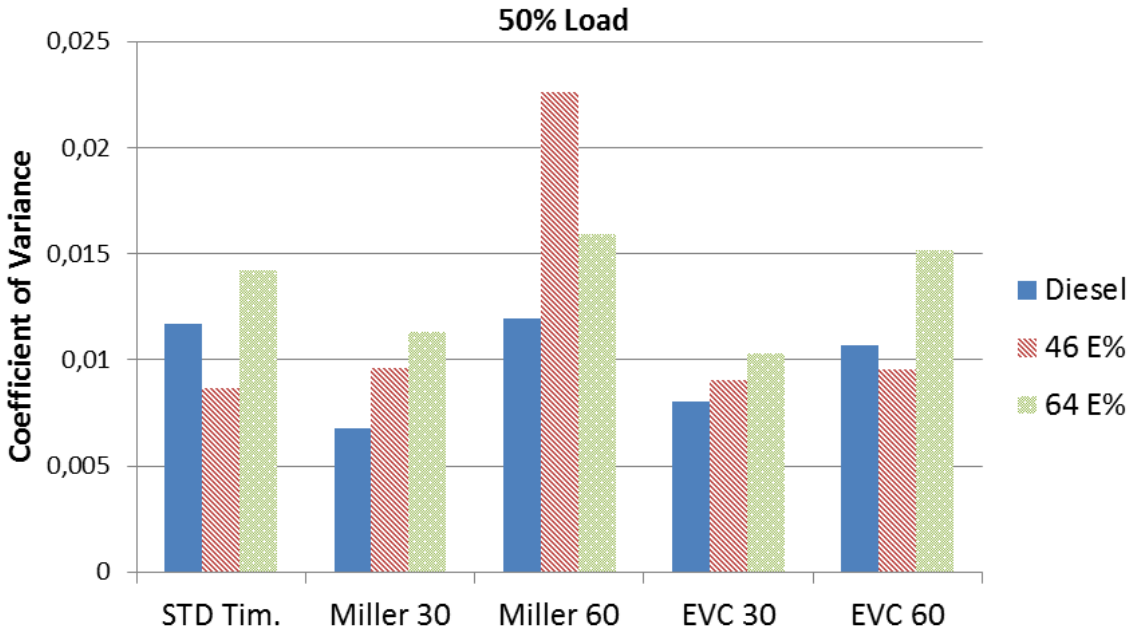

Figure 4.45. Coefficient of Variance with different valve timing configurations at 50% load. The blue columns represent the Diesel mode, red columns 46 E% and green columns 64 E% substitution rates.

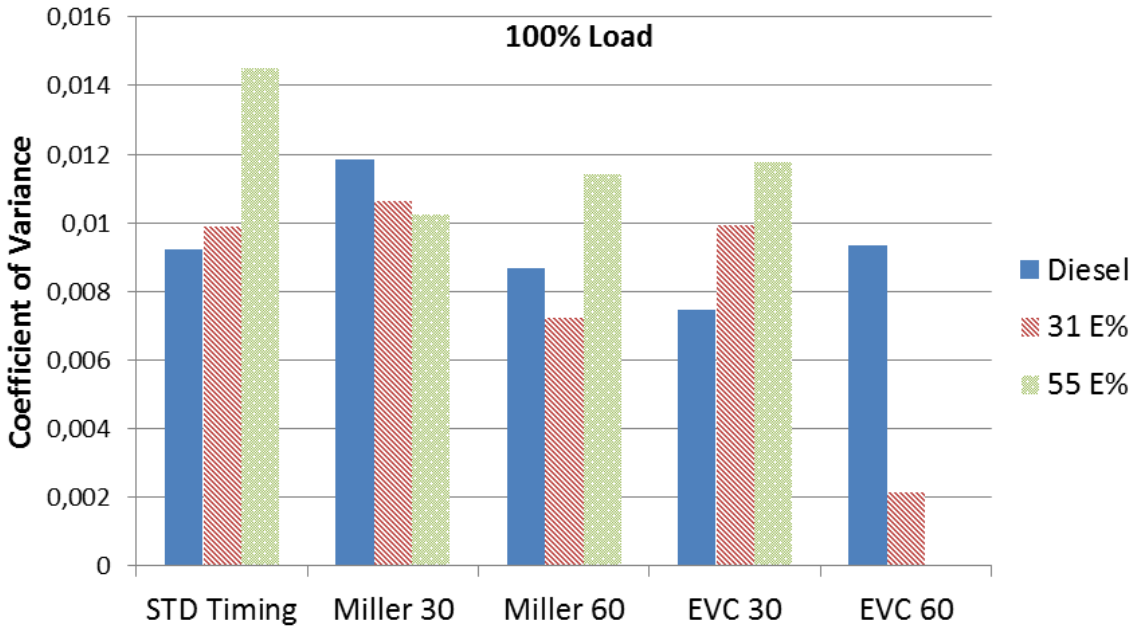

Figure 4.46. Coefficient of Variance with different valve timing configurations at 100% load. The blue columns represent the Diesel reference, red and green columns substitution rates of 31 E% and 55 E%, respectively.

5 Conclusions

The objective of this thesis was to study and analyse the effects of substitution rate and variable valve actuation and related parameters on dual-fuel combustion phenomena and emissions. Probably the greatest challenges in the dual-fuel concept are the relatively high engine-out methane emissions and difficulties in combustion control with lean mixtures. In addition, this thesis suggests that the NO_x emissions are also a matter of concern in dual-fuel engines.

Five valve configurations and different substitution rates were used in the engine tests. The research and analysis of this thesis can be concluded as follows:

- The combustion of the lean methane-air mixture at part load with high substitution rates is often incomplete and high HC emissions are emitted. Implementation of the Miller cycle and the resulting decrease in mixture temperature will aggravate the problem. Early exhaust valve closing strategies significantly reduced the HC emissions.

- The dual-fuel combustion is very sensitive early exhaust valve closing and the resulting increase in the mixture temperature. Elevated mixture temperature will promote the cold combustion and partial oxidation of methane which increases the heat release rate in the early exhaust stroke. Particularly at full load an increase in mixture temperature may also lead to the pre-ignition of the methane-air mixture.

- Rapid combustion of the methane-air mixture causes high NO_x but the HC emissions drop significantly. Increasing the lambda with early exhaust valve closing has the potential to substantially reduce the NO_x emissions while maintaining low HC emissions at part load.

- The NO2 emissions increase with even modest substitution rates regardless of engine load. Possible reasons for this are the decreased combustion peak temperature and the presence of partially oxidized methane products.

- Cycle-to-cycle variation increases with high substitution rates. However, modest substitution rates do not have a clear impact on the coefficient of variance. The cycle-to-cycle variation is generally greater at part load. A low coefficient of variance value is not necessarily linked to low HC emissions.

- The effect of the direct methane slip from the inlet to the exhaust was approximately 15…25 % of the total HC emissions with the most radical Miller cycles. The amount of methane emissions due to scavenging is naturally dependent on the pressure difference between the inlet and the exhaust and on the length of the valve overlap period.

It is clear that the dual-fuel combustion requires sophisticated control of engine parameters in order to maintain acceptable emissions levels while operating at high combustion efficiency. The control of methane lambda is important but also the mixture temperature control offers substantial benefits particularly at part load.

6 Future Work

In order to obtain high-resolution cylinder pressure measurements, it would be necessary to update the control system to match the high-frequency sensors. In addition, fast temperature sensors for monitoring the combustion temperature would provide valuable information regarding the dual-fuel combustion. The natural next step would be to implement a proper lambda control utilizing the valve timing or a separate throttle on the inlet side of the engine. Moreover, the Diesel injection should be updated in order to run the engine at higher substitution rates.

According to the analysis in this thesis, particularly the temperature of the lean methane-air mixture is a subject of interest which requires more in-depth research. Therefore it would be useful to implement a control system for the mixture temperature either by IEGR or by inlet air heaters. Especially the combustion of very lean mixtures at part load should be studied.

In addition to improvements to the actual research engine, a simulation model for the dual-fuel engine would offer indisputable benefits for the future research. A 1-D validated simulation model (e.g. GT-Power) would greatly aid in finding the most interesting parameter combinations and thus reduce the amount of required engine experiments.

Bibliography

[1] International Energy Agency. “Are We Entering the Golden Age of Gas?”. World Energy Outlook. France, 2011.

[2] Directive 2012/33/EU of the European Parliament And of the Council. Official Journal of the European Union. France, 2012.

[3] Evans, R. “Automotive Engine Alternatives: Proceedings Of The International Symposium On Alternative And Advanced Automotive Engines, Vancouver”. Springer Science. USA, 1986.

[4] Karim G. A. “Combustion in Gas Fueled Compression: Ignition Engines of the Dual Fuel Type”. Journal of Engineering for Gas Turbines and Power, Vol. 125. pp. 827-836. 2003. DOI: 10.1115/1.1581894.

[5] Wearer, C & Turner, S.,“Dual Fuel Natural Gas/Diesel Engines: Technology, Performance and Emissions”. SAE technical paper 940548. 1994. DOI: 10.4271/940548

[6] Wärtsilä Corporation. Wärtsilä Image Bank. [Online]. [Cited 19.3.2015]. URL: http://imagebank.wartsila.com/Imagebank/#

[7] Königsson, F., “On Combustion in the CNG - Diesel Dual Fuel Engine”. Doctoral Thesis. Royal Institute of Technology. Sweden, 2014. ISSN 1400-1179.

[8] Papagiannakis R. & Hountalas, D., “Combustion and Exhaust Emission Characteristics af a Dual Fuel Compression Ignition Engine Operated with Pilot Diesel Fuel and Natural Gas,” Energy Conversion and Management, Vol. 45. pp. 2971–2987. Elsevier, 2004. DOI:10.1016/j.enconman.2004.01.013.

[9] American Power Group, Inc., “APG Dual Fuel Gliders^{tm}”. [Online]. [Cited 12.1.2015]. URL: http://www.americanpowergroupinc.com/apg-dual-fuel-gliders%E2%84%A2.html

[10] Bach, C. & Alvarez, R. & Winkler, A., “Exhaust Gas Aftertreatment and Emissions of Natural Gas and Biomethane Driven Vehicles”. Biogasmax - Integrated Project No 0197995. [Online]. [Cited 11.12.2014]. URL: http://biogasmax.eu/media/d5_9_biogasmax_report_final_v4b_20101103__083924400_0948_26012011.pdf

[11] Laguitton, O. et al., “The Effect of Compression Ratio on Exhaust Emissions from a PCCI Diesel Engine,” Energy Conversion and Management, Vol. 48. pp. 2918–2924. Elsevier, 2007. DOI:10.1016/j.enconman.2007.07.016.

[12] Splitter, D et al., “An Experimental Investigation of Fuel Reactivity Controlled PCCI Combustion in a Heavy-Duty Engine,” SAE Technical Paper 2010-01-0345. 2010. ISSN 0148-7191.

[13] Directive 2005/55/EC of the European Parliament And of the Council. Official Journal of the European Union. 2005.

[14] Edwards, R. & Larivé, J-F. & Mahieu, V. & Rouveirolles, P. et al., "Well-to-Wheels Analysis of Future Automotive Fuels and Powertrains in the European Context". Well-to-Tank Report, Version 2c. European Commission Joint Research Centre, 2007.

[15] Directive 1999/96/EC of the European Parliament And of the Council. Official Journal of the European Communities. 1999.

[16] Commission Regulation (EU) No 582/201. Official Journal of the European Union. 2011.

[17] Implats Corporation. "Evolution of Emission Standards" . [Online]. [Cited 15.12.2014]. URL: http://www.implats.co.za/implats/Emission-standards.asp.

[18] Directive 2004/26/EC of the European Parliament And of the Council. Official Journal of the European Union. 2004.

[19] Badr, O; Karim, G. & Liu, B., "Examination of the Flame Spread Limits in a Dual Fuel Engine". Applied Thermal Engineering, Vol. 19. pp. 1071–1080. Elsevier, 1999.

[20] Azimov, U. & Tomita, E. & Kawahara, N., "Ignition, Combustion and Exhaust Emission Characteristics of Diesel Micro-Pilot Ignited Dual-Fuel Engine Operated under PREMIER Combustion Mode". SAE Technical Paper 2011-01-1764. 2011. DOI:10.4271/2011-01-1764.

[21] Tomita, E. & Fukatani, N. & Kawahara, N. & Maruyama, K., "Combustion in a Supercharged Biomass Gas Engine with Micro-Pilot Ignition - Effects of Injection Pressure and Amount of Diesel Fuel". Journal of KONES Powertrain and Transport, Vol. 14. 2007.

[22] Järvi, A. "Methane Slip Reduction in Wärtsilä Lean Burn Gas Engines". CIMAC Congress, Paper No. 106. Bergen, 2011.

[23] Wärtsilä Finland Corporation., "Wärtsilä Medium-Speed Engines"-Brochure. [Online]. [Cited 5.1.2015]. URL: http://pdf.nauticexpo.com/pdf/wartsila-corporation/wartsila-medium-speed-engines/24872-69921.html

[24] Demirbas, A. "Methane Gas Hydrate". Springer Media. pp. 58-76. 2010. ISBN: 978-1-84882-871-1.

[25] Natural & bio Gas Vehicle Association. "Comparison of Energy Contents and CO2 Emissions from Different Fuels". [Online]. [Cited 12.1.2015]. URL: http://www.ngvaeurope.eu/comparison-of-energy-contents-and-co2-emissions-from-different-fuels

[26] Kavalov, B et al., “Liquefied Natural Gas for Europe - Some Important Issues for Consideration”. JRC Reference Reports. European Joint Research Centre, 2009.

[27] Weiland, P., “Biogas Production: Current State and Perspectives”. Applied Microbiology and Biotechnology, Vol. 85. pp. 849–860. Springer, 2010. DOI:10.1007/s00253-009-2246-7

[28] Kim, K. & Kim, H. & Kim, B. & Lee, K. & Lee, K., “Effect of Natural Gas Composition on the Performance of a CNG Engine”. Oil & Gas Science and Technology, Vol. 64. pp 199-206.

[29] M. W. Shin, D. Shin, S. H. Choi, and E. S. Yoon, “Optimal operation of the boil-off gas compression process using a boil-off rate model for LNG storage tanks,” *Korean J. Chem. Eng.*, vol. 25, no. 1, pp. 7–12, 2008. Institut français du pétrole, 2008. DOI:10.2516/ogst:2008044.

[30] International Association for Natural Gas Vehicles. “Fuel Properties”. IANGV Emission Report 31.03.2000.

[31] Semelsberger, T. & Borup, R. & Greene, H., “Dimethyl Ether (DME) as an Alternative Fuel”. Journal of Power Sources, Vol. 156. pp. 497–511. Elsevier, 2006. DOI:10.1016/j.jpowsour.2005.05.082

[32] K. E. Starling, E. R. Ding, J. H. Harwell, and R. G. Mallinson, “Method for Improving Natural Gas Energy Density at Ambient Temperatures,” no. 3, pp. 1062–1064, 2000.

[33] Cummings, Inc. “Cummings Dual Fuel Engines”. [Online]. [Cited 17.1.2015]. URL: http://cumminsengines.com/dual-fuel

[34] Hekkert, M. & Hendriks, F. & Faaij, A. & Neelis, M., “Natural Gas as an Alternative to Crude Oil in Automotive Fuel Chains Well-To-Wheel Analysis and Transition Strategy Development”. Energy Policy, Vol. 33. pp. 579–594. Elsevier, 2005. doi:10.1016/j.enpol.2003.08.018

[35] Green Car Congress. “Bosch Launches Heavy-Duty Natural Gas Dual-Fuel Conversion Kit in Brazil”. [Online]. [Cited 20.1.2015]. URL: http://www.greencarcongress.com/2008/06/bosch-launches.html

[36] McTaggart-Cowan, G. & Rogak, S. & Munshi, S. & Hill, P. & Bushe, W., “The Influence of Fuel Composition on a Heavy-Duty, Natural-Gas Direct-Injection Engine”. Fuel, Vol. 89. pp. 752–759. Elsevier, 2010.

[37] McTaggart-Cowan, G. & Mann, K. & Wu, N & Munshi, S., “An Effiecient Direct-Injection of Natural Gas Engine For Heavy Duty Vehicles”. SAE Technical Paper 2014-01-1332. DOI:10.4271/2014-01-1332.

[38] Andreas, T.; Baumgarten C. & Nisters, C., “Management System for the Efficient Use of Gaseous Fuels”. MTZ Worldwide, Vol. 2/2012. pp. 38–43.

[39] Colvile, R. & Hutchingson, E. & Mindell, J. & Warren, R., "The Transport Sector as a Source of Air Pollution," Atmospheric Environment, Vol. 35. pp. 1537-1565. Elsevier, 2001.

[40] Merker, G. & Schwarz, C. & Teichmann, R., "Combustion Engines Development: Mixture Formation, Combustion, Emissions And Simulation". Springer. Germany, 2009. ISBN: 978-3-64214-094-5

[41] Yoon, S. H. & Lee, C. S., "Experimental Investigation on the Combustion and Exhaust Emission Characteristics of Biogas-Biodiesel Dual-Fuel Combustion in a CI Engine," Fuel Processing Technology. Technol., vol. 92, no. 5, pp. 992–1000, 2011.

[42] Krishnan, S.R. et al.,"Strategies for Reduced NO_x Emissions in Pilot-Ignited Natural Gas Engines," Journal of Engineering for Gas Turbines and Power, Vol. 126. pp. 665-671. ASME, 2004.

[43] Ando, K. & Manabe, A. & Yasuda, A.,"Hardfaced Valve and P/M Valve Seat System for CNG and LPG Fuel Engines" SAE Technical Paper 2005-01-0718.

[44] Heywood, J.B.,"Internal Combustion Engine Fundamentals". McGraw-Hill Series. 1988. ISBN 0-07-100499-8.

[45] Wang, Y.S.,"The Effect of Operating Conditions on Heavy Duty Engine Valve Seat Wear". Wear, Vol. 201. pp. 15-25. Elsevier, 1996.

[46] Martin Wells Industries. "An Answer to Valve Wear" (independent study). [Online]. [Cited 20.11.2014]. URL: [http://www.martinwellsco.com/skin/frontend/default/martinwellsco/downloads/MWI-ValveWearStudyReprint.pdf

[47] Amnéus, P. & Mauss, F. & Kraft, M. & Vressner, A. & Johansson, B., "NO_x and N_2O Formation in HCCI Engines". SAE Technical Paper 2005-01-0126. SAE, 2005. DOI:10.4271/2005-01-0126.

[48] Li, S. C. & Williams, F.A.,"Reaction Mechanisms for Methane Ignition," Journal of Engineering for Gas Turbines and Power, Vol. 124. pp. 471-480. ASME, 2002.

[49] "Bockhorn, H., "Soot Formation in Combustion". Springer-Verlag. Heidelberg, 1994. ISBN: 978-3-642-85169-8.

[50] Pierik R. & Burkhard, J.,"Design and Development of a Mechanical Variable Valve Actuation System". SAE Technical Paper 2000-01-1221. SAE, 2000.

[51] Kiga, S. & Mae, Y. & Akasaka, Y. & Tomogane, K., "Development of Innovative Variable Valve Event and Lift (VVEL) System". SAE Technical Paper 2007-01-3548. SAE International, 2007.

[52] Sellnau, M. & Rask, E.,“Two-Step Variable Valve Actuation for Fuel Economy, Emissions, and Performance”. SAE Technical Paper 2003-01-0029. SAE International, 2003.

[53] Fukuzawa, Y. & Shimoda, H. & Kakuhama, Y. & Hiroyuki, E. & Tanaka, K., “Development of High Efficiency Miller Cycle Gas Engine,” Technical Review, Vol. 38. pp. 146–150. Mitsubishi Heavy Industries, 2001.

[54] Mikalsen, R. & Wang, Y.D. & Roskilly A.P., “A Comparison of Miller and Otto Cycle Natural Gas Engines for Small Scale CHP Applications,” Applied Energy, Vol. 86. pp. 922–927. Elsevier, 2009.

[55] Daw, C. & Kennel, M. & Finney, C. & Connolly, F., “Observing and Modeling Nonlinear Dynamics an an Internal Combustion Engine,” Physical Review E, Vol. 57, no. 3. pp. 2811–2819. APS, 1998.

[56] Qi, Y. & Srinivasan, K. & Krishnan, S. & Yang, H. & Midkiff, K., “Effect of Hot Exhaust Gas Recirculation on the Performance and Emissions of an Advanced Injection Low Pilot-Ignited Natural Gas Engine” Int. J. of Engine Res., Vol. 8, pp. 289–303. USA, 2007. DOI: 10.1243/14680874JER02306

[57] Fackrell, J.E., “A Flame Ionisation Detector for Measuring Fluctuating Concentration”. J. Phys. E: Sci. Instrum., Vol. 13, pp. 888-893. UK, 1980.

[58] Robinson, J. & Bollinger, M. & Birks, J., “Luminol/H2O2 Chemiluminescence Detector for the Analysis of Nitric Oxide in Exhaled Breath,” Analytic Chemistry, Vol. 71, no. 22, pp. 5131–5136, 1999.

[59] Manning, A. & Keeling, R. & Severinghaus, J., “Precise Atmospheric Oxygen Measurements with a Paramagnetic Oxygen Analyzer”. Global Biochemical Cycles, Vol. 13, no. 4, pp. 1107–1115. 1999.

[60] Werle, P. et al., “Near- and Mid-Infrared Laser-Optical Sensors for Gas Analysis”. Optics and Lasers in Engineering, Vol. 37, pp. 101–114. Elsevier 2002.

[61] National Instruments, Inc. “Aliasing and Sampling at Frequencies Above the Nyquist Frequency”. [Online]. [Cited 21.3.2015]. URL: http://www.ni.com/white-paper/3000/en/

Appendices

A1: Wiring Diagram

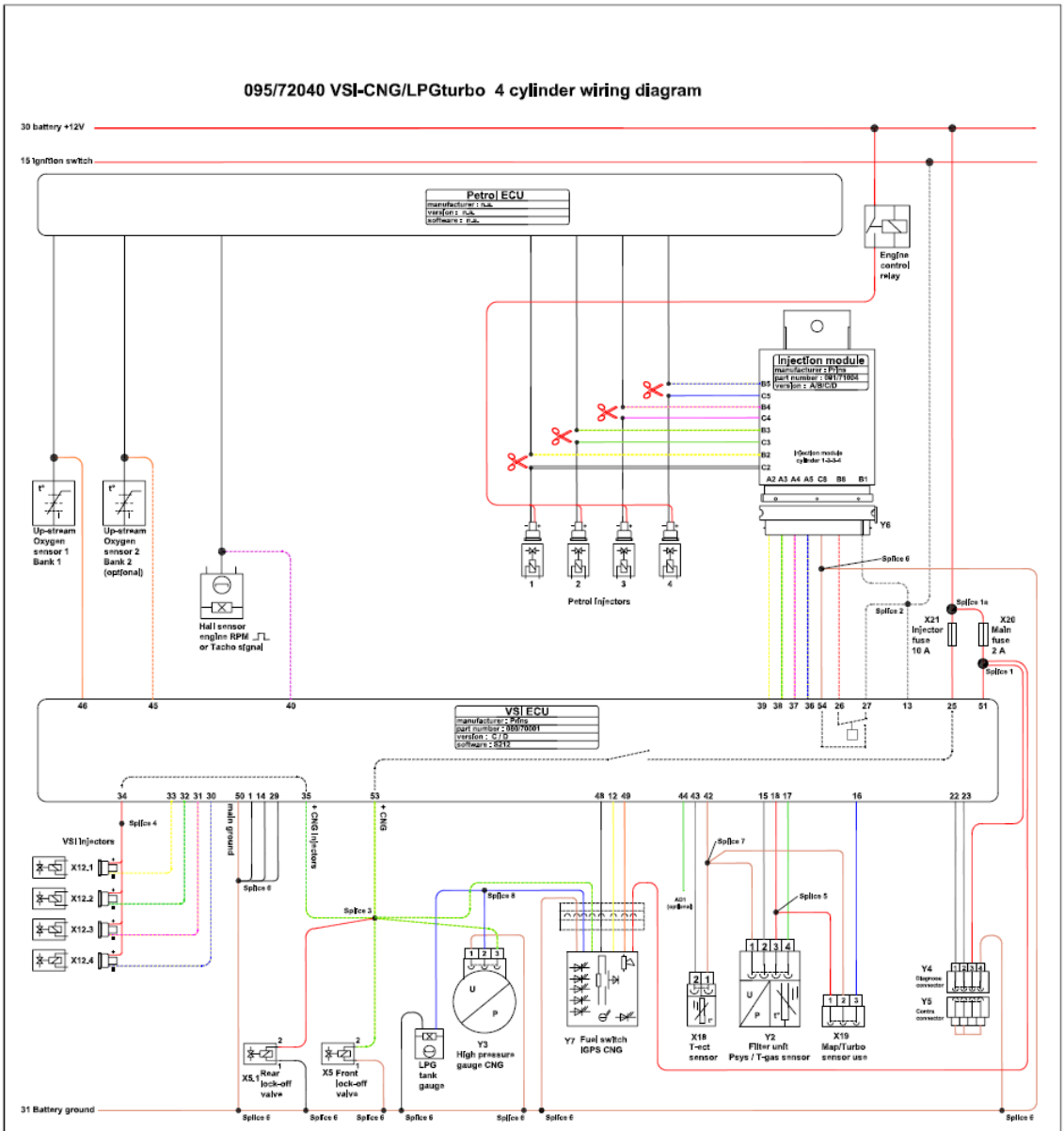

	Injection module		
A1	sealed		
A2	vsi ecu	white-yellow	39 ecu side 1
A3	vsi ecu	green-yellow	38 ecu side 2
A4	vsi ecu	pink-yellow	37 ecu side 3
A5	vsi ecu	blue-yellow	36 ecu side 4
A6	sealed		
A7	sealed		
A8	sealed		
B1	vsi ecu	grey-white	13 Ignition plus
B2	petrol ecu	white-yellow	39 ecu side 1
B3	petrol ecu	green-yellow	38 ecu side 2
B4	petrol ecu	pink-yellow	37 ecu side 3
B5	petrol ecu	blue-yellow	36 ecu side 4
B6	sealed		
B7	sealed		
B8	vsi ecu	red-white	28 Inj. mod. command
C1	sealed		
C2	petrol injector	white	min inj side 1
C3	petrol injector	green	min inj side 2
C4	petrol injector	pink	min inj side 3
C5	petrol injector	blue	min inj side 4
C6	sealed		
C7	sealed		
C8	vsi ecm	brown	54 Inj. mod. ground

pin	vsi wire	color
1	ground	black
2	sealed	
3	sealed	
4	sealed	
5	sealed	
6	sealed	
7	sealed	
8	sealed	
9	sealed	
10	sealed	
11	sealed	
12	pulse fuel switch	yellow
13	+ Ignition	grey-white
14	ground	black
15	T-Gas	grey
16	MAP	blue
17	Psys	green
18	+5V supply P/T sensor	red
18	+5V supply MAP	red
19	sealed	

pin	vsi wire	color
20	sealed	
21	sealed	
22	RS232 TxD	grey
23	RS232 RxD	grey
24	sealed	
25	+12 volt battery	red
26	Inj. mod.command	red-white
27	+ Ignition	grey-white
28	sealed	
29	G INJ A ground	black
30	G INJ OUT 4	blue-yellow
31	G INJ OUT 3	pink-yellow
32	G INJ OUT 2	green-yellow
33	G INJ OUT 1	white-yellow
34	+ G INJ A OUT	red
35	+ G INJ A IN	green-yellow
36	ecu side Inj 4	blue-yellow
37	ecu side Inj 3	pink-yellow
38	ecu side Inj 2	green-yellow
39	ecu side inj 1	white-yellow

pin	vsi wire	color
40	RPM engine speed	purple-white
41	sealed	
42	Sensor ground ECT	brown
42	Sensor ground MAP	brown
42	Sensor ground P/Tsys	brown
43	ECT coolant temp.	grey
44	AD1 Analog-Digital	green
45	lambda bank 2	orange-white
46	lambda bank 1	orange
47	sealed	
48	beeper low switching	black
49	diagnose LED	orange
50	main. ground	brown
50	Lock off valves ground	brown
50	diagnose ground	brown
50	switch ground	brown
50	high p. gauge ground	brown
51	+12 volt fuel switch	red
51	+12 volt diagnose	red
51	+12 volt battery	red

pin	vsi wire	color
52	sealed	
53	+ High p gauge	yellow-green
53	+ tank valve	red
53	+ main valve	yellow-green
53	+ switch	yellow-green
54	INJ module ground	brown
55	sealed	
56	sealed	

Prins Alternative Fuel Systems

Project name :	
Part nr :	095/72040
Description :	CNG/LPGturbo 4 cyl.
Designed by/ date	J.T. / 08-02-08
Checked by / date	J.T. / 08-02-12
Approved by / date	R.K. / 08-02-12
Revision / by / date	C / 08-02-12
Sheet :	1/1

Figure A1.1. VSI ECU Wiring Diagram

A2: Matlab Codes

A2.1: Script for extracting data and for plotting figures

```
% Engine plots

close all
clear all

files50 = dir('*@50*');
files100 = dir('*@100*');
o = size(files50(:,1),1);
p = size(files100(:,1),1);
n = o + p;
line = {'-','--','-','-.',':k'};

% preallocating data
angle = zeros(25001, o);
chargeFlow = zeros(25001, o);
averageChargeFlow = zeros(1, o);
chargePress = zeros(25001, o);
averageChargePress =zeros(1, o);
cylPress = zeros(25001, o);
fuelMassFlow = zeros(25001, o);
averageFuelMassFlow = zeros(1, o);
CH4MassFlow = zeros(25001, o);
averageCH4MassFlow = zeros(1, o);
exhPress = zeros(25001, o);
covdata = zeros(n,8);
Covdata = num2cell(covdata);

% Extracting measurement data:
for i=1:o
load(files50(i,1).name);
for t=1:26
measurements = struct2cell(load(files50(i,1).name));
var = cell2mat(measurements);
data = struct2cell(var);
var2 = data(2,1);
var3 = cell2mat(var2);
Label{t,1} = var3(1,t).Name;
DATA{t,1} = var3(1,t).Data';
end

% arranging data

angle(:,i) = cell2mat(DATA(1,:));
Angle(:,1) = angle(:,i);
chargeFlow(:,i) = cell2mat(DATA(2,:));
averageChargeFlow(:,i) = mean(chargeFlow(:,i));
avg_airflow(:,1) = averageChargeFlow(:,i);
chargePress(:,i) = cell2mat(DATA(3,:));
p_intake(:,1) = chargePress(:,i);
averageChargePress(:,i) = mean(chargePress(:,i));
offset(:,1) = averageChargePress(:,i);
cylPress(:,i) = cell2mat(DATA(6,:));
cyl_P(:,1) = cylPress(:,i);
fuelMassFlow(:,i) = cell2mat(DATA(11,:));
averageFuelMassFlow(:,i) = mean(fuelMassFlow(:,i));
diesel_flow(:,1) = averageFuelMassFlow(:,i)
CH4MassFlow(:,i) = cell2mat(DATA(26,:));
averageCH4MassFlow(:,i) = mean(CH4MassFlow(:,i));
CH4_flow(:,1) = averageCH4MassFlow(:,i)
exhPress(:,i) = cell2mat(DATA(8,:));
p_exhaust(:,1) = exhPress(:,i);
rpm = mean(cell2mat(DATA(18,:)));
```

```
HRR_calc(Angle, cyl_P, p_intake, offset); % heat release calculation

% saving the variables

dQ(i,:) = hr(:,:);
cylPress_hr(i,:) = P_cyl_hr(1,:)/100000;
intake_p_hr(i,:) = P_intake_hr/100000;
Angle_hr(i,:) = angle_hr(1,:);
avg_angle = 720/1002.2; % angle frequency
step(i,:) = avg_angle;
hrr_corr(i,:) = dQ(i,:).*step(i,:);
cumQ(i,:) = cumsum(hrr_corr(i,:))-1100; %setting zero level

cov_calc(cyl_P,Angle); %coefficient of variance calculation
COV_p(i,:) = COV_press(:,:);
d = [1:1:n];


flow_calc(avg_airflow, diesel_flow, CH4_flow, p_intake, p_exhaust, rpm);

Es(i,1) = E_subst;
lambda_df(i,:) = lambda;
lambda_ch4(i,:) = ch4lambda;
chargeP(i,:) = chargeP;
exhP(i,:) = exhP;
stdi_dev(i,:) = stdi_dev;
E_stroke(i,1) = E_cycle;
ci_low(i,:) = ci_low;
ci_high(i,:) = ci_high;
Pmax_mean(i,:) = Pmax_mean;

% creating data matrix
Covdata{i,1} = num2str(files50(i,1).name);
Covdata{i,2} = COV_p(i);
Covdata{i,3} = lambda_df(i);
Covdata{i,4} = Es(i);
Covdata{i,5} = lambda_ch4(i);
Covdata{i,6} = chargeP(i);
Covdata{i,7} = exhP(i);
Covdata{i,8} = stdi_dev(i);
Covdata{i,9} = ci_low(i);
Covdata{i,10} = Pmax_mean(i);
Covdata{i,11} = ci_high(i);
Covdata{i,12} = averageChargeFlow(i);
Covdata{i,13} = averageFuelMassFlow(i);
Covdata{i,14} = averageCH4MassFlow(i);
end

%% Full load measurements

angle2 = zeros(25001, p);
chargeFlow2 = zeros(25001, p);
averageChargeFlow2 = zeros(1, p);
chargePress2 = zeros(25001, p);
averageChargePress2 =zeros(1, p);
cylPress2 = zeros(25001, p);
fuelMassFlow2 = zeros(25001, p);
averageFuelMassFlow2 = zeros(1, p);
CH4MassFlow2 = zeros(25001, p);
averageCH4MassFlow2 = zeros(1, p);
exhPress2 = zeros(25001, p);

for i=1:p
load(files100(i,1).name);
for t=1:26
```

```
measurements = struct2cell(load(files100(i,1).name));
var = cell2mat(measurements);
data = struct2cell(var);
var2 = data(2,1);
var3 = cell2mat(var2);
Label{t,1} = var3(1,t).Name;
DATA{t,1} = var3(1,t).Data';
end

% arranging data

angle2(:,i) = cell2mat(DATA(1,:));
Angle2(:,1) = angle2(:,i);
chargeFlow2(:,i) = cell2mat(DATA(2,:));
averageChargeFlow2(:,i) = mean(chargeFlow2(:,i));
avg_airflow2(:,1) = averageChargeFlow2(:,i);
chargePress2(:,i) = cell2mat(DATA(3,:));
p_intake2(:,1) = chargePress2(:,i);
averageChargePress2(:,i) = mean(chargePress2(:,i));
offset2(:,1) = averageChargePress2(:,i);
cylPress2(:,i) = cell2mat(DATA(6,:));
cyl_P2(:,1) = cylPress2(:,i);
fuelMassFlow2(:,i) = cell2mat(DATA(11,:));
averageFuelMassFlow2(:,i) = mean(fuelMassFlow2(:,i));
diesel_flow2(:,1) = averageFuelMassFlow2(:,i)
CH4MassFlow2(:,i) = cell2mat(DATA(26,:));
averageCH4MassFlow2(:,i) = mean(CH4MassFlow2(:,i));
CH4_flow2(:,1) = averageCH4MassFlow2(:,i)
exhPress2(:,i) = cell2mat(DATA(8,:));
p_exhaust2(:,1) = exhPress2(:,i);
rpm = mean(cell2mat(DATA(18,:)));

HRR_calc(Angle2, cyl_P2, p_intake2, offset2); % heat release calculation

% saving the variables

dQ2(i,:) = hr(:,:);
cylPress_hr2(i,:) = P_cyl_hr(1,:)/100000;
intake_p_hr2(i,:) = P_intake_hr/100000;
Angle_hr2(i,:) = angle_hr(1,:);
hrr_corr2(i,:) = dQ2(i,:)*avg_angle;
cumQ2(i,:) = cumsum(hrr_corr2(i,:))-1715;

cov_calc(cyl_P2, Angle2); %coefficient of variance calculation
COV_p2(i,:) = COV_press(:,:);

flow_calc(avg_airflow2, diesel_flow2, CH4_flow2, p_intake2, p_exhaust2, rpm);
Es2(i,1) = E_subst;
lambda_df2(i,:) = lambda;
lambda_ch42(i,:) = ch4lambda;
chargeP2(i,:) = chargeP;
exhP2(i,:) = exhP;
stdi_dev2(i,:) = stdi_dev;
E_stroke2(i,1) = E_cycle;
ci_low2(i,:) = ci_low;
ci_high2(i,:) = ci_high;
Pmax_mean2(i,:) = Pmax_mean;

Covdata{i+o,1} = num2str(files100(i,1).name);
Covdata{i+o,2} = COV_p2(i);
Covdata{i+o,3} = lambda_df2(i);
Covdata{i+o,4} = Es2(i);
Covdata{i+o,5} = lambda_ch42(i);
Covdata{i+o,6} = chargeP2(i);
Covdata{i+o,7} = exhP2(i);
Covdata{i+o,8} = stdi_dev2(i);
Covdata{i+o,9} = ci_low2(i);
```

```
Covdata{i+o,10} = Pmax_mean2(i);
Covdata{i+o,11} = ci_high2(i);
Covdata{i+o,12} = averageChargeFlow2(i);
Covdata{i+o,13} = averageFuelMassFlow2(i);
Covdata{i+o,14} = averageCH4MassFlow2(i);

end

%% Plots

% 50% HRR

figure ();
for f=1:o
h(f) = plot(Angle_hr(f,:), dQ(f,:),line{f},'LineWidth', 1.5);
hold on
end
h_title = title('50% Load');
set(h_title, 'Fontsize', 12);
set(gcf, 'Position', [100, 100, 1049, 650]);
xlim(gca, [-20 60]);
ylim(gca, [-20 200]);
set(gca, 'xtick',[-20:5:60], 'ytick',[-20:20:200],'FontSize',14);
h_legend = {'64 E%','54 E%','46 E%','29 E%','Diesel'};
order=[5 4 3 2 1];
legend(h(order),h_legend{order});
set(legend, 'FontSize', 12);
xlabel('°CAD','FontSize', 14);
ylabel('Heat Release Rate (J/°CAD)','FontSize', 14);
grid on

%% 50% load cumulative HR
figure();
for f=1:o
plot(Angle_hr(f,:), cumQ(f,:));
xlim(gca, [-30 100]);
ylim(gca, [-20 550]);
hold on
end
Legend=cell(1,1)
for iter=1:o
   Legend{iter}=strcat(num2str(files50(iter,1).name));
end
legend(Legend)

%% 50% cyl press
figure();
hold all
for f=1:o
h(f) = plot(Angle_hr(f,:), cylPress_hr(f,:),line{f},'LineWidth', 1.5);
end
h_title = title('50% Load');
set(h_title, 'Fontsize', 12);
set(gcf, 'Position', [100, 100, 1049, 650]);
xlim(gca, [-30 45]);
ylim(gca, [0 140]);
set(gca, 'xtick',[-30:5:45], 'ytick',[0:10:140],'FontSize',14);
h_legend = {'64 E%','54 E%','46 E%','29 E%','Diesel'};
order=[5 4 3 2 1];
legend(h(order),h_legend{order});
set(legend, 'FontSize', 12);
xlabel('°CAD','FontSize', 14);
ylabel('Cylinder Pressure (bar)','FontSize', 14);
grid on

%%
figure (); %full load HRR
```

```
hold all
for f=1:p
h(f) = plot(Angle_hr2(f,:), dQ2(f,:),line{f},'LineWidth', 1.5);
end
h_title = title('100% Load');
set(h_title, 'Fontsize', 12);
set(gcf, 'Position', [100, 100, 1049, 650]);
xlim(gca, [-20 60]);
ylim(gca, [-20 600]);
set(gca, 'xtick',[-20:5:60], 'ytick',[-20:40:600],'FontSize',14);
h_legend = {'31 E%','18 E%','Diesel','55 E%', '40 E%'};
order=[3 2 1 5 4];
legend(h(order),h_legend{order});
set(legend, 'FontSize', 12);
xlabel('°CAD','FontSize', 14);
ylabel('Heat Release Rate (J/°CAD)','FontSize', 14);
grid on

%%
figure (); %full load cumulative HR
for f=1:p
plot(Angle_hr2(f,:), cumQ2(f,:));
xlim(gca, [-30 100]);
ylim(gca, [-20 550]);
hold on
end
Legend=cell(1,1)
for iter=1:p
   Legend{iter}=strcat(num2str(files100(iter,1).name));
end
legend(Legend)

%%
figure (); %full load cyl press
hold all
for f=1:p
h(f) = plot(Angle_hr2(f,:), cylPress_hr2(f,:),line{f},'LineWidth', 1.5);
end
h_title = title('100% Load');
set(h_title, 'Fontsize', 12);
set(gcf, 'Position', [100, 100, 1049, 650]);
xlim(gca, [-30 45]);
ylim(gca, [0 250]);
set(gca, 'xtick',[-30:5:45], 'ytick',[0:20:250],'FontSize',14);
h_legend = {'31 E%','18 E%','Diesel','55 E%', '40 E%'};
order=[3 2 1 5 4];
legend(h(order),h_legend{order});
set(legend, 'FontSize', 12);
xlabel('°CAD','FontSize', 14);
ylabel('Cylinder Pressure (bar)','FontSize', 14);
grid on
```

A2.2: Heat release calculations

```
% This script performs cylinder pressure and heat release calculations:


function HRR_calc(Angle,cyl_P,p_intake,offset)

conrodLength = 0.232; % Connecting rod length
crankRadius = 0.0725; % Crank radius
lambda= crankRadius/conrodLength; % Cranksaft ratio
Vd1=0.00140315; % Displacement volume
gamma=1.35; % from literature
Rc=16.5; %Compression ratio updated 09.09.2013
Vc=Vd1/(Rc-1); % Free Volume at TDC, updated 09.09.2013
D=0.1108; % Piston Diameter

f=36000;%  sampling frequency
f_cutoff = 2000; % cutoff frequency
fnorm = f_cutoff/(f/2); % normalized cut off freq, you can change it to any
value depending on your requirements
[b1,a1] = butter(10,fnorm,'low'); % Low pass Butterworth filter of order 10
p_cyl = filtfilt(b1,a1,cyl_P); % filtering


assignin('base','P_CYL',p_cyl);
angle_hr = Angle;
assignin('base','Angle360360',angle_hr);

%% re-arregement of the measurement data:
y = 0;
x = 0;
intake = 0;
cycle = 1;
e = 2;

if length(p_cyl) == length(angle_hr);
    len = length(p_cyl);
    y(1,1) = p_cyl(1);
    intake(1,1) = p_intake(1);
    x(1,1) = angle_hr(1);

    for r=2:len

        if (angle_hr(r-1) > 0 && angle_hr(r) < 0)
            cycle = cycle + 1;
            e = 1;
        end
        y(cycle,e) = p_cyl(r);
        intake(cycle,e) = p_intake(r);
        x(cycle,e) = angle_hr(r);
        e = e+1;
    end
end

% removing the first and last row
a = x(2:25, :);
b = y(2:25, :);
c = intake(2:25, :);


% calculate averages for cylinder and intake pressure
avg_p_cyl = mean(b)*100000;
avg_angle = mean(a);
avg_intake_p = mean(c)*100000;
p_cyl = b*100000;
```

```
% Decrease all cylinder pressure measurements to the same length
Avg_p_cyl = zeros(1, 1000);
Avg_angle = zeros(1, 1000);
Avg_intake_p = zeros(1, 1000);

for r=1:1000
Avg_p_cyl(1,r) = avg_p_cyl(1,r);
Avg_angle(1,r) = avg_angle(1,r);
Avg_intake_p(1,r) = avg_intake_p(1,r);
end

Angle_correct = zeros(1, 1000);
Angle_correct(1) = 0.7;
for r=2:1000
    Angle_correct(r) = Avg_angle(r)-Avg_angle(r-1);
end

% set the pressure level
Avg_p_cyl = Avg_p_cyl+(mean(Avg_intake_p(1:200))-mean(Avg_p_cyl(1:200)));
Avg_p_cyl = Avg_p_cyl+offset;

%calculate radian angles for next step
x_rad = Avg_angle/360*2*pi;

% Output the averaged and filtered cylinder pressure to workspace
assignin('base','P_cyl_hr',Avg_p_cyl);
assignin('base','P_intake_hr',Avg_intake_p);
assignin('base','angle_hr',Avg_angle);
dQ = zeros(1,length(x_rad));
dV = Vd1/2.*(sin(x_rad)+lambda.*sin(x_rad).*cos(x_rad)./sqrt(1-
lambda^2.*sin(x_rad).^2));

for s = 2:(length(x_rad)-1)
dQ(1,s) = (gamma/(gamma-1)*Avg_p_cyl(s)*dV(s)+1/(gamma-1)*...
(Vc+pi*D*D/4*(conrodLength+crankRadius-
(crankRadius*cos(x_rad(s))+sqrt(conrodLength*conrodLength-...
crankRadius*crankRadius*sin(x_rad(s))*sin(x_rad(s))))))*(Avg_p_cyl(s+1)-
Avg_p_cyl(s-1))/(x_rad(s+1)-x_rad(s-1)))/(360/(2*pi));
end

%Smoothens heat release curve:

dQ=smooth(Avg_angle,dQ);
dQ_cycle=smooth(dQ_cycle);

assignin('base','hr',dQ);
assignin('base','dQ_cycle',dQ_cycle);
assignin('base', 'Angle_correct', Angle_correct);
```

A2.3: Flow Calculations

```
% subtitution rate and lambda calculation

function flow_calc(avg_airflow, diesel_flow, CH4_flow, p_intake, p_exhaust,
rpm)

E_di = 42.9; % diesel energy content MJ/kg
E_ch4 = 50; % ch4 energy content
AFR_di = 14.7;
AFR_ch4 = 17.2;

if CH4_flow < 0.2;
    CH4_flow = 0;
end

ef_di = diesel_flow*E_di;
ef_ch4 = CH4_flow*E_ch4;

assignin('base', 'ef_di', ef_di);
assignin('base', 'ef_ch4', ef_ch4);

E_subst = ef_ch4/(ef_di+ef_ch4)*100;
m_subst = CH4_flow/(CH4_flow+diesel_flow);
E_cycle = (ef_di+ef_ch4)/(rpm*60/2)*1000000; %energy content per cycle

% lambda calculation

AFR_tot = avg_airflow/(diesel_flow+CH4_flow);

lambda = AFR_tot/(AFR_ch4*m_subst+AFR_di*(1-m_subst));

ch4lambda = (avg_airflow/CH4_flow)/AFR_ch4;

% avg charge and exhaust press

chargeP = mean(p_intake);
exhP = mean(p_exhaust);

assignin('base', 'm_subst', m_subst);
assignin('base', 'E_subst', E_subst);
assignin('base', 'lambda', lambda);
assignin('base', 'ch4lambda', ch4lambda);
assignin('base', 'chargeP', chargeP);
assignin('base', 'ch4lambda', ch4lambda);
assignin('base', 'exhP', exhP);
assignin('base', 'E_cycle', E_cycle);
```

A2.4: Coefficient of Variance Calculation

```
function cov_calc(cyl_P, Angle)

f=36000;%  sampling frequency
f_cutoff = 4000; % cutoff frequency
fnorm = f_cutoff/(f/2); % normalized cut off freq, you can change it to any
value depending on your requirements
[b1,a1] = butter(10,fnorm,'low'); % Low pass Butterworth filter of order 10
p_cyl = filtfilt(b1,a1,cyl_P); % filtering

y = 0;
x = 0;
intake = 0;
cycle = 1;
e = 2;

if length(p_cyl) == length(Angle);
    len = length(p_cyl);
    y(1,1) = p_cyl(1);
    x(1,1) = Angle(1);

    for r=2:len

        if (Angle(r-1) > 0 && Angle(r) < 0)
            cycle = cycle + 1;
            e = 1;
        end
        y(e, cycle) = p_cyl(r);
        x(e, cycle) = Angle(r);
        e = e+1;
    end
end

ANG = x(:, 2:25); % removing the first and last column
CYL = y(:, 2:25);

[Pmax, p_ind] = max(CYL);

Pmax_mean = mean(Pmax); % mean of max cyl press
std_dev = std(Pmax); % std deviation of cyl press
stdi_dev = std(p_ind);
COV_press = std_dev/Pmax_mean

n = 24
s_vect = zeros(1,24);
for i=1:n
    s_vect(i) = (Pmax(i)-Pmax_mean)^2;
end

s = sqrt(sum(s_vect)/(n-1));
S = s/sqrt(n);
ci_low = Pmax_mean - S*1.96; % 95% confidence interval
ci_high = Pmax_mean + S*1.96;

assignin('base', 'COV_press', COV_press);
assignin('base', 'stdi_dev', stdi_dev);
assignin('base', 'ci_low', ci_low);
assignin('base', 'ci_high', ci_low);
assignin('base', 'Pmax_mean', Pmax_mean);
```

A3: Mean Cylinder Pressure Confidence Intervals

Table A3.1. Average cylinder pressure 95% confidence intervals of the measurements. The files are named as follows: "d<Diesel inj. Duration(us)>_g<gas inj. duration>_<valve config.>_<load>.mat". (ml=late miller, cp=high charge press). The maximum deviation of the average cylinder pressure at this confidence interval relative to the average value is calculated in the rightmost column.

Measurement file name	Lower limit	Average	Upper limit	Max dev.
d508_g77_iegr30_@50.mat	127,88	128,41	128,93	0,58 %
d508_g77_iegr60_@50.mat	174,65	175,72	176,78	0,41 %
d508_g77_iegr60_cp_@50.mat	189,40	190,61	191,81	0,61 %
d508_g77_l30_@50.mat	126,97	127,85	128,72	0,63 %
d508_g77_m0_press_@50.mat	129,62	130,20	130,78	0,68 %
d508_g77_m30_@50.mat	134,86	135,47	136,08	0,44 %
d508_g77_m30_press_@50.mat	128,93	129,46	130,00	0,45 %
d508_g77_m60_@50.mat	122,83	123,62	124,40	0,41 %
d508_g77_m60_press_@50.mat	123,05	123,74	124,44	0,64 %
d508_g77_ml30_@50.mat	136,37	136,93	137,50	0,56 %
d508_g77_ml60_@50.mat	151,23	151,77	152,31	0,41 %
d520_g77_@50p.mat	123,35	124,05	124,75	0,35 %
d585_g71_@50p.mat	120,37	121,12	121,87	0,57 %
d670_g58_@50p.mat	126,94	127,40	127,87	0,62 %
d670_g58_iegr30_@50.mat	145,05	145,58	146,10	0,36 %
d670_g58_iegr60_@50.mat	172,65	173,31	173,97	0,38 %
d670_g58_iegr60_cp_@50.mat	190,04	191,08	192,13	0,36 %
d670_g58_l30_@50.mat	140,18	140,75	141,31	0,38 %
d670_g58_m0_@50.mat	141,13	141,61	142,10	0,55 %
d670_g58_m30_@50.mat	147,80	148,37	148,94	0,40 %
d670_g58_m60_@50.mat	133,55	134,77	135,99	0,35 %
d720_g52_@50p.mat	125,51	126,01	126,50	0,38 %
d834_g00_@50p.mat	126,54	126,97	127,39	0,91 %
d834_g00_iegr30_@50.mat	147,72	148,19	148,67	0,39 %
d834_g00_iegr60_@50.mat	137,24	137,82	138,41	0,33 %
d834_g00_iegr60_cp_@50.mat	159,75	160,08	160,41	0,32 %
d834_g00_l30_@50.mat	143,86	144,30	144,74	0,43 %
d834_g00_m0_@50.mat	143,02	143,69	144,36	0,21 %
d834_g00_m30_@50.mat	148,14	148,54	148,95	0,31 %
d834_g00_m60_@50.mat	133,45	134,09	134,73	0,47 %
d1200_g64_@100.mat	233,16	234,00	234,84	0,27 %
d1200_g64_iegr30_@100.mat	201,44	202,24	203,05	0,48 %
d1200_g64_iegr60_@100.mat	240,04	240,24	240,45	0,36 %
d1200_g64_l30_@100.mat	196,01	196,64	197,26	0,32 %
d1200_g64_m0_@100.mat	207,23	208,06	208,88	0,40 %
d1200_g64_m30_@100.mat	200,25	201,11	201,97	0,09 %
d1200_g64_m60_@100.mat	181,89	182,42	182,95	0,32 %

d1500_g50_@100.mat	229,24	229,93	230,62	0,40 %
d2200_g00_@100.mat	217,71	218,19	218,67	0,43 %
d2200_g00_iegr30_@100.mat	183,26	183,81	184,36	0,29 %
d2200_g00_iegr60_@100.mat	184,27	184,96	185,65	0,30 %
d2200_g00_l30_@100.mat	178,15	178,89	179,62	0,22 %
d2200_g00_m0_@100.mat	185,79	186,48	187,16	0,29 %
d2200_g00_m30_@100.mat	187,57	188,46	189,36	0,30 %
d2200_g00_m60_@100.mat	171,61	172,21	172,81	0,37 %
d620_g95_@100.mat	237,41	238,45	239,48	0,41 %
d620_g95_iegr30_@100.mat	211,72	212,72	213,72	0,37 %
d620_g95_l30_@100.mat	200,62	201,79	202,96	0,47 %
d620_g95_m30_@100.mat	197,79	198,61	199,42	0,35 %
d620_g95_m60_@100.mat	176,83	177,64	178,45	0,43 %
d620_g95_ml30_@100.mat	198,51	199,06	199,61	0,44 %
d620_g95_ml60_@100.mat	231,54	232,55	233,56	0,47 %
d820_g81_@100.mat	236,24	236,95	237,66	0,58 %